iEnergy
REVIEW
https://doi.org/10.23919/IEN.2023.0026

Major strategies for improving the performance of perovskite solar cells

Lixiu Zhang[1], Hang Li[2], Kai Zhang[3], Wenzhe Li[8], Chuantian Zuo[1], George Omololu Odunmbaku[6], Jingde Chen[9], Cong Chen[5], Luozheng Zhang[10], Ru Li[11], Yuping Gao[12], Baomin Xu[10], Jiangzhao Chen[11], Yongsheng Liu[12], Yang Wang[13], Yanlin Song[13], Jianxin Tang[9], Feng Gao[14], Qing Zhao[14], Yong Peng[15], Mingzhen Liu[16], Lei Tao[17], Yuelong Li[17], Zhimin Fang[18], Ming Cheng[7] ✉, Kuan Sun[6] ✉, Dewei Zhao[5] ✉, Yixin Zhao[4] ✉, Shihe Yang[3] ✉, Chenyi Yi[2] ✉ and Liming Ding[1] ✉

ABSTRACT

Metal halide perovskite solar cell (PSC) has successfully distinguished itself in optoelectronic field by virtue of the sharp rise in power conversion efficiency over the past decade. The remarkable efficiency breakthrough at such a fast speed can be mainly attributed to the comprehensive study on film deposition techniques, especially the effective management of surface and interfacial defects in recent works. Herein, we summarized the current trends in performance enhancement for PSCs, with a focus on the generally applicable strategies in high-performance works, involving deposition methods, compositional engineering, additive engineering, crystallization manipulation, charge transport material selection, interfacial passivation, optical coupling effect and constructing tandem solar cells. Promising directions and perspectives are also provided.

KEYWORDS

Perovskite solar cells, efficiency improvement, strategies, milestones.

Perovskite solar cells (PSCs) have emerged as a promising technology for achieving high performance. Solution processibility and the low levelized cost of electricity (LCOE) (3.5–4.9 US cents/kWh) further add its market attractiveness[1]. The rapid advance is the joint consequence of the increasing understanding of film processing techniques and the superior intrinsic photoelectric properties of perovskite, e.g., strong light absorption, long and balanced carrier diffusion length, benign defect tolerance, easily tunable bandgaps, etc. These merits endow PSCs with the capability to achieve up to certified 26.1% efficiency in a short time period[2], which is around 82% of S-Q limit. Compared with the relatively mature photovoltaic technologies like Si and GaAs solar cells, there is still room for improvement, and thus understanding the mechanisms behind high performance is critical.

Metal halide perovskite materials were first utilized as the sensitizer in dye-sensitized solar cells in 2009 by Kojima et al., and the methyl ammonium lead iodide ($MAPbI_3$)-based solar cells showed a power conversion efficiency (PCE) of 3.8%[3]. Based on this pioneering work, numerous studies on PSCs have sprung up, where the milestone efficiency enhancement works are summarized in Figure. 1. At the early stage, the efficiency breakthrough was mainly driven by the optimization of device structure, precursor composition and film formation processes. Park's group innovatively substituted spiro-OMeTAD for liquid electrolyte as the hole transport layer and constructed all-solid-state PSC with 9.7% PCE[4]. Subsequently, in 2012, Snaith's group constructed meso-superstructure OIHP device by replacing TiO_2 with the insulating scaffold Al_2O_3 and the PCE exceeded 10% for the first time[5]. This work proved the bipolar charge transport nature of perovskite materials, inspiring the development of the first planar-heterojunction PSCs[6]. The inferior morphology and crystal quality were the major reasons for poor device performance in that period. Many approaches were proposed to improve the film formation

[1]Center for Excellence in Nanoscience (CAS), Key Laboratory of Nanosystem and Hierarchical Fabrication (CAS), National Center for Nanoscience and Technology, Beijing 100190, China; [2]State Key Laboratory of Power System, Department of Electrical Engineering, Tsinghua University, Beijing 100084, China; [3]Shenzhen Graduate School, Peking University, Shenzhen 518055, China; [4]School of Environmental Science and Engineering, Shanghai Jiao Tong University, Shanghai 200240, China; [5]College of Materials Science and Engineering & Engineering Research Center of Alternative Energy Materials & Devices, Sichuan University, Chengdu 610065, China; [6]School of Energy & Power Engineering, Chongqing University, Chongqing 400044, China; [7]Institute for Energy Research, Jiangsu University, Zhenjiang 212013, China; [8]Institute of New Energy Technology, Department of Electronic Engineering, College of Information Science and Technology, Jinan University, Guangzhou 510631, China; [9]Institute of Functional Nano & Soft Materials (FUNSOM), Soochow University, Suzhou 215123, China; [10]Department of Materials Science and Engineering, Southern University of Science and Technology, Shenzhen 518055, China; [11]College of Optoelectronic Engineering, Chongqing University, Chongqing 400044, China; [12]College of Chemistry, Nankai University, Tianjin 300071, China; [13]Institute of Chemistry, Chinese Academy of Sciences, Beijing 100190, China; [14]State Key Lab for Mesoscopic Physics and Frontiers Science Center for Nano-optoelectronics, School of Physics, Peking University, Beijing 100871, China; [15]State Key Laboratory of Advanced Technology for Materials Synthesis and Processing, Wuhan University of Technology, Wuhan 430070, China; [16]School of Materials and Energy, University of Electronic Science and Technology of China, Chengdu 611731, China; [17]Institute of Photoelectronic Thin Film Devices and Technology, Nankai University, Tianjin 300350, China; [18]School of Materials Science and Engineering, Shaanxi Normal University, Xi'an 710119, China
Address correspondence to Ming Cheng, mingcheng@ujs.edu.cn; Kuan Sun, kuan.sun@cqu.edu.cn; Dewei Zhao, dewei.zhao@scu.edu.cn; Yixin Zhao, yixin.zhao@sjtu.edu.cn; Shihe Yang, chsyang@pku.edu.cn; Chenyi Yi, yicy@mail.tsinghua.edu.cn; Liming Ding, ding@nanoctr.cn

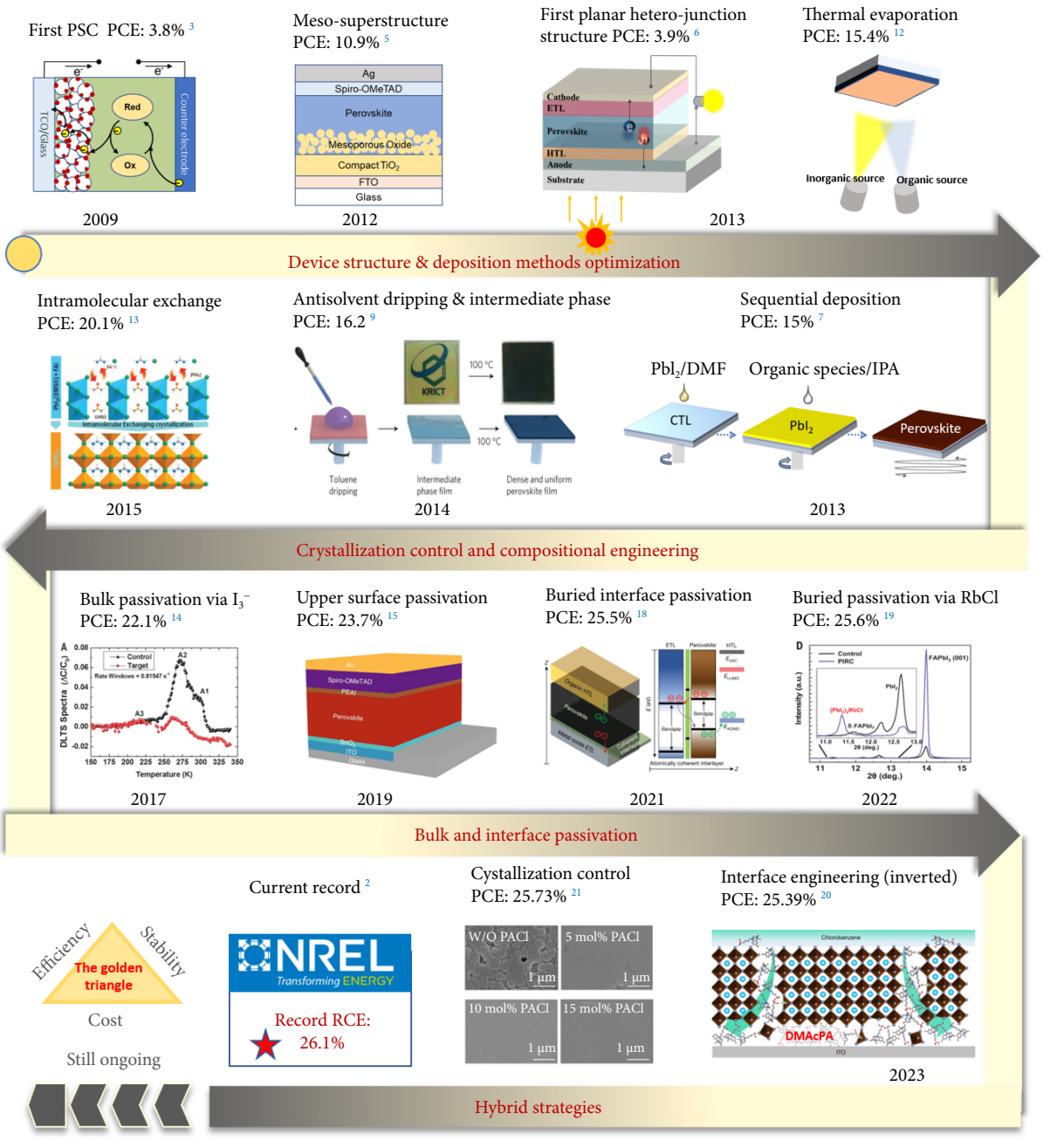

Fig. 1 The milestone works in the efficiency enhancement history of PSCs (reprinted with permission from Ref. [9], © 2014 Macmillan Publishers Limited. All rights reserved; Ref. [13], © 2015, American Association for the Advancement of Science; Ref. [14], © 2017 The Authors, some rights reserved; exclusive licensee American Association for the Advancement of Science. No claim to original U.S. Government Works; Ref. [15], © The Author(s), under exclusive licence to Springer Nature Limited 2019; Ref. [18], © The Author(s), under exclusive licence to Spring; Ref. [19], © 2022 The Authors, some rights reserved; exclusive licensee American Association for the Advancement of Science. No claim to original U.S. Government Works; Ref. [20], © The Author(s), under exclusive licence to Spring 2023; Ref. [21], © © The Author(s), under exclusive licence to Spring 2023).

process of perovskite, e.g., sequential deposition[7], antisolvent dripping[8], intermediate phase[9, 10], solvent annealing[11], etc. Snaith's group developed dual-source thermal evaporation method to deposit planar-heterojunction PSCs and raised the PCE to 15.4% in 2013[12]. In 2014, the construction of intermediate phase in the antisolvent dripping process through the addition of dimethylsulphoxide (DMSO) effectively retarded the crystallization process, yielding uniform and dense film with a PCE of 16.2%[9]. Through composition engineering and intramolecular exchange, the PCE of formamidinium lead iodide ($FAPbI_3$)-based PSCs passed the 20% watershed in 2015 by Seok and his collegues[13].

Subsequent performance enhancement was mainly enabled by charge transport material design and passivation. The solution-processed perovskite films will inevitably involve large amount of defect, which can act as non-radiative recombination centers, induce ion migration and impede charge transport. Up to now, various charge transport modification and passivation strategies to reduce defects at grain boundary, top and buried interface have been proposed, which greatly enhance the performance of PSCs. Excess PbI_2, halide or pseudo halide anions, alkylammonium halogen, Lewis acid and base are proved to be effective passivators, which motivates the further efficiency improvement. In 2017, by

adding extra triiodide ions during two-step deposition process of $FAPbI_3$, the deep-level traps were effectively reduced and a certified PCE of 22.1% was achieved[14]. In 2019, You's group used phenethylammonium iodide (PEAI) to passivate the upper surface of perovskite film, further increasing the efficiency to 23.7%[15], the analogues of which were widely adopted to form 2D capping layer for passivation in the latest high-efficiency works[16, 17]. In 2021, Seok's group. further raised the PCE to 25.5% by passivating the defects at buried interface[18]. You's group found out that the excess PbI_2 could benefit the photovoltaic performance but undermine the long-term stability of perovskite solar cells. They utilized RbCl additive to convert the excess PbI_2 during sequential deposition into an inactive $(PbI_2)_2RbCl$ compound and enabled a 25.6% certified PCE with high stability[19]. Noticeably, PSCs with inverted configuration (p-i-n) have made great progress these days through charge transport layer and interface engineering. He's group utilized dimethylacridine-based molecular doped in perovskite precursor to construct a well-matched *p*-perovskite/ITO contact, together with all-round grain boundaries passivation, yielding a certified PCE of 25.39%[20]. Nowadays, the reported efficiency of regular (n-i-p) PSCs has reached 25.7%, enabled by the high-quality film derived from alkylammonium chlorides (RACl) controlled crystallization[21].

Further improvement of performance for single-junction PSCs will be hard since it has approached the Shockley–Queisser (SQ) limit. Constructing tandem cells is an effective way to break the SQ limit. Notably, all-perovskite tandem solar cells have achieved 28% PCE for 0.049 cm^2, surpassing the record efficiency for single-junction single-crystal silicon solar cells (26.8%)[22]. Recently, a breakthrough has been made for perovskite-Si tandem solar cells, in which an impressive PCE of 33.7% was achieved by researchers in King Abdullah University of Science and Technology[2]. Since Si solar cell still occupies the mainstream market (over 90%), combining perovskite with the already mature manufacturing process flow of Si solar cells could be a plausible way for it to step into the efficiency and cost-driven photovoltaic market.

In this review, the driving force behind the fast performance enhancement of PSCs since beginning is analysed and summarized, which mainly involves deposition process optimization, compositional engineering, additive engineering, crystallization manipulation, charge transport materials, interfacial engineering, optical coupling effect and constructing tandem solar cells. Furthermore, the remaining challenges and promising directions for some strategies are also provided. This review aims to provide an empirical guidance to the development of PSCs and stimulate further research activity towards the goal of fabricating efficient and stable perovskite solar cells for commercial use.

1 Typical deposition methods of perovskite films

1.1 Solution-based deposition methods

The film morphology of the light-absorbing layer in perovskite solar cells has a direct impact on the optoelectronic properties of the film, including light absorption, carrier diffusion and recombination, which dominates the photovoltaic parameters. The morphology of perovskite films, including surface coverage, flatness, thickness and grain distribution, is highly dependent on the preparation processes[23]. A variety of fabrication technologies have been developed, among which the solution-based deposition method is the current mainstream method[24]. The solution process refers to dissolving the precursor components of perovskite into a suitable solvent in advance, then depositing the precursor solution on the substrate by means of spin coating, drop coating, blade coating, spraying or inkjet printing, and finally crystallizing into a film after annealing to remove the solvent. The commonly used deposition methods for perovskite solar cells are summarized in Figure 2.

1.1.1 One-step spin-coating

The one-step spin-coating method, also called the one-pot method, was once the most commonly used method to prepare perovskite films due to its simplicity. In this method, lead salts and organic ammonium salts are dissolved together in polar solvents (including dimethylformamide (DMF), dimethyl sulfoxide (DMSO) and γ-butyrolactone (GBL)) to form a precursor solution, which is then spin-coated in a single pass to form a film[25]. Due to the high boiling point and poor volatility of such polar solvents, the formed perovskite film suffers from serious agglomeration[26]. To improve the morphology, a series of measures, including adjusting the composition ratio, replacing the solvent, optimizing the intermediate phase and introducing anti-solvent, were proposed by the researchers.

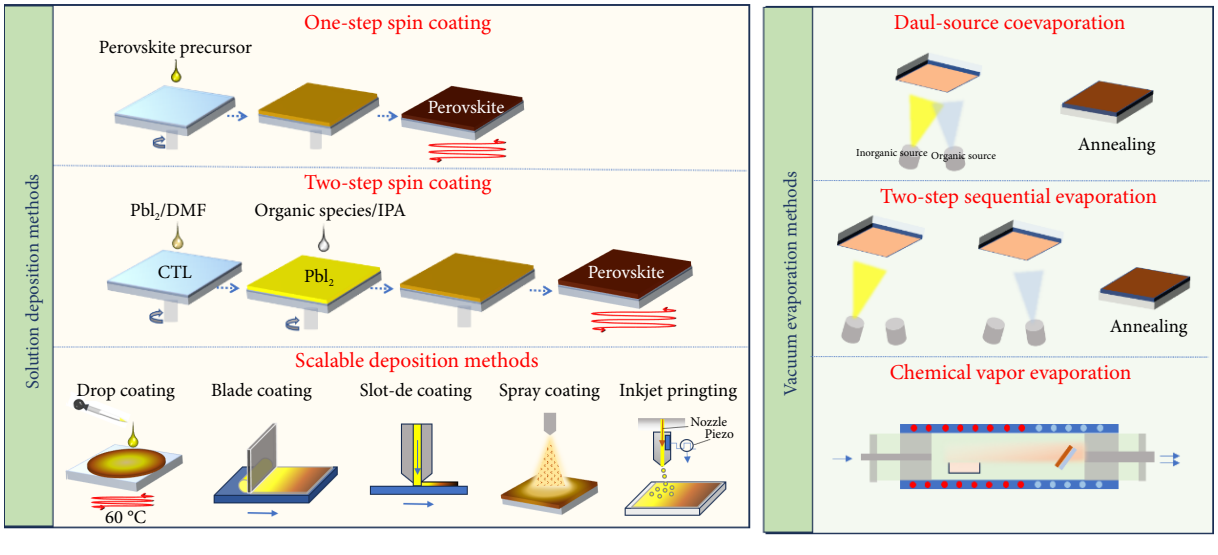

Fig. 2 Summary of commonly used deposition methods for perovskite solar cells.

Anti-solvent engineering is a milestone in the development of a one-step method. The anti-solvent is added dropwise during spin-coating of the precursor solution. Anti-solvent is miscible with the host solvent without dissolving the perovskite, which can induce rapid supersaturation and manipulate the crystallization process of perovskite[27]. The fast speed of supersaturation induced by anti-solvent splashing makes the nucleation rate greater than the crystal growth rate, leading to rapid crystallization to form a dense film. In 2014, Seok's group introduced toluene as an anti-solvent for the first time to obtain a flat and dense perovskite film. The perovskite device obtained by this method showed a remarkable efficiency of 16.2% with no hysteresis. Since then, anti-solvent engineering has become indispensable in one-step methods. After a detailed classification of more than a dozen common anti-solvents, Taylor et al. proposed a universal method to prepare high-quality films by optimizing the time window[28].

Intermediate phase engineering is another important mean to improve the quality of crystallization[29]. The one-step deposition process of films can be roughly divided into three parts: precursor solution, intermediate phase and crystal growth. Due to the robust coordination ability, the lead salts, organic ammonium salts and polar solvents in the precursor solution could constitute a solid intermediate phase. DMSO was introduced into the DMF solvent system because of the easier formation of a stable intermediate phase with PbI_2. By adding N-methyl-2-pyrrolidone (NMP) to the precursor solution to regulate the intermediate phase, Bu et al. fabricated high-performance perovskite solar cells without using anti-solvent in ambient air[30] PbI_2 preferentially combined with NMP rather than DMF to form stable adducts, which greatly suppressed the formation of δ-phase perovskite Figure 3(a). PbI_2•NMP served as a template to react with FAI/CsI in situ, thereby transforming into the needy α-phase perovskite. The above method could also be further extended to the preparation of large-area devices.

1.1.2 *Two-step spin-coating*

The two-step method was first introduced in perovskite by Grätzel's group which split the spin-coating process into two

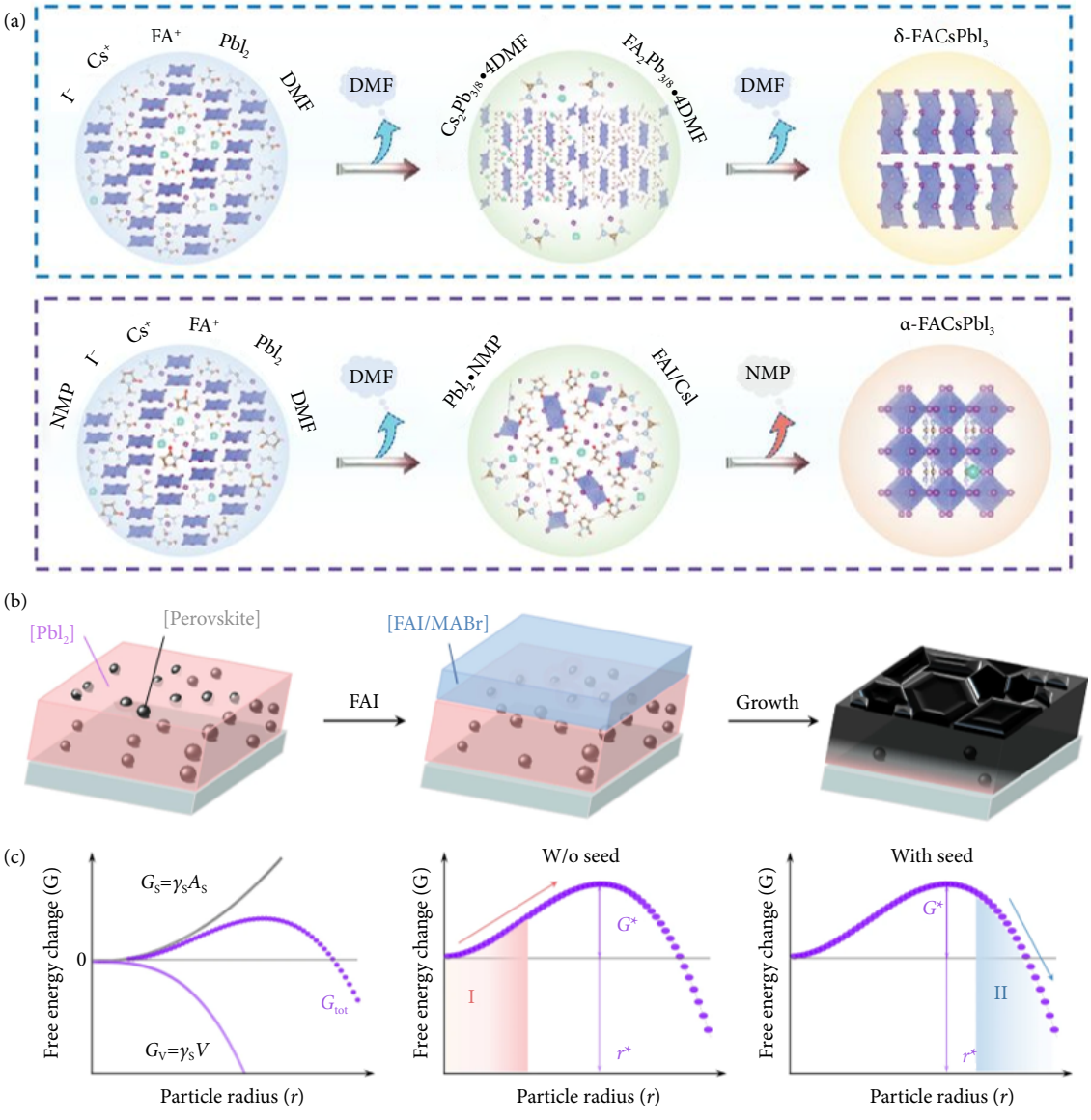

Fig. 3 **(a)** Schematic diagram of crystal growth for the formation of $FAPbI_3$ perovskites with or without NMP (reprinted with permission from Ref. [30], © 2021 The Authors, some rights reserved; exclusive licensee American Association for the Advancement of Science. No claim to original U.S. Government Works). **(b)** Procedure of perovskite seeding growth method. **(c)** Growth dynamics of the seed-assisted growth method. Reproduced with permission from Ref. [34], © The Author(s) 2018.

steps[7]. In this method, lead salts and organic ammonium salts are dissolved in different solvents, and the PbI_2 layer and organic amine salt components are spin-coated successively. Benefiting from the layered loose structure, PbI_2 and organic ammonium salts can be transformed into dense perovskite films through solid-liquid diffusion reactions[31]. The alcoholic solvent of the organic ammonium salts is dried immediately after being dropped, so thermal annealing is crucial for crystallization[32]. Owing to better experimental operability and repeatability, the two-step method has gradually gained the favor of researchers. For the two-step method, substantial works have concentrated on the regulation of components in the precursor solution and the annealing conditions. For instance, Park's group revealed the effect of organic ammonium salt concentration on grain size, obtaining a PCE of 17%[33]. Recently, You's group added RbCl to the lead salt precursor to convert PbI_2 into an inactive $(PbI_2)_2RbCl$ compound, which stabilized the perovskite phase and yielded the currently highest certified PCE of 25.6% for $FAPbI_3$ perovskite solar cells via two-step methods[19].

Inspired by epitaxial growth in silicon solar cells, Zhao's group proposed a seed-assisted growth method to further improve the film quality of the two-step method[34]. Different from spontaneous growth in the traditional method, they introduced submicron perovskite seeds in PbI_2 precursor solution as nuclei to induce subsequent growth of perovskite from bottom to top Figure 3(b). The seeded region and the unseeded region exhibited two distinct growth kinetics modes. Obviously, the seed-assisted growth mode was significantly faster than the random nucleation growth, occupying the dominant position. In fact, spontaneous crystallization consists of two stages, nucleation and growth, bounded by the critical radius r^*. The growth stage can only proceed when the nucleus radius exceeds the critical radius r^*. With the help of the ready-made nucleus provided by perovskite seeds, the crystal growth of perovskite can easily overcome the Gibbs free energy barrier and commence directly from the seeds Figure 3(c). As a result, a highly crystalline perovskite film with significantly reduced grain boundaries will be obtained. Therefore, the perovskite solar cells based on the seed-assisted growth method achieved a PCE of 21.5% and better operating stability (60% of the initial PCE after 140 h). Later, Li et al. developed CsCl-enhanced perovskite seeds with bromide-rich composition through halogen engineering and component regulation, which further expanded the grain size to 1.5 μm with more vertical cylindrical grains[35,36].

The seed-assisted growth method provides a new path for modulating crystallization dynamics, grains dimensions and perovskite composition. On this basis, researchers have successively devised many different types of perovskite seeds. For example, different from other types, all-inorganic perovskite seeds ($CsPbBr_3$ and $RbPbI_3$, etc.) can be used not only as nucleation sites but also as a stabilizer for the $FAPbI_3$ black phase[37,38]. In addition, the 2D perovskite seeds were found to endow the PbI_2 film with a mesoporous structure, facilitating the penetration of organic salts[39]. Recently, Shen et al. realized array-distributed perovskite crystallites on a substrate through a polydimethylsiloxane (PDMS) template, which greatly improved the controllability of the growth of the perovskite light-absorbing layer[40]. Another role of seed-assisted growth is to tailor the facet orientation. The carrier lifetimes, defect types and densities of perovskite films with different crystal facet orientations are quite different[41]. Usually, perovskite film with preferred facet orientation showed favorable photovoltaic performance in solar cell devices. Recently, Luo et al. selected highly oriented low-dimensional perovskites as seeds to induce the growth of 3D perovskites, thereby obtaining the desired crystal plane orientation and stacking mode[42]. The selected Dion–Jacobson (DJ) phase perovskite crystal grew along the (00L) crystal direction; thus, the 3D perovskite grew from this template epitaxially presented a preferred orientation in the (00L) direction. As a result, the obtained perovskite films exhibited excellent crystal quality. More interestingly, the low-dimensional perovskite seeds diffused to the grain boundaries of 3D perovskite, forming a type-I band structure to passivate defects. This novel approach enabled dramatic performance improvements in perovskite photovoltaic devices, with a PCE of 23.95% and an FF of 0.847.

1.1.3 Other solution-based methods

Spin-coating is the mainstream method for laboratory fabrication of high-efficiency perovskite solar cells, but unfortunately, it is not suitable for large-scale industrial production due to inhomogeneity of scale-up and waste of raw materials[43]. To adapt to large-scale production, many new manufacturing processes have been developed. The drop-coating method was developed for large-area devices owing to the facile procedure[44]. However, when the substrate area is larger than 100 cm^2, it is powerless for this method to guarantee the uniformity of the film. Spraying-coating and inkjet printing were applied to the preparation of perovskite films as early as 2014, but the difficulty of thickness control and crystallization speed hinder their further development[45,46]. In contrast to the above methods, meniscus coating is a new technology with high material utilization and compatibility with roll-to-roll production lines[46]. According to whether the blade is in contact with the substrate, it can be divided into blade coating and slot-die coating[43]. Benefiting from the precise adjustment of the moving speed and distance of the blade, the efficiency of large-area devices obtained by meniscus coating has exceeded 20%[30]. The advantages and disadvantages of different preparation processes are compared in Table 1[18,43,47–57].

1.2 Vacuum evaporation methods

Although most of the reported high-efficiency PSCs were fabricated by solution-based methods, the solution-processed PSCs still face several formidable challenges to meet the requirements of future commercialization[58]. The first key issue is the uniformity limitation of the spin-coating method. Most of the high-PCE devices were achieved on small-area devices via spin-coating, while the uniformity and homogeneity of the perovskite film may be deteriorated on large-scale substrates. Furthermore, the remaining solvent may damage the underlying layers (e.g., hole transport layer (HTL) in p-i-n PSCs), undermining the device performance and long-term stability. Moreover, the soluble lead used in the solution method (e.g., PbI_2-DMSO complexes) has the risk of contaminating the soil and groundwater. In addition, the solvent used, usually with high purity, is rather expensive, costly and time-consuming and is difficult to recycle. Last, it remains difficult to fabricate tandem solar cells on textured silicon cells with a solution-based method.

Decades of practices in PV technologies like CIGS, CdTe, Ⅲ-Ⅴ and HJT silicon solar cells have shown the preference for vacuum-based technologies in industrial production due to superior uniformity, conformality and reproducibility in large scale while fabricating thin films (~1 um or less thickness)[59]. The vacuum evaporation procedure is usually performed in a vacuum chamber, and no solvent is used during the process, eliminating the risk of environmental pollution caused by the lead halide and saving the solvent cost. Furthermore, the film thickness can be precisely controlled by monitoring the deposition rate with a quartz crystal

Table 1 Comparison of commonly used fabrication technologies for perovskite films

Method	Strength	Weakness	Highest PCE
One-step spin-coating	Facile and easy to operate.	The uniformity of perovskite films decreases sharply with increasing area; massive raw materials are wasted.	25.8% (0.1 cm^2)[18]
Two-step spin-coating	Excellent experimental operability and repeatability.		25.03% (0.08 cm^2)[51]
Drop-coating	The experimental process is the easiest and can resist high humidity.	The experimental conditions are not easy to control and difficult to repeat.	21.08% (0.04 cm^2)[52]
Spraying-coating	Suitable for low cost, high volume, and rapid manufacturing.	Difficult to control film thickness and quality.	19.4% (0.025 cm^2)[53]
Inkjet-printing	Easy to print specific preset patterns.	There are special requirements for the annual perovskite ink; lack of a suitable printer.	22.1% (0.16 cm^2)[54]
Blade-coating	The structure of the equipment is simple and the utilization rate of materials is high.	Squeegee may cause contamination.	23.19% (0.04 cm^2)[55]
Slot-die coating	The coating is noncontact, and the ink will not splash; the film formation uniformity is good.	Difficult to achieve patterned coating.	22.7% (0.09 cm^2)[56]
Solution-vapor combination	The vacuum deposition of FAI produces a homogeneous FAI film.	Solution processed PbI_2 is inhomogeneous and is unfavorable for large-scale devices.	24.1% (0.1 cm^2)[48]
Dual-source evaporation	Dual-source evaporation can fabricate highly uniform perovskite layer in a single process.	The evaporation rate and thickness of each precursor cannot be decided. Mutual interference between FAI and PbI_2 may exist.	20.28% (0.16 cm^2)[47]
Sequential evaporation	Both the evaporation rate of the lead halide and the ammonium salt can be monitored.	More expensive instruments needed.	24.42% (0.1 cm^2)[49]
Chemical vapor deposition	Chemical vapor deposition can produce high-quality perovskite film with over an area of m^2 scale.	Unsuitable for depositing lead halide layer. The related parameters are complex and need to be carefully controlled.	15.5% (0.1 cm^2)[50]

microbalance (QCM), and the evaporated precursors can be uniformly and evenly deposited onto the rotating substrate, which is conducive to large-scale industrial fabrication[60]. Three main technical routines have been developed: co-evaporation, two-step sequential routine and chemical vapor deposition[61–66] among which the former two are commonly used and their schematics and development timeline are shown in Figures 4(a) and 4(b). Co-evaporation and two-step sequential routine are all based on thermal evaporation, which belongs to physical vapor deposition. The reactants are either simultaneously or sequentially evaporated onto the substrate and react in-situly to produce perovskite layer. While chemical vapor deposition (CVD) utilizes gas-state precursors to deposit perovskite layers through chemical reactions. CVD is commonly carried out in a tube furnace, which contains a high-temperature region for material sublimation, and low-temperature region for precursor deposition.

1.2.1 Dual-source coevaporation

To date, many efforts have been made to fabricate PSCs using the vacuum thermal evaporation method. Nevertheless, the PCE of evaporated PSCs still lags behind that of the solution-based method. The dual-source coevaporation method is first explored and demonstrates the uniformity of the vacuum thermal evaporation method. Early in 2013, Liu's group first proposed the coevaporation of $PbCl_2$ and MAI to fabricate $MAPbI_{3-x}Cl_x$ and achieved a PCE of 15.4%[12]. In 2017, Bolink's group developed multi-sources (3 and 4) vapor deposition technologies and succeeded a best PCE of 16% based on the multi-cation perovskite materials[67]. Meanwhile, the crystal growth mechanisms of multi-cation perovskite films and the interface defects between perovskite and charge transport layers under co-evaporation have also been noticed as main factors to further push the performance of PSCs. In 2020, Bruno's group coevaporated MAI and PbI_2 and reached a PCE as high as 20.28%. Albrecht et al. in 2021[68] and Johnston et al. in 2022[69] reported their champion devices under three- and four-sources vapor deposition with PCEs of 20.4% and 19.3%, respectively, by carefully controlling the process of perovskite crystal growth. At present, PSCs based on the co-evaporated perovskite films have a record efficiency of 20.6%, which was reported by Bruno's Group on the year of 2021[70] and Albrecht's Group on the year of 2020[71].

Although the dual-source coevaporation process can fabricate PSCs with good uniformity, it still has several drawbacks. First, the much higher vapor pressure of the ammonium salt compared with that of lead halide makes it difficult to simultaneously evaporate both precursors with a stable evaporation rate. The temperature of the crucible for evaporating lead halide is much higher than that for ammonium salt, which can significantly change the pressure of ammonium molecules in the chamber, making evaporation difficult to control. In addition, it is difficult to identify the exact evaporation rate of the lead halide and ammonium salt with a single QCM. Last, it is found that a minor amount of the ammonium salt may remain in the chamber after evaporation, which may affect the subsequent evaporation process and reduce the batch-to-batch reproducibility.

1.2.2 Two-step sequential routine

A typical sequential routine consists of two steps: inorganic precursors (PbX_2 and CsX) were firstly evaporated, then inorganic precursors reacted with such organic vapor (FAX, MAX and/or mixtures) to form perovskite films. Compared with the dual-source coevaporation method, the two-step sequential evaporation method avoids the risk of mutual interference by evaporating precursors separately. Both the evaporation rate of the lead halide and the ammonium salt can be monitored by the QCM, and thus the film thickness of each layer can be controlled precisely[72]. This technology was first reported by Lin's group in 2014[73]. In this initial attempt, $MAPbI_3$ PSCs received an efficiency of 15.4%. Soon after that, in 2016 the same group improved the PCE of $MAPbI_3$ PSCs to 17.6%[74], and revealed that extremely high vacuum degree, e.g., ~10^{-2} Pa, was not necessary for high-efficiency devices. This implies that vacuum-based PSCs are affordable to the industry because expensive high vacuum equipment is not inevitable. In 2018, Tong et al. applied defect passivation strategies to enhance

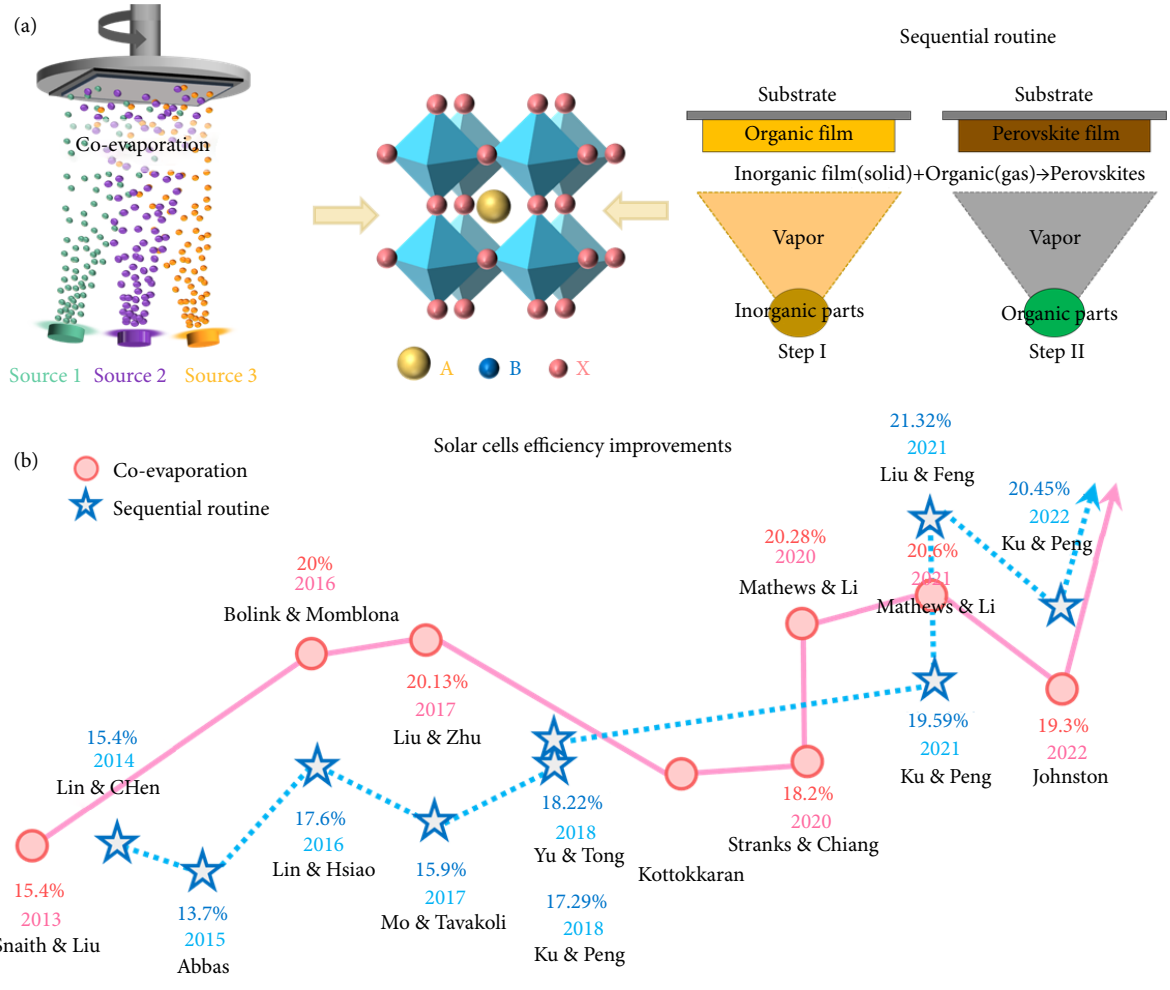

Fig. 4 Vacuum fabrication for perovskite solar cells. (a) Schematic diagram of fabricating perovskite films through co-evaporation method and Sequential routine. **(b)** Solar cells efficiency timeline for the PSCs based on co-evaporation method and Sequential routine.

the PCE up to18.2%[75]. In 2021, Ku's and Peng's group. optimized their interphase-related defects passivation strategies and reported a PCE of 20.45%[76–78]. Up-to-date, the champion PCE for all-vacuum-processed PSC is 21.32%, which was reported by Feng et al. in 2021[72]. Recently, Zhang et al. combined single-source evaporation of FAI and spin-coating of lead halide to fabricate MA-free PSCs[48], which achieved a PCE of 24.1% (certified 23.9%) and 22.8% for 0.1 cm^2 and 1 cm^2 Cs-FA-based devices, respectively. They demonstrated the uniformity of the vacuum-deposited FAI layer and obtained the highest reported PCE of MA-free devices with good stability. Li's group proposed a Cl-containing alloy-mediated sequential vacuum thermal evaporation approach and systematically studied the crystallization process of evaporated PSCs[49]. They coevaporated $PbCl_2$, PbI_2 and CsI to form the Cl-alloyed film, on which a FAI layer was deposited. They demonstrated that the Cl-alloyed lead halide precursor film ($Cs_{0.05}PbI_{2.05-x}Cl_x$) exhibited better crystallinity and a stronger degree of preferential orientation. The resulting PSCs yielded PCEs of 24.42%, 23.44% (certified 22.6%) and 19.87% for 0.1 cm^2, 1 cm^2 and 14.4 cm^2 devices, respectively, which is the highest PCE of evaporated PSCs to date. The sequential vacuum evaporation method has proven its feasibility and industrial potential in fabricating PSCs and other photoelectronic devices.

1.2.3 Chemical vapor deposition

Chemical vapor deposition (CVD) has attracted increasing attention due to its film homogeneity and industrial compatibility. The CVD method can produce highly uniform layers with an area over 1 m^2, which has been demonstrated in the silicon photovoltaic industry. Different from the vacuum thermal evaporation method, CVD uses gas-state precursors to deposit perovskite films through chemical reactions[59]. In 2014, Qi's group first introduced hybrid chemical vapor deposition (HCVD) to fabricate PSCs[79]. A PCE of 11.8% with good stability was achieved. Recently, they demonstrated the upscaling ability of the HCVD method[80]. They deposited a C_{60} interlayer to avoid the damage to the sputtered SnO_2 (ETL) during the HCVD process and fabricated $Cs_{0.1}FA_{0.9}PbI_{2.9}Br_{0.1}$ PSCs with enhanced phase and thermal stabilities. They obtained more than 10% efficiency in a PSC module with a designed area of 91.8 cm^2. Nevertheless, most of the reported literature focused on the vapor deposition of ammonium salt, while the lead halide layer is still based on vacuum evaporation or solution-based methods due to the waste of material and the much higher temperature of the furnace in comparison with ammonium salt. Furthermore, the furnace pressure, flow rate of gas, heating temperature of the substrate, ammonium salt, and distance between the substrate and precursor need to be carefully controlled during the CVD process, increasing the complexity of the experiment[50]. In addition, it is difficult to deposit an ultrathin layer at the interface of the perovskite layer or charge transport layer by the CVD process for surface passivation or interface modification, which may potentially become a hazard toward fab-

ricating PSCs with high efficiency and good stability.

Challenges PCEs of vacuum-based PSCs are still lagging behind solution-based PSCs. One of the main challenges is that organic precursors sublimed but not evaporated slowly, resulting in complicated control of perovskite crystals and thereby forming large amount of defect in target perovskites. Although researchers have already realized the importance of passivating defects in vacuum-based perovskite films, only a few choices are available. Therefore, it is urgent for chemists and material researchers to inventing or developing materials adopting to vacuum technologies.

2 Compositional engineering of lead halide PSCs

2.1 Mainstream 3D perovskite materials

In the initial stage, 3D structured organic-inorganic hybrid perovskite materials $MAPbI_3$ and $MAPbBr_3$ were firstly utilized as light harvesting material in liquid-state solar cells by Miyasaka T., demonstrating a PCE of 3.81% with extremely poor stability[3]. Following that, Kim et al. reported the first full solid-state $MAPbI_3$-based PSC with impressive efficiency exceeding 9% and dramatically improved stability, which was recognized as the landmark breakthrough in PSCs field[4]. Since then, dramatic attentions have been paid to composition engineering of perovskite materials to further improve the photovoltaic performance.

One effective engineering strategy is anionic component regulation[9, 57–83]. Partly substituting I with Br or Cl ions can easily tune the bandgap and regulate the crystallization process of perovskite films. Especially, the introduction of Cl anion can extend the charge carrier lifetime and diffusion length, which is essential for restricting the charge recombination[12, 84]. The other strategy is the optimization of A-site cation. FA^+ and Cs^+ are the most frequently used A-site cations except MA^+[85]. Substituting the MA^+ with a slightly larger FA^+ decreases the bandgap, from which higher photo absorption and higher theoretical efficiency limit can be expected for FA-based perovskites[86]. However, $FAPbI_3$ suffers from poor crystallinity and phase instability, which limited the development progress of the corresponding PSCs at the starting stage[87, 88]. To tackle these issues, multiple cations and certain ratio of bromine anion were introduced to stabilize the black-phase $FAPbI_3$ (e.g., $FA_{1-x}MA_xPb(I_{1-y}Br_y)_3$ and $FA_{0.95-x}MA_xCs_{0.05}Pb(I_{1-y}Br_y)_3$) through reducing the Goldschmidt tolerance factor τ, which became the dominant compositions in highly-efficient PSCs at that time[13, 89,90]. However, the incorporation of MA^+ and Br^- comes at the cost of a blue-shifted absorption spectrum, limiting the further enhancement of J_{sc} and PCE. Moreover, MA erodes the thermal stability and Br induces phase segregation of relative compositions. Therefore, stabilizing α-$FAPbI_3$ while maintaining its inherent bandgap is highly desirable for highly-efficient and stable PSCs[91]. How to produce pure α-$FAPbI_3$ films with high film quality and high phase stability at room temperature become one of the research hotspots recently. Additive engineering of precursor solution is one of the most commonly used method to stabilize black phase $FAPbI_3$. Several reports proposed that adding slightly excess methylammonium chloride (MACl) or methylenediammonium dichloride ($MDACl_2$) can successfully stabilize the pure α-phase $FAPbI_3$, facilitate the crystallization and increase grain size of $FAPbI_3$ films, yielding a certified PCE of more than 23% for the resulting PSCs[91, 92]. Lu et al. used methylammonium thiocyanate (MASCN) vapor treatment to convert yellow δ-$FAPbI_3$ to the kinetically stable α-$FAPbI_3$. The vapor-treated α-$FAPbI_3$ PSCs achieved a PCE greater than 23% together with excellent long-term operational stability[93]. Jeong et al. introduced a pseudo-halide anion formate ($HCOO^-$) to reduce anion-vacancy defects in the $FAPbI_3$ perovskite films, which suppressed the non-radiative recombination of charge carriers[17]. With the improved crystallinity of the α-phase $FAPbI_3$ films, an impressive PCE of 25.6% (certified 25.2%) was obtained with a J_{sc} of 26.35 mA/cm^2, a V_{oc} of 1.189 V and *FF* of 81.7%.

2.2 3D/low-dimensional perovskite integrated light absorption layer

Even though the efficiency has been greatly improved, the long-term stabilities of 3D organic-inorganic hybrid perovskite materials mentioned above are still lagging far behind commercialization requirements. Constructing low-dimensional (LD) and all-inorganic $CsPbX_3$ compositions are adopted to enhance the stability. All-inorganic $CsPbX_3$ composition engineering will be discussed in the following sections. LD perovskites with 2D, 1D and 0D structures present superior moisture stability than 3D perovskites[94–96]. Besides, the incorporation of low-dimensional (LD) perovskites in 3D perovskites have the ability to reduce trap density and impede the ions migration no matter in the bulk or on the surface[97–99]. In this scenario, LD/3D hybrid perovskites might be one of the ideal candidates for solar cell commercialization.

The 2D perovskites are comprised of alternating organic spacer layers and inorganic frameworks. Most of the existing literature focused on 2D bulk incorporation, which incorporates single or multiple long carbon-chain organic ammoniums into precursor[100–102]. Snaith's group introduced n-butylammonium cations into a mixed-cation lead mixed-halide 3D perovskite. The 2D thin sheets were inserted into the highly orientated 3D perovskite grains, leading to the efficient suppression of non-radiative charge recombination. The solar cells with an optimal n-butylammonium content exhibited average stabilized PCE of 17.5 ± 1.3%[103]. The oriented growth of layered organic molecules inhibited the charge transfer in the vertical direction. Yuan et al. introduced the π-conjugated terpyridyl coordinated Cr^{3+} ion in perovskite precursor, enabling multi-interactive charge-carrier transport channels within 3D perovskites[104]. Recently, the surface treatment with 2D perovskite generally enables higher conversion efficiencies, which was attributed to the effective passivation of surface defects[99, 105]. Jang et al. grew a stable and highly crystalline 2D $(C_4H_9NH_3)_2PbI_4$ film on top of a 3D film using a solvent-free solid-phase in-plane growth method. The resulted 2D/3D PSCs achieved a certified steady-state efficiency of 24.35%, owing to an intact 2D/3D heterojunction with a thick 2D film. The encapsulated device retained 94% of its initial efficiency after 1056 h under the damp heat test (85 °C/85% relative humidity)[106]. At the interface of 3D/2D perovskite, a transition layer with $n > 1$ was formed. Tailoring the dimensionality (n) of the 2D perovskite fragments at the electron-selective interface of inverted PSCs by applying oleylammonium iodide (OLAI) was essential to enable efficient top-contact passivation. The resulting inverted PSCs delivered a 24.3% PCE and retained >95% of their initial value after >1000 hours at damp-heat test conditions, thereby meeting one of the critical industrial stability standards for PV modules[102].

While tremendous progress has been realized in 3D/2D perovskite research in recent years, the 1D/3D and 0D/3D perovskites remain relatively underexplored. In the case of 1D perovskites, $[MX_6]^{4-}$ octahedra are connected in chain through face-sharing, edge-sharing or corner-sharing formation and surrounded by

organic ammonia cations. Fan et al. obtained a series of 1D and 1D/3D hybrid perovskite materials. Based on the 1D/3D hybrid perovskite, the solar cells presented self-healing properties and long-term stability[107]. Likewise, Liu et al. made a 1D PbI_2-bipyridine (BPy) (II) perovskite, which was further utilized to prepare 1D–3D PSCs. The good lattice-matching blocked negative ion migration channel in 1D–3D heterojunction domains, accounting for the good stability[108]. Bi and coworkers employed 2-diethylaminoethylchloride hydrochloride (DEAECCl) to induce the formation of 1D/3D perovskite. The devices exhibited good stability under ambient air, 85 °C and illumination conditions[109]. However, the stability enhancement came at the cost of the device PCE, which was mainly due to the low carrier mobility of as-induced 1D perovskites. Building charge transport channel via organic groups with π–π conjugate structure is one of the effective methods to improve charge-transport properties in 1D perovskites. Fan, Li and coworkers introduced 5-aminoquinoline (Aq) and terpyridine (Tpy) as organic spacer with π–π conjugate structure to construct 1D perovskites. The electron mobility of 1D/3D hybrid perovskite was increased by nearly three orders of magnitude[110, 111]. Additionally, the residual strain release in the heterojunction is conducive to optimize the carrier transport of the low-dimensional perovskite. The *in-situ* cross-linkable polymerizable propargylammonium (PA^+) was introduced at the surfaces and grain boundaries to form a 1D/3D perovskite heterostructure, which could significantly improve the interfacial carrier transport in the perovskite films. Remarkably, the cross-linked 1D/3D perovskite solar cells achieved a champion PCE of 21.19%, which maintained 93% of their initial efficiency after 3055 h of continuous illumination under the maximum power point (MPP) operation conditions[112]. Perovskites with 0D structures at the molecular level are bulk assemblies of individual metal halide octahedral units. Li et al. realized 3D/0D $Cs_xFA_{1-x}PbI_3$–$[GaAA_3]_4$ ($0 < x < 1$) hybrid perovskites with core-shell grain structure, which remarkably enhanced the long-term stability of perovskite solar cells while remaining high efficiency[113]. Besides, the Cs_4PbI_6 and Cs_4PbBr_6 compounds with 0D structure can surround the black-phase perovskite grains to passivate the defects and stabilized the phase stability[114, 115].

In summary, compositional engineering plays a vital role in breaking the bottleneck of PSCs performance. α-phase $FAPbI_3$ composition is still the ideal choice for the record high-efficiency PSCs in the foreseeable future. Moreover, it is crucial to balance the trade-off between stability and efficiency through the construction of LD-3D perovskite structure.

3 Additive engineering

Additives play an important role in the development of perovskite solar cells. Unlike dopants, additives can't alloy into the crystal lattice of perovskites[116], but additives can affect the crystallization process and thereby affect the morphology, crystallinity and optoelectronic properties of the perovskite films. Various additives have been reported, such as chlorides, iodides, pseudo-halides, surfactants, ionic liquids, Lewis acids or bases and polymers. The reported additives can be divided into two types: volatile additive and incorporated additive (Figure 5). The main role of volatile additives is regulating the crystallization process of perovskite, thus improving crystallinity and film morphology. The incorporated additives have different functions depend on their chemical structure, such as defect passivation, suppressing ion migration, enlarging grain size, improving uniformity, releasing stress and stabilizing crystal structure. In this section, we introduce some representative additives for using in perovskite solar cells.

3.1 Volatile additives

Volatile additive doesn't exist in the final perovskite films, but it exists in some intermediate phases, thus affecting nucleation and crystal growth and resulting in perovskite films with improved morphology, crystallinity and photovoltaic performance. Chlorides are the earliest and most commonly used additives in solutions of perovskites. For the $MAPbI_3$ films made by one-step method without anti-solvent quenching, the solution without MACl additive will end up crystalizing into needle-like crystals[117]. The large

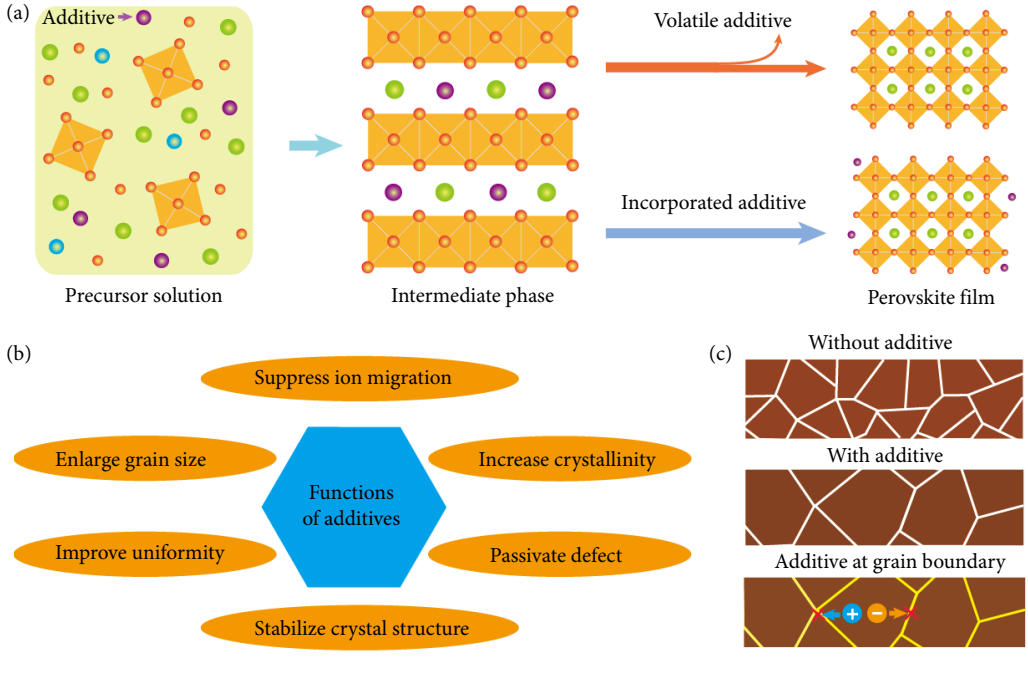

Fig. 5 **(a)** Illustration of volatile additive and incorporated additive. **(b)** Main functions of additives for perovskite films. **(c)** Illustration of perovskite films with enlarged grain size and suppressed ion migration.

voids among the needle-like crystals lead to insufficient light absorption and leakage of photocurrent, resulting in low device performance. By adding MACl into the $MAPbI_3$ solution, smooth and compact $MAPbI_3$ film with increased crystallinity and significantly enhanced PCE was achieved. No Cl^- can be detected in the final perovskite films, suggesting that MACl escaped from the film during crystallization and thermal annealing[117, 118]. TGA-MS measurement further confirms the sublimation of MACl during thermal annealing[118]. MACl were also used in FA-rich perovskites, enabling preparation of perovskite films without using anti-solvent[119]. Using NH_4Cl as additive results in similar effect but the crystallization speed is faster than the film with MACl, which may be due to that NH_4Cl is more volatile[120]. To date, almost all of the high-performance perovskite solar cells have incorporated chloride additives in the precursor solutions.

For the two-step deposition of perovskites, additives can be used in the first step (deposition of PbI_2) and/or the second step (deposition of ammonium salts). By adding MACl into PbI_2 solution, a porous PbI_2 film can be prepared after volatilization of MACl, which facilitates the reaction with MAI[121] MACl additive is also a commonly used additive for the second step, which facilitates the fabrication of the perovskite solar cells with the highest PCE that uses the two-step method[15,91].

Additives also play an important role in inorganic perovskite solar cells. Hydroiodic acid (HI) was found effective to improve film quality in some early works, but subsequent works showed that HI can react with DMF and produce a new compound of DMAI[122]. Then DMAI became a popular additive for the preparation of $CsPbI_3$-based perovskite solar cells. ToF-SIMS and nuclear magnetic resonance (NMR) results confirmed the absence of DMA^+ residue in final $CsPbI_3$ perovskite film, indicating that DMAI would not alloy into the crystal lattice of $CsPbI_3$ perovskite[123]. Both DMAI (volatile additive) and phenyltrimethylammonium iodide (PTAI) (incorporated additive) were used in the preparation of the state-of-the-art inorganic perovskite solar cells with a PCE of 21.0%[124]. Unlike DMAI, PTAI remains in the final perovskite film, forming low-dimensional perovskites with PbI_2, which enhances the phase stability of $CsPbI_3$ and suppresses non-radiative recombination.

3.2 Incorporated additives

The incorporated additive remains in the final perovskite film and plays the roles of defect passivation, inhibiting ion migration and stabilizing perovskites. Pseudo-halides, such as SCN^-, BH_4^- and $HCOO^-$, which show similar chemical properties with halides, can also be used as additives. Early works reported that SCN^- may substitute part of the I^- in perovskite lattice, but subsequent works showed that it forms a layered structure with Pb^{2+} and I^-[125]. Kim et al. found that pseudo-halide anion formate ($HCOO^-$) can suppress anion-vacancy defects at grain boundaries and on the surface of perovskite films[17]. Moreover, the crystallinity was augmented for the films with $HCOO^-$. A certified PCE of 25.2% was achieved for perovskite solar cells with $HCOO^-$ additive.

Potassium (K^+) containing additives were recently found effective to reduce hysteresis of perovskite solar cells. Stranks's group investigated the existence of potassium in perovskite films by using scanning transmission electron microscopy–energy dispersive X-ray spectroscopy (STEM–EDX), grazing-incidence wide-angle X-ray scattering (GIWAXS) and hard-X-ray photoelectron spectroscopy (HAXPES)[126]. They found a potassium-rich phase at the grain boundaries as well as at the interface. They concluded that potassium does not incorporate into the perovskite lattice, but plays a role of surface passivation, which enhances photoluminescence and reduces hysteresis of the perovskite solar cells. Huang's group used KPF_6 as additive for MA-free perovskite and achieved PCEs of 20.42% and 19.54% for 17.1 cm^2 and 65.0 cm^2 cells, respectively. Recently, a certified PCE of 25.5% was achieved for perovskite solar cells with KI additive and $MDACl_2$ dopant[18]. All these examples have proved the effectiveness of potassium on enhancing the photovoltaic performance of perovskite solar cells.

Ionic liquid is another type of frequently used additives. Bai et al. incorporated ionic liquid of $BMIMBF_4$ into perovskite film and achieved enhanced PCE with markedly improved long-term stability[127]. XRD measurement suggests that neither $[BMIM]^+$ nor $[BF_4]^-$ incorporates into the perovskite crystal lattice. ToF-SIMS measurement suggests that the $[BF_4]^-$ locates mainly at the perovskite/NiO interface, while the $[BMIM]^+$ exists throughout the film. Some ionic liquid can be used as solvent, such as methylamine formate (MAFa). When using MAFa as the solvent for PbI_2, the residual Fa^+ in PbI_2 precursor facilitates the reaction with MAI, resulting in improved film quality and device performance.

Surfactant additives can be used to improve the wettability of perovskite solution and the uniformity of perovskite films, especially for making large-area films on non-wetting surface. Huang's group added a small amount (tens of parts per million) of L-α-phosphatidylcholine (LP) into perovskite solution to alter the fluid drying dynamics and increase the adhesion of the perovskite ink to the underlying PTAA[128]. The additive enables the blading of smooth perovskite films at a high coating rate of 180 $m{\cdot}h^{-1}$. By adding carbohydrazide (CBH) into perovskite solution, the contact between perovskite and substrate interface can be improved. By combining CBH with a series of additives (n-dodecylammonium iodide, LP, MAH_2PO_2, and p-F-PEA), perovskite films with a PCE of 23.6% were made by blade-coating[129].

Polymers can be used as additives in both perovskite and charge transport layers. Bi et al. incorporated poly(methyl methacrylate) (PMMA) into the anti-solvent and found that PMMA can be a template for the nucleation and crystal growth of perovskite, resulting in larger grains and enhanced PCE[130]. Peng et al. used PMMA:PCBM as an ultrathin interface passivation layer in perovskite solar cells, achieving a fill factor of >86% and a PCE of 22.6% for a 1 cm^2 cell[131]. The most common ground for polymer additives is that almost all of their structures contain C=O or C-O, which can interact with PbI_2 in the precursor solution, thereby affecting the crystallization and passivating the defects in perovskite films. Polymer additives can also be used to improve the tolerance for humidity during film and device preparation, such as poly(ethylene oxide) (PEO) and polyvinylpyrrolidone (PVP)[44,132].

4 Crystallization control of perovskite films through precursor and anti-solvent engineering

Printing solar panels at a low cost and large scale has been a long-standing pursuit to secure a clean and sustainable future. This hope is recently fueled by the solution processability of halide perovskites, which have become the driving force for the burgeoning perovskite solar cell technology. To unleash the commercial potential of the technology, it is of paramount importance to control perovskite crystallization from solution and minimize defects that may compromise optoelectronic performance of the perovskite. Currently, the widely used solvents for dissolving the reagents, viz. lead halide and amine halide, are the aprotic polar solvents by virtue of their amenability to form Lewis acid-base adducts with the reagent ions. Naturally, the control of crystallization can be divided into intrinsic adjustment of perovskite precursor solution and extrinsic adjustment of anti-solvent, perhaps in conjunction

with other auxiliary operations.

4.1 Precursor engineering

Three prime factors for processing a perovskite film need to be considered while preparing the perovskite precursor solution, namely the components of perovskite, thickness of the perovskite film and the anti-solvent dripping window. In order to obtain a compact precursor film, adjustment of precursor solvents will be the first measure coming to mind. Indeed, the solvent engineering pioneered the early development of perovskite solar cells[133–135]. The upshot was the consensus on utilizing mixed solvent dimethylformamide (DMF) and dimethyl sulfoxide (DMSO) for processing perovskite solar cells (PSCs), and the DMF/DMSO ratio has basically remained unchanged along the way. In a nutshell, the hallmark of a good precursor solvent is its ability to optimize the anti-solvent dripping window, perovskite grain size and film thickness, which conduces to the quality of perovskite films and efficiency of PSCs.

Next, the ratio of reagents has important influences on the crystallization processes, such as the anti-solvent dripping, the formation of intermediate phases and the process of annealing. To fabricate perovskite with the ABX_3 structure, one would naturally start with equimolar amount of AX and BX_2, where A denotes methylamine (MA), formamidine (FA) or cesium (Cs); B denotes lead (Pb) or tin (Sn); X denotes halogen. However, it turned out that high-efficiency PSCs are difficult to obtain with the use of stoichiometric reagents and in the absence of anti-solvent dripping. The actual situation of perovskite crystallization is more complicated due to a tangled interplay among solution supersaturation, solvent evaporation during coating, intermediate formation, aging and annealing, perovskite phase transition, etc. Zhao et al. reported the positive influence of methylamine hydrochloride (MACl) on the perovskite film in 2014 by regulating crystallization and significantly improving the PSC efficiency. In 2015, Yan et al. studied the colloidal chemistry of perovskite precursor solution and exploited the strategy of excess AX to greatly improve the coverage and quality of perovskite films, reaping a PSC efficiency of over 17% even without anti-solvent dripping[136]. The need for excess AX is posed by the tendency of the precursor solution to form AX-lacking intermediates such as PbI_2•2DMSO, Pb_2I_4•2DMSO and $MA_2Pb_3I_8$•2DMSO, which can be smoothly transformed to high-quality $MAPbI_3$ films only when the MAI supply is sufficient[137]. Among the various AX, MACl in excess is especially helpful for the fabrication of a suite of perovskites with different compositions, primarily because it is relatively volatile and thus can be easily removed from the film during annealing at a later stage of the crystallization[137–139]. Besides, MACl not only improves the crystal quality of perovskite films but also assists the phase transformation of δ-$FAPbI_3$ to α-$FAPbI_3$[140, 141], making it applicable to the fabrication of FA-based perovskites.

Now using excess ammonium halide has become a time-proven strategy to fabricate high-quality perovskite films. Interestingly, this strategy can be extended to other A cations to fabricate high-quality films of mixed cation perovskites, even the inorganic perovskite[142] and the Pb-free perovskite $FASnI_3$[143]. For example, the incorporation of excess CsI could stabilize the $CsPbI_2Br$ phase by reducing the surface Gibbs free energy, forming peculiar microphase-separated perovskite films[142]. The incorporation of additional halide piperazine dihydriodide (PDI_2) could tune the crystallization kinetics of precursor solution and reduce the energy barrier of nucleation in the fabrication of $FASnI_3$[143]. In practice, one needs to consider how much excess AX is required to fabricated a desirable perovskite film. If AX can be removed during annealing or excess AX can play useful roles in the target film, the precursor solution can allow AX to exceed the stoichiometric ratio by a larger margin. However, if AX cannot be removed during annealing or excess AX can only do harm to optoelectronic performance of the perovskite film, the precursor solution then needs to be prepared to limit the excess AX.

For large-scale perovskite fabrication in the future, the excess AX strategy could be the most potential path to expand the solution-processed method. It can effectively restrain the phase segregation that is adverse to photovoltaic performance, and simultaneously optimize the perovskite crystallization. In particular, the excess AX strategy opens many possibilities for the fabrication of perovskites to couple with more scalable fabrication methodologies and machineries. Although the protocols and technical details may alter during upscaling, the basic principles still apply. Taken together, precursor engineering, e.g., with the excess of AX, will have major impacts on the development of perovskite optoelectronics.

4.2 anti-solvent engineering

anti-solvent method is a standard trick for growing single crystals by introducing the anti-solvent into a miscible solvent that contains the dissolved precursor. It was adapted to the spin-coating fabrication of perovskite films, and the most general implementation of this method is through anti-solvent dripping during the high-speed spin-coating of the precursor solution. The anti-solvent can partly remove the solvent from the liquid film with the help of the centrifugal force. During the anti-solvent dripping, the elevated supersaturation results in rapid nucleation and crystallization, forming a compact precursor film. Since the pioneering introduction of the anti-solvent dripping method in 2014[144], researchers have been able to fabricate high-quality perovskite films in a simple way, which brought laboratory-scale PSCs into the racing stage of efficiency record. As such, anti-solvent dripping has become the most popular fabrication method in the research laboratories worldwide. However, with the increasing urgency of scaling-up production, the limitations of anti-solvent dripping have increasingly come to attention. First, anti-solvent dripping is faced with difficulties in operation and repeatability. The dripping operation seriously relies on skills of the operators, so it has proved difficult to repeat the high-efficiency PSCs even when fabricated using the same formulation but in a different environment with a different machine. Second, when anti-solvent dripping is applied to the fabrication of large-area perovskite films, these difficulties of operation will multiply.

To solve these problems, it is necessary to analyze and control the crucial operating parameters in the anti-solvent dripping process. The effectiveness of anti-solvent dripping largely depends on the intrinsic properties of the anti-solvent and the composition of perovskite precursor solution. The selection criteria of anti-solvent include toxicity, polarity, boiling point, dipole moment, miscibility, etc. In actual experiments, the operator needs to judge the anti-solvent dripping window, which is commonly taken as a performance metric of a given anti-solvent. First of all, the dripping quantity and dripping rate will influence the resulting precursor film, which is composed of the Lewis acid-base adducts and a certain amount of solvents, and will be completely transformed into a perovskite film only after annealing. When the dripping quantity is insufficient, the supersaturation will be too low to achieve rapid crystallization. On the other hand, when the dripping rate is too fast, the dwell time of dripping will be too short to reach adequate

supersaturation in a typical spin-coating process. Second, the judgement of anti-solvent dripping window is also influenced by other factors, such as the time point, position and direction of dripping, even the operator per se. Note that the judgement of anti-solvent dripping window is often based on visual inspection of film quality, PSC efficiency measurements or other characterizations, which are either rough or time-consuming. In order to obtain a compact precursor film, a balance need to be struck between coordination and crystallization. Precursor solvent is required to have an appropriate coordination ability, and if too low, the negative influences from anti-solvent dripping will dominate, but if too high, the formed perovskite will react with the solvent. Meanwhile, anti-solvent is required to have an appropriate miscibility with the precursor solvent. Enhancing extraction ability of the anti-solvent can guarantee a rapid crystallization, but too strong extraction may lead to precipitation of PbI_2. The relation between coordination and crystallization with respect to the performance metrics of precursor solvent and anti-solvent need to be further systematically investigated.

Summarizing the above, the operational precision of anti-solvent dripping needs to be improved, perhaps through automation. Ultimately, the anti-solvent dripping should be adapted to large-scale production technologies. In this direction, any prospective extension of the anti-solvent method will need to inherit its advantages of system homogeneity and adjustability while striving for good repeatability.

4.3 Promising directions

Given that the solvent engineering is relatively mature for small-area spin-coating processing of perovskite films, now it is the right time to move it in the direction of commercial front. Large-scale fabrication of perovskite films can draw lessons from small-area spin-coating experience in terms of solvent engineering. For instance, the precursor solutions and intermediate phases remain similar, and the strategies and mechanisms that are effective on the fabrication of small-area perovskite films should be also operative in the fabrication of large-area perovskite films. What does differ between the two are the coating equipment and the auxiliary crystallization methods, which need to be designed to work on the shared principles of the respective crystallization processes. In fact, the strategy of excess AX has been demonstrated recently to work well for the large-scale fabrication of perovskite films by Bu et al. using a self-drying precursor ink[144]. In this case, anti-solvent-free fabrication was achieved by employing the strategy of excess MACl and the co-solvent system of DMF/NMP, which lowered the formation energy by forming a mixed-cation perovskite and enlarged the grain size of the resultant perovskite film. Such use of excess AX in partnership with a low-solubility solvent is expected to afford an indispensable formulation for the large-scale fabrication of perovskite films. Here the deficiencies of both partners can be mutually offset. For example, the excess AX increases the solubility of PbI_2 to complement the low solubility deficiency of the solvent. In the meantime, volatilization of the low-solubility solvent can sensitively boost the supersaturation to complement the low supersaturation deficiency of the excess AX.

Regarding extension of the anti-solvent method to the large-scale fabrication of PSCs, certain modifications and optimizations are necessary. Some developments in this direction are already ongoing with hopes looming on the horizon, such as alternatives to spin-coating coupled anti-solvent dripping, mixed anti-solvent and functionalized anti-solvent. First, anti-solvent bathing in lieu of anti-solvent dripping was used by Kim et al. for the roll-to-roll (R2R) production of perovskite films with the advantages of high throughput, low cost and flexible substrates[145]. The researchers could fabricate uniform FA-based perovskite films on both rigid and flexible substrates by the anti-solvent bathing method in tert-butyl alcohol (tBuOH) and ethyl acetate (EA). anti-solvent bathing is expected to expand the application scope of the anti-solvent method for the large-scale fabrication of perovskites. More interestingly, some of the deficiencies of anti-solvent dripping can be avoided by using the anti-solvent bathing method. Second, the properties of anti-solvent can be well adjusted by using a mixed anti-solvent instead of the pure solvent to achieve synergistic extraction of the precursor solvent[134, 146–148]. One can optimize polarity, miscibility and volatility of the mixed anti-solvent against those of the individual components. For example, the mixed anti-solvent of EA and toluene was developed for the fabrication of large-area perovskite films[148]. Even using the anti-solvent dripping, the uniformity of large-area perovskite films can be greatly improved with the mixed anti-solvent. From a technological point of view, the mixed anti-solvent strategy can significantly promote the effectiveness of the anti-solvent dripping method. Further developments towards large-scale fabrication require to upgrade the anti-solvent dripping to other operating modes, such as anti-solvent bathing, anti-solvent dipping, anti-solvent spraying and anti-solvent blading. To accomplish the development, appropriate equipment will need to be customized.

Another development path in the future could be functionalized anti-solvent. One example is the use of a saturated solution of phenethylammonium iodide (PEAI) and toluene as the anti-solvent to form 3D-2D ($MAPbI_3$-$PEA_2Pb_2I_4$) graded perovskite interface[149]. Such 3D-2D graded interface with changed energy levels helped to obtain an open-circuit voltage of 1.17 V and improve the device stability. An ethanol solution of methylamine bromide (MABr) was also used as the anti-solvent to improve the perovskite film quality and passivate the surface defects despite the ethanol dissolving FAI, thanks to the compensation effect of the MABr[150]. Similarly, an isopropanol (IPA) solution of FAI and MABr was used as the anti-solvent to improve the quality of perovskite films and optimize the energy level alignment of PSCs[151]. The charge transport materials, such as PCBM, fullerene derivative α-bis-PCBM and ITIC, were doped into the anti-solvent to passivate the grain boundaries[152–154]. An anti-solvent can dissolve ordinary polymers and the functional conjugated polymers to form functionalized anti-solvents. For example, researchers dissolved poly(methyl methacrylate) (PMMA) into a mixed anti-solvent to control nucleation and crystallization of perovskites, achieving a film with a low defect density and large grain size. P-type and n-type conjugated polymers were also doped into anti-solvents to passivate the grain boundaries and improve the water resistance of PSCs[155]. In a word, by modulating nucleation and crystallization, functionalized anti-solvents can modify perovskite films *in-situ* and in-time, and thus facilitate the development of PSCs.

5 Charge transport materials design and passivation strategies

Depending on the deposition order of electron transport layer (ETL) and hole transport layer (HTL), the cell structure can be divided into regular (n-i-p) or inverted (p-i-n) architectures. Notably, the two device structures typically require systematic development of suitable ETLs and HTLs. The ideal ETLs and HTLs should possess the following properties: (1) appropriate energy level matched with absorption layer to reduce the V_{oc} loss;

(2) high conductivity and charge mobility to reduce series resistance; (3) high film quality and good coverage to avoid current leakage; (4) good defect passivation capability at the perovskite interface. In this section, we briefly review the evolution of the charge transport materials, grain boundary passivation and contact passivation for highly efficient and stable PSCs, which are illustrated in Figure 6.

5.1 Development of the charge transport materials

The evolution of ETLs has played an important contributing factor to the rapid progress in high-performance PSCs. Historically, the first n-i-p PSC reported by Miyasaka[3], employed mesoporous titanium dioxide (m-TiO_2) as the ETL. Since then, PSCs based on the mesoporous structure of dye-sensitized solar cells (DSSCs) have achieved rapid efficiency development. However, it was found that TiO_2-based PSCs had an inherent instability under UV illumination arising from light-induced desorption of surface-adsorbed oxygen[156]. Furthermore, the high sintering temperature (400–500 °C) required for the m-TiO_2 films complicated the manufacture process, and hinders their application in flexible modules and perovskite-based tandem devices. To date, many ETLs have been explored to replace the m-TiO_2 stack in PSCs, e.g., low-temperature processed metal oxides SnO_2[15], ZnO[157], $BaSnO_3$[158], Zn_2SnO_4[159] as well as sulfides CdS[160]. Among all these materials, SnO_2 has been considered as the most promising alternative to TiO_2 in n-i-p structured devices due to its excellent properties, such as wide bandgap with high optical transmittance over the whole visible range, a high electron mobility, deep conduction

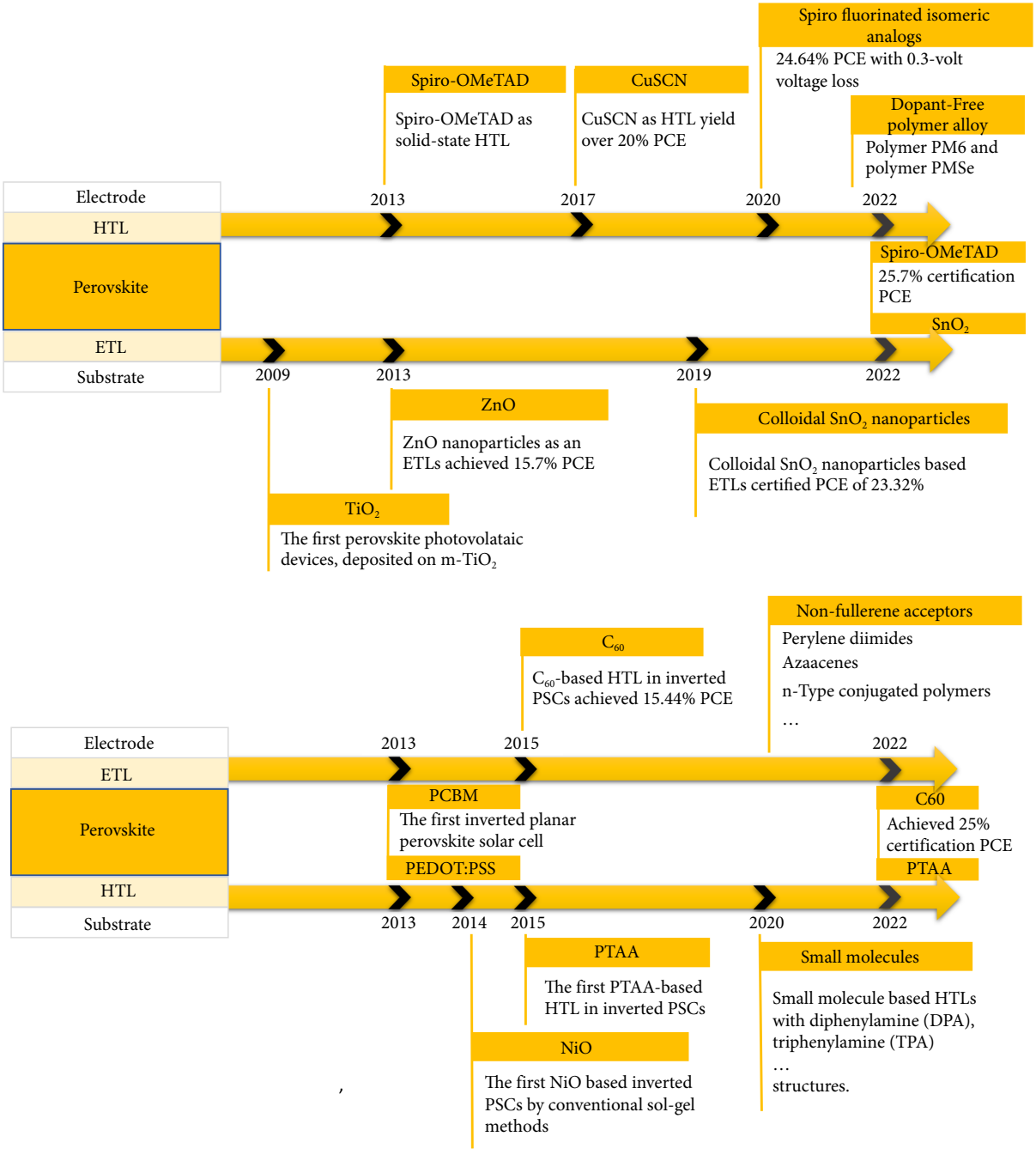

Fig. 6 Evolution of the charge transport materials in perovskite solar cells.

band and good energy level alignment with absorption layer. At present, the PCE of SnO_2-based planar structured PSCs has been increased to 25.7%[18], the highest certified efficiency of single-junction PSCs.

Meanwhile, organic conducting materials such as graphene, fullerene, and its derivatives (such as PCBM and C_{60}[161]) have been widely used as ETLs in p-i-n structured PSCs. The first inverted planar PSC selecting fullerene derivative PCBM as the ETL, achieving a PCE of 3.9%. Using non-fullerene acceptors as ETLs in inverted PSCs is also one of the directions that is worth exploring.

HTLs with the function of hole extracting and electron blocking can largely boost the photovoltaic performance of PSCs. Park and Grätzel first introduced 2,2′,7,7′-tetrakis (N,N-di-pmethoxyphenylamine) 9,9′ -spirobifluorene (spiro-OMeTAD) as the solid-state HTL to replace liquid electrolyte, resulting in much improved efficiency (9.7%) and stability. Up to now, spiro-OMeTAD is the dominated HTL material in high-performance n-i-p structured PSCs. However, the hygroscopic dopants used in sprio-OMeTAD[162] as well as the necessary oxidation process in air[163] inevitably cause stability problems. So new HTLs needs to be explored to obtain PSCs with both high efficiency and superior stability. Jeong et al. developed spiro-OMeTAD analogues (spiro-Naph series) and obtained a high PCE of 24.43%[164]. Jeong et al. used P_3HT as the HTL in contact with the modified perovskite layer without any dopants to improve the stability[165]. Furthermore, dopant-free polymer materials are also the materials of choice. Fu et al. developed a solution-processable two-dimensional (2D) polymer 2DP-TDB, exhibiting a high PCE of 22.17% as dopant-free HTL[166], and then featured an excellent PCE of 24.53% by blending the polymer PM6 and polymer PMSe as HTL without any ionic dopants[167]. Furthermore, some inorganic materials such as CuSCN[168] and CuI[169], were also scrutinized to obtain more stable PSCs.

In inverted structure, poly (3,4-ethylene dioxythiophene): poly (4-styrenesulfonate) (PEDOT:PSS) was initially used as the HTL. Its green-solvent processibility and tunable conductivity provide it a promising prospect[170, 171]. Unfortunately, the intrinsic work function of PEDOT:PSS is only 5.2 eV, leading to low open circuit voltage. Subsequently, poly-bis (4-phenyl) (2,4,6-trimethylphenyl) amine (PTAA) was developed to substitute PEDOT:PSS, and the highest certified efficiency (25%) for single-junction inverted PSCs adopted PTAA as the HTL[172]. Nevertheless, the hydrophobic nature of PTAA presents great challenges for perovskite deposition. Alternatively, inorganic p-type metal oxide semiconductors may replace these organic HTLs for inverted PSCs, such as NiO_x[173], MoO_x[174], and V_2O_5[175] with outstanding chemical stability and acceptable hydrophilicity.

5.2 Grain boundary passivation

In polycrystalline films, point defects such as vacancies and interstitials as well as impurities usually diffuse and concentrate at grain boundaries, thereby serving as major sites for bulk nonradiative recombination within the perovskite absorber. Interstitial and substitutional defects [Pb_i, I_{Pb}, I_{MA}, Pb_I] with low formation energies constitute potential deep-level traps within the perovskite absorber that can induce nonradiative recombination losses[176]. While predominant positively charged iodide vacancies (V^{+}_{I}) along with Pb^{2+} (V_{Pb}^{2-}) form shallow-level traps [cation vacancies, anion vacancies and anti-site substitutional defects][177].

Self-passivation effects resulting from perovskite grains being encapsulated by a thin layer of excess PbI_2 to form type-I straddling gap heterojunction reduces carrier recombination at GBs. However, the thickness of encapsulating PbI_2 must be optimized to prevent charge accumulation effects at GBs. Extrinsic wide-gap additives for encapsulating perovskite grains such as Al_2O_3 and oligomeric silica[178] have been employed.

Alkylammonium halogen salts can also serve as passivation agents, via hydrogen or ionic bonding, for cation and anion defects at GBs. These include linear alkylammonium halogen compounds such as n-butylammonium, iso-butylammonium, ethylammonium, and guanidinium can induce the formation of a wider bandgap low-dimension perovskite phases at GBs similar to the excess PbI_2 passivation mechanism. While longer linear alkylammonium radicals such as octlyammonium can directly passivate GBs without the formation of a low-dimension perovskite phases[179]. Meanwhile benzene-containing alkylammonium halogen compounds have an excellent multifunctional passivation effect at GBs and surfaces due to the formation of ordered layered 2D-perovskite phase. The multifunctional passivation can be attributed to the fact that π-conjugated benzene unit promotes charge transfer and minimizes neutral iodine defects, amine group coordinates with interstitial Pb^{2+} cations and forms a halogen bond with the iodide ion, and the iodide ions fill the vacant iodine sites. Furthermore, the hydrophobicity of the phenyl group enhances the moisture resistance and stability of PSCs.

An extensive range of additives including small molecules, fullerene derivatives, inorganic acids, ionic liquids[180], polymers[181], nanoparticles[182] and solvents have been employed to tune the crystal growth mechanism and resulting morphology for enhanced perovskite grain linkage and to minimize GB surface area. As a result of the wide range of available additives, this approach remains one of the key strategies to enhance both the performance and stability of PSCs.

Electron pair acceptors (Lewis acids) and donors (Lewis bases) serve as an important class of passivating agents for charged traps at perovskite GBs and surfaces[183]. Lewis acids form adducts with free halide ions and Pb_I anti-site defects while Lewis bases bond to under-coordinated Pb^{2+} interstitial ions[184] without electron transfer. Fullerene and its derivatives, also employed as ETLs, are popular Lewis acids candidates resulting from their electron affinity. Whereas compounds containing atoms with electron lone pairs such as nitrogen, sulfur, or oxygen, and phosphorus atoms serve as Lewis bases. These include derivatives of pyridine, thiophene, and imidazole derivatives as well as the impressive outcome of employing trioctylphosphine oxide (TOPO)[185–187] for perovskite passivation to yield very high PL quantum efficiencies. More recently, molecules with polyfunctional groups allow for interaction with multiple defect sites to yield enhanced passivation effects. The introduction of molecules such as 11-Maleimidoundecanoic acid (11MA) and (5-mercapto-1,3,4-thiadiazol-2-ylthio)acetic acid containing multiple active Lewis base sites for GB and surface passivation has led to enhanced performance and stability[188, 189]. Furthermore, zwitterion molecules containing both Lewis acid and Lewis base units, such as choline halides, can simultaneously passivate cation and anion related defects.

5.3 Contact passivation

5.3.1 Perovskite/ETL interface

In the case of planar and mesoporous n-i-p structured devices, the most employed ETLs are SnO_2 and TiO_2, respectively. The n-type character of both transport layers is derived from the presence of oxygen vacancies, which in turn, can serve as electron traps[190].

Surface passivation with halide and alkaline ions have proven to ameliorate some of these issues[191]. More recently, the use of additives with multiple interaction sites for multifunctionality at the perovskite/ETL interface results in enhanced performance and stability[192]. Adamantane derivatives at the perovskite/SnO_2 interface have been used for the synergistic effect of defect passivation and interfacial residual strain release[193]. Biguanide hydrochloride has been demonstrated to simultaneously enhance the electron extraction across the perovskite/SnO_2 interface and the perovskite growth, leading to the highest efficiency of 24.4% till date for two-step deposited perovskite films[194]. However, the most significant development regards the use of multiple hydrogen and coordinative interactions via carboxyl groups on polyacrylic acid (PAA) to ensure conformal contact between SnO_2 quantum dots and the underlying compact TiO_2 layer[195].

For PSCs with inverted structures, the Lewis base approach for surface passivation at the perovskite/C_{60} interface via the use of polyfunctional groups attached to an electron-rich unit has been very effective and the PCE was improved to over 25%. This work is very promising as it provides alternative fabrication routes to achieve high performance other than regular structured cells adopting p-doping of the spiro-OMeTAD HTL. Furthermore, low-dimensional quasi-2D perovskite passivation approach has recently been successfully introduced, e.g., introducing oleylammonium iodide at the perovskite/C_{60} interface to achieve efficient heat-stable PSCs.

5.3.2 Perovskite/HTL interfaces

At the perovskite/spiro-OMeTAD interface (commonly encountered in regular structured PSCs), the formation of a wider bandgap Ruddlesden-Popper 2D-perovskite phase using relatively long alkylammonium spacer cations to form a 2D/3D heterojunction has proven to be very effective at passivating surface defects, suppressing ion migration, and provides a moisture-resistant surface capping layer. In a recent work, a pseudo-halide anion engineering approach introduced formate ions at surfaces and GBs to strongly interact with undercoordinated Pb^{2+} and passivate iodide vacancies, which resulted in a PCE of 25.6%. Similar anion engineering approach has been previously employed for an ion-exchange between iodide and PF_6^- ions to enhance moisture-resistance and performance[196]. The functional polymers have also been used as an interface layer between perovskite and spiro-OMeTAD layers. This layer could not only passivate surface defects but also improve device stability owing to their superior hydrophobic properties[181]. In 2018, Yang's group first introduced a conjugated polymer (PTQ10) as an interfacial layer in PSCs and obtained a PCE of 21.2% with improved stability[197]. The PCE was improved to over 24% when using a two-dimensional polymer interface layer[198]. Depositing a hydrophobic functional interlayer between the perovskite and spiro-OMeTAD layers has been proved to be an efficient strategy to improve the device performance.

In inverted structures, the buried interface is typically perovskite/PTAA; whereby pre-washing with solvents is typically carried out to improve the wettability of the perovskite precursor solution on hydrophobic PTAA. Recent work has shown that the inclusion of PEAI in the pre-washing step led to enhanced performance due to uniform perovskite film growth on PTAA[199]. Besides, embedding alkaline metal salts such as NaCl[200] or RbCl[201] in the HTL proves to be a universal method to enhance perovskite crystal growth.

5.4 Perspectives

In sum, the works described above clearly highlight the efficacy of the two general passivation schemes-molecules with polyfunctional groups for the passivation of various defect sites; and wide-gap materials such as 2D-perovskite phases—along with halide ion engineering approach within the bulk and at interfaces. There is no doubt that, over the coming years, new multifunctional additives to simultaneously ameliorate various interfacial and bulk defect sites for enhanced performance and operational stability shall be discovered. However, there remain challenges to be overcome, some of which include: the development of dopant-free HTL alternatives to spiro-OMeTAD, such as dopant-free polymer alloys in regular structured devices whose dopants trigger perovskite degradation; a deeper knowledge of the structure-property relationships and relative strengths of various chemical interactions upon the introduction of multifunctional additive molecules in order to fully understand the chemical passivation process and speed up the additive material discovery. Furthermore, the development of advanced post-treatment processing methods and materials characterization techniques is necessary for advancing interfacial engineering[191]. For example, further advancements in solution-processed techniques will be required for tailored dimensionality, growth direction and phase purity of low-dimensional perovskite formation over their 3D counterparts to ensure atomically sharp 2D/3D heterojunctions for optimal charge extraction. In addition, the development of advanced material characterization and data analysis techniques is vital for a full understanding of the defect distribution at the buried perovskite-transport layer interface closer to the bottom contact.

6 Optical management through optical coupling effect

Beyond the optimization of the perovskite active layer, optical coupling plays an important role in boosting the device performance. As perovskite devices consist of multiple functional layers and corresponding interfaces, their light utilization efficiency is limited due to interference, reflection, and fixed optical path. Effective optical structure design and construction significantly suppress the optical loss of perovskite optoelectronic devices via optical in-coupling for light trapping in photovoltaic devices and optical out-coupling for light extraction in luminescent devices.

6.1 Optical in-coupling for light trapping

For the perovskite photovoltaic devices, the utilization of incident light is restrained by the Yablonovitch limit of $4n^2$ (where n is the refractive index of the absorbing material)[202]. Fortunately, the designed micro-nano structure provides an opportunity to break the absorption limit of films through the optical in-coupling for light trapping. The incident light is folded into the absorber layer with elongated optical paths and thus the photocarriers generation is increased, which is favorable for perovskite optoelectronic devices.

Various approaches have been introduced to make structured devices, including laser ablation, photolithography, and nanoimprinting. Usually, light harvesting strategies using single micro-nano structures toward optical in-coupling mode mainly include the antireflection (such as grating[203], moth-eye[204], whispering-gallery[205] and inverse opal[206]), back scattering[207], scatter enhancement[208] and surface plasmon polariton (SPP) resonances (Figure 7)[209]. The micro-nano structures can remarkably improve the light harvesting efficiency and enhance the performance of devices. Earlier, the top and bottom surface of thin films have been independently designed and optimized with different periods and grating structures to enhance light trapping[210, 211]. To achieve

hierarchical light-trapping nano-architectures, Song et al. in 2021 developed moiré interference structures using the DVD imprinting method for the efficient moiré-PSCs. The light harvesting ability of the fabricated PSCs was greatly enhanced and could be well manipulated through changing the rotation angle. Moiré interference structure boosted the light harvesting to approach the practical $4n^2$ limit with the reduction of reflection loss within the whole visible light range, even exceeding the average value of the practical $4n^2$ limit ranging from 400 nm to 500 nm[212, 213]. As a result, the efficiencies of the PSCs were increased to 20.17% ($MAPbI_3$) and 21.76% ($(FAPbI_3)_{1-x}(MAPbBr_3)_x$).

6.2 Optical out-coupling for light extraction

Although the quantum efficiency of perovskite emitters is approaching unity, the device efficiency of perovskite luminescent devices is still limited because of the unsatisfactory light extraction. This stems from optical loss mechanisms including SPP modes and waveguide modes caused by the commonly used planar device architecture that features narrow light escaping cone[214, 215]. Optical out-coupling micro-nano structures including nanograting[216], nanophotonic[217], down-converter[218], nanoarray[219] and moth eye[220] have been developed to suppress SPPs and waveguide modes for efficient perovskite luminescent devices (Figure 7).

The light emitted from perovskite emitters may couple with free electron gas at the adjacent metal surface and excite plasma oscillations, namely SPP. The SPP decays exponentially along the metal surface, thereby leading to optical loss[221]. Given that the coupling of SPP to light in a dielectric medium is forbidden due to the mismatch of wavevector, periodic optical structures that can provide additional wavevector are proposed to reduce the SPP loss. Directly patterning the perovskite film to generate a 1D grating-featured emitting layer has been proposed by Mao et al.[216]. A twofold increase in radiance was achieved. In contrast, indirect patterning approach that constructs perovskite layer on a patterned structure to obtain conformal morphology seems to be a more reliable way to reduce SPP loss without affecting the crystallinity of perovskite film. Zhang et al. fabricated PeLED based on an anodic alumina membrane with periodic structure as the substrate

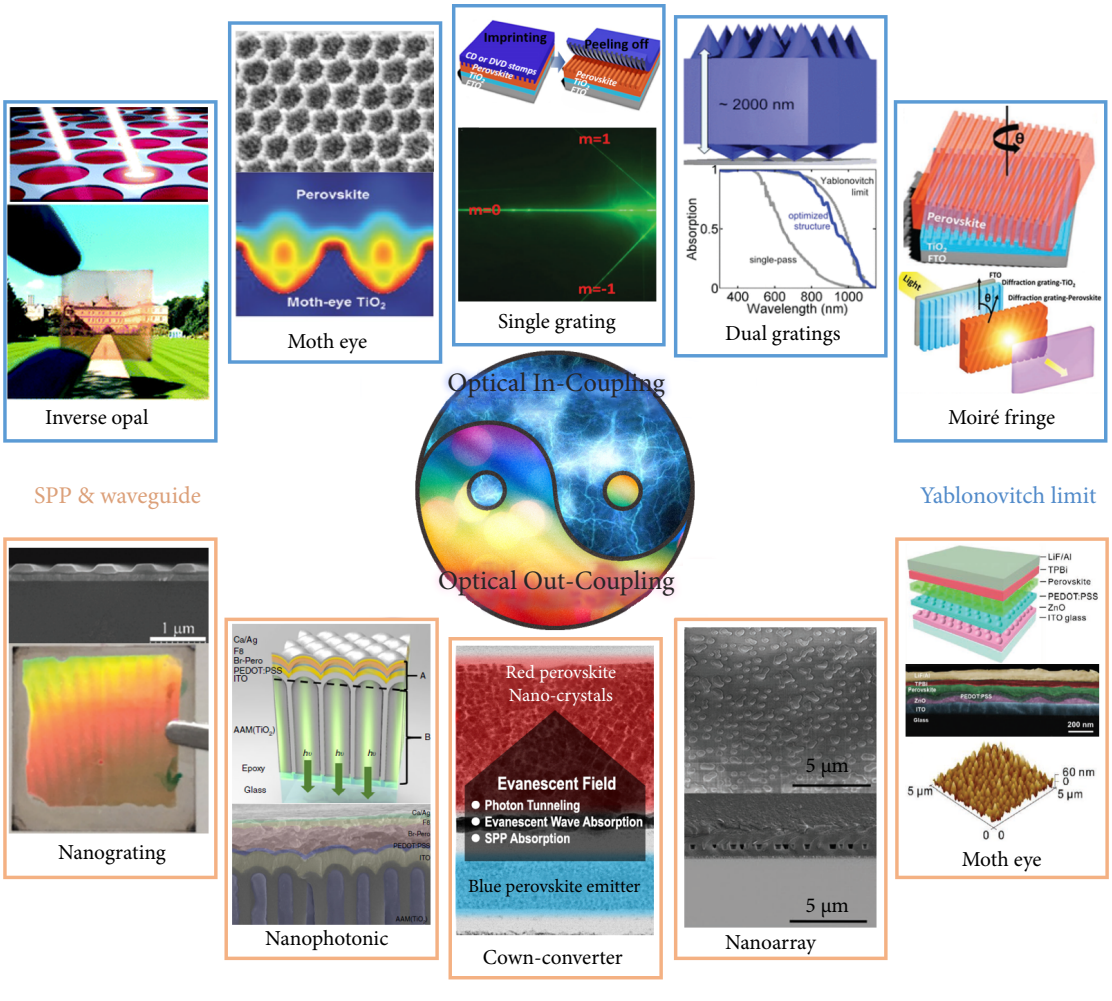

Fig. 7 Optical in-coupling micro-nano structures including inverse opal (reprinted with permission from Ref. [206], © The Royal Society of Chemistry 2015), moth eye (reprinted with permission from Ref. [204], © 2016 WILEY-VCH Verlag GmbH & Co. KGaA, Weinheim), Single Grating (reprinted with permission from Ref. [203], © 2018 WILEY-VCH Verlag GmbH & Co. KGaA, Weinheim), dual gratings (reprinted with permission from Ref. [211], © 2012 American Chemical Society) and Moiré fringe (reprinted with permission from Ref. [212], © 2021 Wiley-VCH GmbH), aiming to reach the Yablonovitch limit of perovskite films for efficient photoelectric conversion. Optical out-coupling micro-nano structures including nanograting (reprinted with permission from Ref. [216], © 2017 WILEY-VCH Verlag GmbH & Co.), nanophotonic (reprinted with permission from Ref. [217], © The Author(s) 2019), down-converter (reprinted with permission from Ref. [218], © 2020 Elsevier Inc.), nanoarray (reprinted with permission from Ref. [219], © 2019 WILEY-VCH Verlag GmbH & Co. KGaA, Weinheim), and moth eye (reprinted with permission from Ref. [220], © 2019 WILEY-VCH Verlag GmbH & Co. KGaA, Weinheim), aiming to suppress SPPs and waveguide modes for efficient perovskite luminescent devices.

and obtained a breakthrough in device efficiency with EQE increasing from 8.19% to 17.5%[217]. Different from direct coupling of SPPs to light, Chen et al. utilized red perovskite nanocrystal to absorb SPPs excited by sky-blue light and reemitted them as red light[218].

Owing to the total internal reflection at the interfaces that have high refractive index mismatch, light emitted from perovskite emitters may be coupled into waveguide modes and be trapped in perovskite emitters. It is possible to suppress waveguide modes by reducing the thickness of the emission layer, but the raise in SPP loss and drop in electrical property of perovskite film may occur simultaneously. Accordingly, destructing the Fabry–Perot cavities that support the waveguide modes is regarded as the most effective strategy to reduce waveguide loss. Li et al. directly printed the perovskite film using thermal nanoimprint lithography, thereby obtaining a periodically patterned perovskite/air interface[222]. Besides the significantly enhanced emission characteristics, the patterned perovskite film acts as a high-*Q* cavity with large mode confinement, which enables the application of an optically pumped laser. Similarly, depositing the perovskite film on a patterned polymer resist can also generate a perovskite/air interface with periodic pattern and enhance the optical out-coupling[223]. For PeLEDs, the waveguide modes are mainly supported by interfaces of perovskite/charge injection layer, ITO/glass, and glass/air due to the high refractive index mismatch. Accordingly, Jeon et al. introduced a randomly distributed nanohole array into SiN film surrounded by ITO and glass to extract the light from perovskite film and boosted the EQE of near-infrared PeLEDs to 14.6%[219]. Shen et al. patterned the front electrode with quasi-random moth-eye nanostructure to control the morphology of the lower surface of perovskite film and obtained a 1.5-fold increase in EQE[220]. The integration of moth-eye nanostructure also enhanced the efficiency in flexible PeLED[224]. Besides the destruction of the planar device structure, inserting metal nanoparticles that feature localized surface plasmon resonance (LSPR) is another approach to suppress the waveguide modes. Shi et al. demonstrated a 1.55-fold emission enhancement by embedding Au nanoparticles into PeLED[225].

For perovskite optoelectronic devices, the implementation of optical coupling structures can boost the light propagation from source to acceptor, improving the device efficiency without causing any loss in electrical performance of functional layers. However, optical coupling in perovskite devices involves many optical phenomena, while the contribution of different mechanisms and corresponding optimization strategies have not been fully understood. In addition, for the manufacturing of large-scale devices, issues including the fabrication of large-area templates and precise control of the layer morphology need more investigation.

7 Perovskite-based tandem solar cells

The certified record-efficiency 26.1% of single-junction perovskite solar cells has approached the S-Q limit[2]. Multi-junction tandem solar cells (TSCs) consisting of a wide-bandgap (wide-E_g: 1.65–1.9 eV) top subcell and a low-E_g (1.1–1.3 eV) bottom subcell have the theoretical efficiency of ~44% to break this S-Q limit via minimizing the thermalization losses[226, 227]. Wide tunability of perovskite bandgaps ranging from ~1.2 to 2.3 eV offers great opportunities for applications in various perovskite-based tandem configurations, such as perovskite/Si, perovskite/perovskite (all-perovskite), perovskite/CIGS, and perovskite/OPV, as shown in Figures 8(a) and 8(b).

Perovskite-based tandems have two configurations, i.e., two-terminal (2-T) and four-terminal (4-T), where the former is realized by optically and electrically connecting two subcells together, and the latter is constructed by mechanically stacking two subcells. Here, we will mainly focus on the milestone achievements and future perspectives for 2-T perovskite-based tandems.

7.1 Development milestones

In the past years, the efficiencies of 2-T perovskite/Si, all-perovskite, perovskite/CIGS, and perovskite/organic tandems have been rapidly boosted to certified 31.3%, 28%, 24.2% and 23.1%, as shown in Figure 8(c), respectively, showing great promise for industrialization of perovskite-based tandem PV technology.

7.1.1 Perovskite/Si tandem

2-T perovskite/Si TSCs have compatibility with current Si technology, and therefore, it is currently the focus of TSCs. The usage of a nanocrystal Si recombination junction that provides high resilience to shunts was demonstrated by Sahli et al. A fully textured monolithic perovskite/SHJ TSC delivered a certified PCE of 25.2%[228]. In 2020, Hou et al. reported TSCs combing fully textured Si heterojunction bottom cells with solution-processed micrometer-thick perovskite top cells[229]. The combined enhancements from enhanced depletion width at the bases of Si pyramids, increased carrier diffusion length, and suppressed halide phase segregation enabled an independently certified PCE of 25.7% for such perovskite/Si TSCs. Xu and his co-workers reported the usage of triple-halide alloys (I/Br/Cl) to adjust the bandgap and stabilize the semiconductor under illumination[230]. Al-Ashouri et al. demonstrated a 2-T perovskite/Si TSC with a certified PCE of 29.15% by using a SAM layer, i.e, methyl-substituted carbazole, that facilitates fast hole extraction and efficient passivation at the hole-selective interface[231]. A very recent record efficiency of 33.7% suggests the promising future of 2-T perovskite/ Si TSCs[2].

7.1.2 All-perovskite tandem

Snaith's group reported the monolithic all-perovskite TSC with a 1.2 eV mixed Sn-Pb low-E_g perovskite as the bottom subcell absorber in 2016, delivering an efficiency of 17.0%[232]. Jen's group utilized the synergistic effect of interfacial modification with Indene-C_{60} bis-adduct ($IC_{60}BA$) for ~1.2 eV low-E_g PSCs and compositional engineering for ~1.8 eV wide-E_g PSCs to obtain the 2-T all-perovskite TSC, showing a high V_{oc} of 1.98 V and a stabilized PCE of 18.5%[233].

Zhao et al. employed a bulk passivation strategy via chlorine doping to enlarge grain sizes and reduce electronic disorder in low-E_g (~1.25 eV) perovskite layers. Combined with effective Ag/MoO_3/ITO ICL, efficient 2-T all-perovskite TSCs with 21% efficiency were achieved, which was the highest value for monolithic all-perovskite TSCs in 2018[234]. Further replacing Ag/MoO_3/ITO with sole ITO as ICL effectively increase the near-infrared transmittance of ICL to enhance the J_{sc} and thus the PCE to 23.1%[235]. ITO not only protects the underneath layers from damages when depositing the subsequent subcell, but also acts as part of the ICL for charge recombination.

Besides ITO, the atomic layer deposited (ALD) SnO_2/Au ICL has been developed[236–239]. Tan's group exploited the comproportionation reaction of metallic Sn and the oxidized Sn^{4+} to reduce the Sn vacancies in Sn-Pb low-E_g (1.22 eV) perovskites, which increased the carrier diffusion length to 3 μm and led to impressive certified PCE of 24.8% for 0.049 cm^2-area all-perovskite TSCs[237]. Strongly reductive surface-anchoring zwitterionic molecules were introduced into the low-E_g perovskite precursor to inhibit Sn^{2+} oxidation and passivate defects at the grain surface, leading to a certified PCE of 24.2% for ~1 cm^2-area tandem devices[236]. A recently certified record efficiency of 26.4% for 0.049 cm^2-area all-

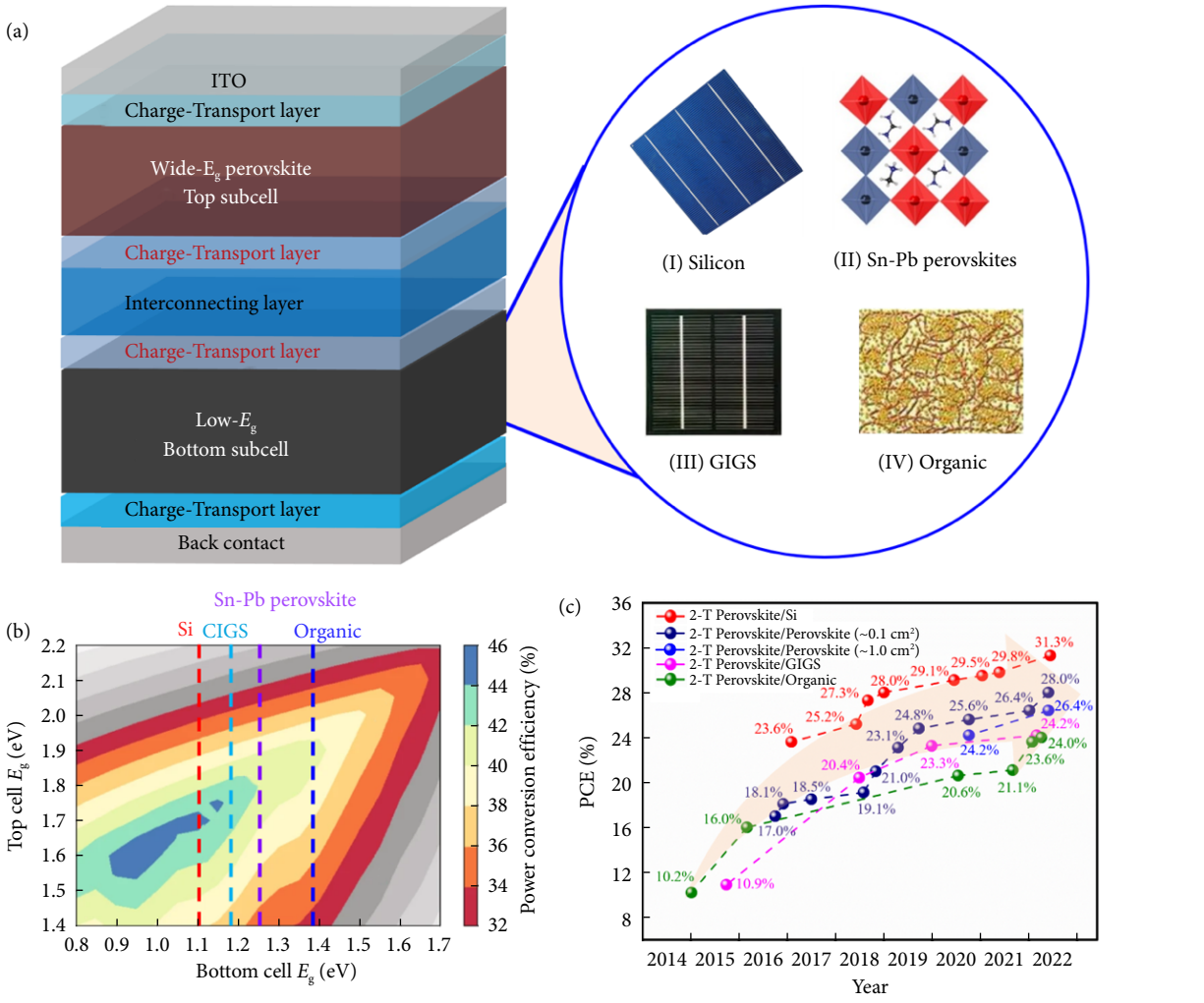

Fig. 8 **(a)** Typical device structure of 2-T perovskite-based tandems. **(b)** Theoretical simulation of PCEs for 2-T perovskite-based tandems with different bandgap combinations (reprinted with permission from Ref. [227], © 2018, The Author(s)). **(c)** The efficiency progress of 2-T perovskite-based tandems.

perovskite TSCs was again reported by Tan group in 2022 via incorporating 4-trifluoromethyl-phenylammonium passivators to improve the quality of thick (~1.2 μm) low-E_g perovskite absorber[239] contributing to a higher J_{sc} of 16.5 mA/cm² in the tandem device.

Very recently, the highest certified efficiencies of small-area (~0.1 cm²) and large-area (~1 cm²) for all-perovskite TSCs have reached 28.0% and 26.4%, respectively[240].

In addition to these accomplishments achieved on rigid substrates, significant progress has also been made for all-perovskite TSCs on flexible substrates and tandem solar minimodules (~20 cm²)[238, 241, 242]. These excellent achievements pave the way to future commercialization of all-perovskite TSCs.

7.1.3 Perovskite/CIGS tandem

$Cu(In,Ga)Se_2$ (CIGS) typically has the E_g of 1.1 eV, which is suitable for the bottom subcell absorber. Perovskite/CIGS tandems possess the following distinct advantages: (1) Higher absorption coefficient of CIGS can reduce the film thickness and thus lower the fabrication cost. (2) Perovskite/CIGS tandem cells can be prepared by all solution processing, compatible with flexible photovoltaics[243–245].

Todorov et al. reported the first 2-T perovskite/CIGS TSC in 2015, which delivered a PCE of 10.9%[246]. The main challenge for high-performance 2-T perovskite/CIGS TSC is the significant electrical loss originating from the poor interfacial contact between CIGS and perovskite layers. Due to the rough surface of CIGS, it is difficult to deposit uniform and dense perovskite film on the CIGS subcells, leading to large nonradiative charge recombination and low FFs. In 2018, Han et al. deposited boron-doped ZnO (BZO) and ITO layer atop the CIGS film, followed by chemical mechanical polishing (CMP) to smoothen the ITO surface, promoting the formation of uniform and dense perovskite films and a certified PCE of 22.43% for 2-T perovskite/CIGS TSC[247]. Taking advantage of self-assembled materials (SAMs), it is possible to directly deposit a conformal HTL on the rough surface. Albrecht's group employed self-assembled monolayer (SAM) 2PACz ((2-(9H-carbazol-9-yl) ethyl) phosphonic acid) to replace PTAA as HTL and obtained a certified PCE of 23.26% on 1.03 cm²-area cells[248]. Later, they utilized Me-4PACz ((4-(3,6-dimethyl-9H-carbazol-9-yl) butyl) phosphonic acid) as SAM and a 1.68 eV-perovskite as top cell, leading to a certified record PCE of 24.2%[249].

7.1.4 Perovskite/organic tandem

Perovskite/organic TSCs have been attracting increasing attention due to the recent advances of organic solar cells (OSCs) with the extension of the spectral response beyond 1000 nm using non-fullerene acceptors, as well as solution processability, light weight, and flexibility[150, 250–253]. Most importantly, orthogonal solvents for preparing the perovskite and organic absorbers make it feasible for large-area solution-processing.

Except for large V_{oc} loss in wide-E_g (~1.80 eV) subcells, the optical loss in the ICL limits the PCE enhancement of perovskite/organic TSCs, where thin metals (Ag or Au) and organic/inorganic charge transport layers as ICLs are typically employed. However, such thin metal-based ICLs would induce notable optical loss, which significantly sacrifices the J_{sc} and limits the PCE below 22%[254–259]. Recently, Chen et al. reported a BCP/IZO (4 nm)/MoO_x sandwich layer as ICL and demonstrated a PCE of 23.6% (22.95% certified), which is much higher than that of ICL using BCP/Ag/MoO_x[260]. Moreover, Brinkmann et al. inserted ALD-InO_x between ALD-SnO_x and MoO_x as ICL, yielding a record PCE of 24.0% (23.1% certified) for 2-T perovskite/organic TSC[261]. These two works set a milestone for highly efficient perovskite/organic tandems.

7.2 Challenges and perspectives

Although great progress of perovskite-based tandems has been made, further development of this promising PV technology could focus on the perovskite top/bottom subcells, design of ICL, stability, and scaling-up manufacture.

7.2.1 Minimizing V_{oc} deficit

One limiting factor of 2-T perovskite-based tandem device performance lies in the wide-E_g perovskite top subcells[262, 263]. First, large V_{oc} deficit (typically >400 mV) limits the performance of wide-E_g perovskite top subcells, especially for P-I-N type 2-T perovskite-based tandems. In order to achieve higher V_{oc}, minimizing or passivating various defects in the bulk or surface of perovskite absorbers is of extreme significance, which can be well tackled with high-quality perovskite films and multifunctional passivation agents. Moreover, interfacial energy levels between wide-E_g perovskite absorbers and charge transporting layers should be aligned to minimize the interfacial recombination. Therefore, effective charge transport materials with proper energy levels should be carefully selected and developed. Interfacial modification layers are another effective strategy to reduce losses at the interfaces of perovskite/charge transport layers/metal electrode. Ideally, the 2-T perovskite-based tandems could achieve the highest V_{oc} of ~2.0 V for perovskite/Si tandem[264], ~2.25 V for all-perovskite tandem, ~2.01 V for perovskite/CIGS tandem[249] and ~2.15 V for perovskite/organic tandem[261].

7.2.2 Current matching for higher J_{sc}

Current matching of subcells governs the J_{sc} of 2-T perovskite-based tandems, as the lower J_{sc} of the subcells determines the overall J_{sc} of monolithic TSCs.

The future trend of N type Si solar cells requires N-I-P type perovskite top subcells for efficient TSCs. However, parasitic absorption of Spiro-OMeTAD limits the J_{sc} of N-I-P type top cells for 2-T perovskite/Si TSCs. Although P-I-N type perovskite top subcells is popular recently[240], further development of novel thin inorganic HTLs is highly desired to replace thick organic ones. Therefore, low-temperature processed NiO_x will be the focus in the future. Moreover, depositing inorganic charge transport layer directly on wide-E_g perovskite absorbers may reduce the cost and simplify the fabrication process by completely removing inorganic buffer layers (e.g., SnO_x, MoO_x) which are normally deposited to protect weak organic charge transport layers (e.g., Spiro-OMeTAD, C_{60}, PCBM) from the bombardment of sputtering of transparent conductive electrodes (TCOs). Additionally, stacking materials with gradient refractive index, especially at front incident surface and ICLs, should suppress reflection loss at interfaces to achieve higher J_{sc}. Fully textured c-Si bottom subcells for perfect light trapping is still necessary to guarantee the maximum J_{sc} of 2-T perovskite/Si TSCs, although this complicates the fabrication process of wide-E_g perovskite top cells[228, 229]. Parasitic absorption of the TCOs in the NIR region affects J_{sc} as well. Selection of proper TCOs with higher charge mobility instead of higher carrier density (e.g., IZO, IO:H, and IZrO) may deliver a higher overall J_{sc} of 2-T perovskite/Si TSCs[265]. Finally, design of metal grids is another factor affecting the J_{sc} since the cell under the shade of metal grid hardly contributes current[266]. Theoretically, half of the maximum J_{sc} (42.5 mA/cm^2) of c-Si solar cell[240], i.e., approximately 20 mA/cm^2, is achievable as the J_{sc} for high-performance 2T PVK/c-Si TSCs.

For all-perovskite TSCs, thick Sn-Pb (over 1 μm) perovskite absorber is extremely significant to enhance the spectral response in NIR region to get the current matched from both subcells. Therefore, the addition of antioxidants in the precursor and the passivation of bulky and interfacial defects will prolong the carrier lifetimes and diffusion length, thus enhancing the performance. Over 17 mA/cm^2 for all-perovskite TSCs is expectable.

Optimizing the interfacial contact between CIGS and perovskite subcells to reduce the electrical loss is critical for the J_{sc} improvement. Since CIGS and silicon have similar bandgaps, approximately 20 mA/cm^2 is also achievable for 2-T perovskite/CIGS TSCs[249].

The low J_{sc} (~15 mA/cm^2) is the major obstacle that limits the efficiency of 2-T perovskite/organic TSCs, primarily due to photocurrent limits from OSCs. Developing more efficient low-E_g donor and acceptor materials with high carrier mobility and absorption coefficients, as well as optimizing the morphology of heterojunction film are crucial for high-performance OSCs. J_{sc} of around 16 mA/cm^2 for perovskite/organic TSCs is expected.

7.2.3 Rational design of ICLs

ICLs should have high vertical conductivity for effective charge recombination, low lateral conductivity for less current leakage, and balanced spectral distribution for current matching of subcells. Ideally, when the refractive indices of ICLs approximately amounts to the geometric mean of perovskites and other absorbers, the minimized reflection is obtained when the optical thickness equals to one fourth of the wavelength irradiating on the bottom subcell. However, refractive index of commonly used TCO such as IZO and ITO is approximately 2, which results in internal reflection at the interfaces due to a large refractive index contrast. Nanocrystalline Si with lower lateral conductivity is a promising recombination junction candidate to reduce interfacial reflection losses and parasitic absorption as well as suppress shunt paths between the top and bottom subcells, thus increasing the J_{sc} and FF of bottom subcell.

In particular, for solution-processed all-perovskite and perovskite/organic tandems, protecting the underneath existing layers is very crucial when depositing the subsequent layers. Multi-layer stacking ICLs could function well, but parasite absorption across these layers should also be minimized. Meanwhile, thin metals are likely to damage the device stability. Therefore, searching new materials with high NIR transmittance is feasible to further reduce parasite absorption losses.

7.2.4 Improving stability of perovskite absorbers

The instability of wide-E_g perovskite top absorbers mainly originates from the perovskite top cells. Instability intriguing factors include: external factors (humidity, oxygen, heat, UV light, electrical field, etc.) and internal factors (ion migration, defects). Proper encapsulation can eliminate the external factors such as humidity, oxygen, and even UV light if UV protection layer is applied during the encapsulation[267]. Intrinsic factors can be tackled by successful

engineering of single-junction PSCs in crystallization[125], composition[230], interface[231] and passivation[268]. Moreover, layers delamination during the temperature-cycling test happens due to a huge thermal expansion coefficient contrast[269] and charge transporting layer with suitable thermal coefficient to adjacent layers (perovskite and TCOs) needs to be considered to avoid physical failure of device.

Phase segregation is severe in Br-rich wide-E_g perovskites. High content of Br could accelerate the crystallization rate of wide-E_g perovskites, leading to the separation of I-rich and Br-rich domains as well as small grain size. Therefore, the usage of appropriate additives into the precursor to modulate the crystallization process is urgent, which could inhibit the phase segregation. In addition, surface modifications are also beneficial to mitigate the migration of halide ions on the wide-E_g perovskite surface, which could make the phase more stable[270].

Easy oxidation of Sn hinders high-performance all-perovskite tandems. Except for the protection via effective encapsulation, antioxidants, reducing agents, and defect passivators applied to Sn-Pb low-E_g perovskite absorbers would largely enhance the stability of low-E_g perovskite bottom subcells, benefiting the overall stability of all-perovskite tandems.

7.2.5 Scaling-up manufacture

The wafer-scale manufacture of 2-T PVK/ Si TSCs is another big challenge. Previous reports of 2-T perovskite/Si TSCs are mostly based on small area and spin-coating technique[228, 231, 271–274]. Some attempts have also been tried to scale up the devices but the efficiency declines as area increases[266, 275, 276]. Historically, Oxford PV recently announced a record efficiency of 26.8% with a full area of 274 cm^2, which is the first time for 2-T perovskite/ Si TSCs to exceed the efficiency of 26.6% of single-junction c-Si solar cell in full size[240]. There is still much room for efficiency improvement compared with the fresh record 31.3% especially in V_{oc} and J_{sc}[240].

Techniques such as slot-die coating and vapor depositions for fully textured TSCs are suitable for scalable fabrication, which demonstrates satisfactory compatibility with commercial manufacture of mature Si and emerging photovoltaic technology.

Considering that all-perovskite, perovskite/CIGS, and perovskite/organic tandems can all be fabricated by solution processing, it is very promising to expect flexible devices based on high-throughput and low-cost roll-to-roll manufacturing, enabling flexible and lightweight applications for building-integrated photovoltaics (BIPV) and portable power supply.

8 Conclusions

The past few years has witnessed great progress for PSCs through comprehensive tools controlling the film deposition process. This review gives an overall analysis over the efficiency improvement strategies since the beginning of first PSC device. At the early stage, the performance enhancement is mainly driven by the development of fabrication methods and device structures. Whereafter, the research focus concentrates on the deposition of high-quality perovskite thin films through compositional engineering, additive engineering and crystallization manipulation, which pushes the efficiency to over 20%. At the very recent stage, interfacial engineering including charge transport layer modification and passivation are indispensable strategies for achieving high performance in state-of-art PSCs. Moreover, optical management through the proper use of optical coupling effect to reduce optical loss and constructing tandem solar cells are also effective tools to further raise the efficiency. Finally, we believe that the better understanding of different passivation mechanisms and better defect management, especially at buried interface, is the breakthrough point for performance leap in the foreseeable future.

Acknowledgements

The work was supported by the National Key Research and Development Program of China (2022YFB3803300), the open research fund of Songshan Lake Materials Laboratory (2021SLABFK02), and the National Natural Science Foundation of China (21961160720 and 52203217), and the China Postdoctoral Science Foundation (2021M690805).

Article history

Received: 30 August 2023; Revised: 25 September 2023; Accepted: 27 September 2023

Declaration of competing interest

The authors have no competing interests to declare that are relevant to the content of this article.

References

[1] Cai, M., Wu, Y., Chen, H., Yang, X., Qiang, Y., Han, L. (2017). Cost-performance analysis of perovskite solar modules. *Advanced Science*, 4: 1600269.

[2] National Renewable Energy Laboratory (2023). Best research-cell effiencies. Available at https://www.nrel.gov/pv/cell-efficiency.html

[3] Kojima, A., Teshima, K., Shirai, Y., Miyasaka, T. (2009). Organometal halide perovskites as visible-light sensitizers for photovoltaic cells. *Journal of the American Chemical Society*, 131: 6050–6051.

[4] Kim, H. S., Lee, C. R., Im, J. H., Lee, K. B., Moehl, T., Marchioro, A., Moon, S. J., Humphry-Baker, R., Yum, J. H., Moser, J. E., et al. (2012). Lead iodide perovskite sensitized all-solid-state submicron thin film mesoscopic solar cell with efficiency exceeding 9%. *Scientific Reports*, 2: 591.

[5] Lee, M. M., Teuscher, J., Miyasaka, T., Murakami, T. N., Snaith, H. J. (2012). Efficient hybrid solar cells based on meso-superstructured organometal halide perovskites. *Science*, 338: 643–647.

[6] Jeng, J. Y., Chiang, Y. F., Lee, M. H., Peng, S. R., Guo, T. F., Chen, P., Wen, T. C. (2013). $CH_3NH_3PbI_3$ perovskite/fullerene planar-heterojunction hybrid solar cells. *Advanced Materials*, 25: 3727–3732.

[7] Burschka, J., Pellet, N., Moon, S. J., Humphry-Baker, R., Gao, P., Nazeeruddin, M. K., Grätzel, M. (2013). Sequential deposition as a route to high-performance perovskite-sensitized solar cells. *Nature*, 499: 316–319.

[8] Xiao, M., Huang, F., Huang, W., Dkhissi, Y., Zhu, Y., Etheridge, J., Gray-Weale, A., Bach, U., Cheng, Y. B., Spiccia, L. (2014). A fast deposition-crystallization procedure for highly efficient lead iodide perovskite thin-film solar cells. *Angewandte Chemie International Edition*, 53: 9898–9903.

[9] Jeon, N. J., Noh, J. H., Kim, Y. C., Yang, W. S., Ryu, S., Seok, S. I. (2014). Solvent engineering for high-performance inorganic-organic hybrid perovskite solar cells. *Nature Materials*, 13: 897–903.

[10] Ahn, N., Son, D. Y., Jang, I. H., Kang, S. M., Choi, M., Park, N. G.

(2015). Highly reproducible perovskite solar cells with average efficiency of 18.3% and best efficiency of 19.7% fabricated via lewis base adduct of lead(II) iodide. *Journal of the American Chemical Society*, 137: 8696–8699.

[11] Xiao, Z., Dong, Q., Bi, C., Shao, Y., Yuan, Y., Huang, J. (2014). Solvent annealing of perovskite-induced crystal growth for photovoltaic-device efficiency enhancement. *Advanced Materials*, 26: 6503–6509.

[12] Liu, M., Johnston, M. B., Snaith, H. J. (2013). Efficient planar heterojunction perovskite solar cells by vapour deposition. *Nature*, 501: 395–398.

[13] Yang, W. S., Noh, J. H., Jeon, N. J., Kim, Y. C., Ryu, S., Seo, J., Seok, S. I. (2015). High-performance photovoltaic perovskite layers fabricated through intramolecular exchange. *Science*, 348: 1234–1237.

[14] Yang, W. S., Park, B. W., Jung, E. H., Jeon, N. J., Kim, Y. C., Lee, D. U., Shin, S. S., Seo, J., Kim, E. K., Noh, J. H., et al. (2017). Iodide management in formamidinium-lead-halide-based perovskite layers for efficient solar cells. *Science*, 356: 1376–1379.

[15] Jiang, Q., Zhao, Y., Zhang, X., Yang, X., Chen, Y., Chu, Z., Ye, Q., Li, X., Yin, Z., You, J. (2019). Surface passivation of perovskite film for efficient solar cells. *Nature Photonics*, 13: 460–466.

[16] Jeong, M., Choi, I. W., Go, E. M., Cho, Y., Kim, M., Lee, B., Jeong, S., Jo, Y., Choi, H. W., Lee, J., et al. (2020). Stable perovskite solar cells with efficiency exceeding 24.8% and 0.3-V voltage loss. *Science*, 369: 1615–1620.

[17] Jeong, J., Kim, M., Seo, J., Lu, H., Ahlawat, P., Mishra, A., Yang, Y., Hope, M. A., Eickemeyer, F. T., Kim, M., et al. (2021). Pseudo-halide anion engineering for α-$FAPbI_3$ perovskite solar cells. *Nature*, 592: 381–385.

[18] Min, H., Lee, D. Y., Kim, J., Kim, G., Lee, K. S., Kim, J., Paik, M. J., Kim, Y. K., Kim, K. S., Kim, M. G., et al. (2021). Perovskite solar cells with atomically coherent interlayers on SnO_2 electrodes. *Nature*, 598: 444–450.

[19] Zhao, Y., Ma, F., Qu, Z., Yu, S., Shen, T., Deng, H. X., Chu, X., Peng, X., Yuan, Y., Zhang, X., et al. (2022). Inactive $(PbI_2)_2RbCl$ stabilizes perovskite films for efficient solar cells. *Science*, 377: 531–534.

[20] Tan, Q., Li, Z., Luo, G., Zhang, X., Che, B., Chen, G., Gao, H., He, D., Ma, G., Wang, J., et al. (2023). Inverted perovskite solar cells using dimethylacridine-based dopants. *Nature*, 620: 545–551.

[21] Park, J., Kim, J., Yun, H. S., Paik, M. J., Noh, E., Mun, H. J., Kim, M. G., Shin, T. J., Seok, S. I. (2023). Controlled growth of perovskite layers with volatile alkylammonium chlorides. *Nature*, 616: 724–730.

[22] Green, M. A., Dunlop, E. D., Siefer, G., Yoshita, M., Kopidakis, N., Bothe, K., Hao, X. (2023). Solar cell efficiency tables (Version 61). *Progress in Photovoltaics: Research and Applications*, 31: 3–16.

[23] Chen, Z., Dong, Q., Liu, Y., Bao, C., Fang, Y., Lin, Y., Tang, S., Wang, Q., Xiao, X., Bai, Y., et al. (2017). Thin single crystal perovskite solar cells to harvest below-bandgap light absorption. *Nature Communications*, 8: 1890.

[24] Gao, F., Zhao, Y., Zhang, X., You, J. (2020). Recent progresses on defect passivation toward efficient perovskite solar cells. *Advanced Energy Materials*, 10: 1902650.

[25] Hui, W., Chao, L., Lu, H., Xia, F., Wei, Q., Su, Z., Niu, T., Tao, L., Du, B., Li, D., et al. (2021). Stabilizing black-phase formamidinium perovskite formation at room temperature and high humidity. *Science*, 371: 1359–1364.

[26] Huang, F., Li, M., Siffalovic, P., Cao, G., Tian, J. (2019). From scalable solution fabrication of perovskite films towards commercialization of solar cells. *Energy & Environmental Science*, 12: 518–549.

[27] Wang, X., Han, Z., Gao, F., Luo, C., Zhao, Q. (2022). Facet orientation and intermediate phase regulation via a green antisolvent for high-performance perovskite solar cells. *Solar RRL*, 6: 2100973.

[28] Taylor, A. D., Sun, Q., Goetz, K. P., An, Q., Schramm, T., Hofstetter, Y., Litterst, M., Paulus, F., Vaynzof, Y. (2021). A general approach to high-efficiency perovskite solar cells by any antisolvent. *Nature Communications*, 12: 1878.

[29] Xiang, W., Zhang, J., Liu, S., Albrecht, S., Hagfeldt, A., Wang, Z. (2022). Intermediate phase engineering of halide perovskites for photovoltaics. *Joule*, 6: 315–339.

[30] Bu, T., Li, J., Li, H., Tian, C., Su, J., Tong, G., Ono, L. K., Wang, C., Lin, Z., Chai, N., et al. (2021). Lead halide-templated crystallization of methylamine-free perovskite for efficient photovoltaic modules. *Science*, 372: 1327–1332.

[31] Han, Y., Xie, H., Lim, E. L., Bi, D. (2022). Review of two-step method for lead halide perovskite solar cells. *Solar RRL*, 6: 2101007.

[32] Gao, F., Luo, C., Wang, X., Zhao, Q. (2021). Alkali metal chloride-doped water-based TiO_2 for efficient and stable planar perovskite photovoltaics exceeding 23% efficiency. *Small Methods*, 5: e2100856.

[33] Im, J. H., Jang, I. H., Pellet, N., Grätzel, M., Park, N. G. (2014). Growth of CH_3NH_3PbI3 cuboids with controlled size for high-efficiency perovskite solar cells. *Nature Nanotechnology*, 9: 927–932.

[34] Zhao, Y., Tan, H., Yuan, H., Yang, Z., Fan, J. Z., Kim, J., Voznyy, O., Gong, X., Quan, L. N., Tan, C. S., et al. (2018). Perovskite seeding growth of formamidinium-lead-iodide-based perovskites for efficient and stable solar cells. *Nature Communications*, 9: 1607.

[35] Li, Q., Zhao, Y., Fu, R., Zhou, W., Zhao, Y., Liu, X., Yu, D., Zhao, Q. (2018). Efficient perovskite solar cells fabricated through CsCl-enhanced PbI_2 precursor via sequential deposition. *Advanced Materials*: e1803095.

[36] Li, Q., Zhao, Y., Zhou, W., Han, Z., Fu, R., Lin, F., Yu, D., Zhao, Q. (2019). Perovskite solar cells: Halogen engineering for operationally stable perovskite solar cells via sequential deposition. *Advanced Energy Materials*, 9: 1902239.

[37] Xie, L., Lin, K., Lu, J., Feng, W., Song, P., Yan, C., Liu, K., Shen, L., Tian, C., Wei, Z. (2019). Efficient and stable low-bandgap perovskite solar cells enabled by a $CsPbBr_3$-cluster assisted bottom-up crystallization approach. *Journal of the American Chemical Society*, 141: 20537–20546.

[38] Alharbi, E. A., Baumeler, T. P., Krishna, A., Alyamani, A. Y., Eickemeyer, F. T., Ouellette, O., Pan, L., Alghamdi, F. S., Wang, Z., Alotaibi, M. H., et al. (2021). Formation of high-performance multi-cation halide perovskites photovoltaics by δ-$CsPbI_3$/δ-$RbPbI_3$ seed-assisted heterogeneous nucleation. *Advanced Energy Materials*, 11: 2003785.

[39] Zhou, T., Xu, Z., Wang, R., Dong, X., Fu, Q., Liu, Y. (2022). Crystal growth regulation of 2D/3D perovskite films for solar cells with both high efficiency and stability. *Advanced Materials*, 34: e2200705.

[40] Shen, Z., Han, Q., Luo, X., Shen, Y., Wang, T., Zhang, C., Wang, Y., Chen, H., Yang, X., Zhang, Y., et al. (2022). Crystal-array-assisted growth of a perovskite absorption layer for efficient and stable solar cells. *Energy & Environmental Science*, 15: 1078–1085.

[41] Li, W., Rothmann, M. U., Zhu, Y., Chen, W., Yang, C., Yuan, Y., Choo, Y. Y., Wen, X., Cheng, Y. B., Bach, U., et al. (2021). The critical role of composition-dependent intragrain planar defects in the performance of $MA_{1-x}FA_xPbI_3$ perovskite solar cells. *Nature Energy*, 6: 624–632.

[42] Luo, C., Zheng, G., Gao, F., Wang, X., Zhao, Y., Gao, X., Zhao, Q. (2022). Facet orientation tailoring via 2D-seed- induced growth enables highly efficient and stable perovskite solar cells. *Joule*, 6: 240–257.

[43] Li, D., Zhang, D., Lim, K. S., Hu, Y., Rong, Y., Mei, A., Park, N. G., Han, H. (2021). A review on scaling up perovskite solar cells. *Advanced Functional Materials*, 31: 2008621.

[44] Zuo, C., Ding, L. (2021). Drop-casting to make efficient perovskite solar cells under high humidity. *Angewandte Chemie International Edition*, 60: 11242–11246.

[45] Barrows, A. T., Pearson, A. J., Kwak, C. K., Dunbar, A. D. F., Buckley, A. R., Lidzey, D. G. (2014). Efficient planar heterojunction mixed-halide perovskite solar cells deposited *via* spray-deposition. *Energy & Environmental Science*, 7: 2944–2950.

[46] Wei, Z., Chen, H., Yan, K., Yang, S. (2014). Inkjet printing and instant chemical transformation of a $CH_3NH_3PbI_3$/nanocarbon electrode and interface for planar perovskite solar cells. *Angewandte Chemie International Edition*, 53: 13239–13243.

[47] Li, J., Wang, H., Chin, X. Y., Dewi, H. A., Vergeer, K., Goh, T. W., Lim, J. W. M., Lew, J. H., Loh, K. P., Soci, C., et al. (2020). Highly efficient thermally co-evaporated perovskite solar cells and mini-modules. *Joule*, 4: 1035–1053.

[48] Zhang, Y., Zhang, Z., Yu, W., He, Y., Chen, Z., Xiao, L., Shi, J. J., Guo, X., Wang, S., Qu, B. (2022). Lead-free double perovskite $Cs_2AgIn_{0.9}Bi_{0.1}Cl_6$ quantum dots for white light-emitting diodes. *Advanced Science*, 9: e2102895.

[49] Li, H., Zhou, J., Tan, L., Li, M., Jiang, C., Wang, S., Zhao, X., Liu, Y., Zhang, Y., Ye, Y., et al. (2022). Sequential vacuum-evaporated perovskite solar cells with more than 24% efficiency. *Science Advances*, 8: eabo7422.

[50] Qiu, L., He, S., Liu, Z., Ono, L. K., Son, D. Y., Liu, Y., Tong, G., Qi, Y. (2020). Rapid hybrid chemical vapor deposition for efficient and hysteresis-free perovskite solar modules with an operation lifetime exceeding 800 hours. *Journal of Materials Chemistry A*, 8: 23404–23412.

[51] Luo, X., Shen, Z., Shen, Y., Su, Z., Gao, X., Wang, Y., Han, Q., Han, L. (2022). Effective passivation with self-organized molecules for perovskite photovoltaics. *Advanced Materials*, 34: e2202100.

[52] Liu, L., Zuo, C., Ding, L. (2021). Self-spreading produces highly efficient perovskite solar cells. *Nano Energy*, 90: 106509.

[53] Bishop, J. E., Read, C. D., Smith, J. A., Routledge, T. J., Lidzey, D. G. (2020). Fully spray-coated triple-cation perovskite solar cells. *Scientific Reports*, 10: 6610.

[54] Huang, Z., Hu, X., Zhao, Z., Meng, X., Su, M., Xue, T., Chi, J., Xie, H., Cai, Z., Chen, Y., et al. (2021). Releasing nanocapsules for high-throughput printing of stable perovskite solar cells. *Advanced Energy Materials*, 11: 2101291.

[55] Liang, Q., Liu, K., Sun, M., Ren, Z., Fong, P. W. K., Huang, J., Qin, M., Wu, Z., Shen, D., Lee, C. S., et al. (2022). Manipulating crystallization kinetics in high-performance blade-coated perovskite solar cells via cosolvent-assisted phase transition. *Advanced Materials*, 34: e2200276.

[56] Du, M., Zhu, X., Wang, L., Wang, H., Feng, J., Jiang, X., Cao, Y., Sun, Y., Duan, L., Jiao, Y., et al. (2020). High-pressure nitrogen-extraction and effective passivation to attain highest large-area perovskite solar module efficiency. *Advanced Materials*, 32: e2004979.

[57] Noh, J. H., Im, S. H., Heo, J. H., Mandal, T. N., Seok, S. I. (2013). Chemical management for colorful, efficient, and stable inorganic-organic hybrid nanostructured solar cells. *Nano Letters*, 13: 1764–1769.

[58] Wang, S., Li, X., Wu, J., Wen, W., Qi, Y. (2018). Fabrication of efficient metal halide perovskite solar cells by vacuum thermal evaporation: A progress review. *Current Opinion in Electrochemistry*, 11: 130–140.

[59] Jiang, Y., He, S., Qiu, L., Zhao, Y., Qi, Y. (2022). Perovskite solar cells by vapor deposition based and assisted methods. *Applied Physics Reviews*, 9: 021305.

[60] Ávila, J., Momblona, C., Boix, P. P., Sessolo, M., Bolink, H. J. (2017). Vapor-deposited perovskites: The route to high-performance solar cell production. *Joule*, 1: 431–442.

[61] Momblona, C., Gil-Escrig, L., Bandiello, E., Hutter, E. M., Sessolo, M., Lederer, K., Blochwitz-Nimoth, J., Bolink, H. J. (2016). Efficient vacuum deposited p-i-n and n-i-p perovskite solar cells employing doped charge transport layers. *Energy & Environmental Science*, 9: 3456–3463.

[62] Zhu, X., Yang, D., Yang, R., Yang, B., Yang, Z., Ren, X., Zhang, J., Niu, J., Feng, J., Liu, S. F. (2017). Superior stability for perovskite solar cells with 20% efficiency using vacuum co-evaporation. *Nanoscale*, 9: 12316–12323.

[63] Kottokkaran, R., Gaonkar, H. A., Abbas, H. A., Noack, M., Dalal, V. (2019). Performance and stability of co-evaporated vapor deposited perovskite solar cells. *Journal of Materials Science: Materials in Electronics*, 30: 5487–5494.

[64] Chiang, Y. H., Anaya, M., Stranks, S. D. (2020). Multisource vacuum deposition of methylammonium-free perovskite solar cells. *ACS Energy Letters*, 5: 2498–2504.

[65] Abbas, H. A., Kottokkaran, R., Ganapathy, B., Samiee, M., Zhang, L., Kitahara, A., Noack, M., Dalal, V. L. (2015). High efficiency sequentially vapor grown n-i-p $CH_3NH_3PbI_3$ perovskite solar cells with undoped P3HT as p-type heterojunction layer. *APL Materials*, 3: 016105.

[66] Tavakoli, M. M., Simchi, A., Mo, X., Fan, Z. (2017). High-quality organohalide lead perovskite films fabricated by layer-by-layer alternating vacuum deposition for high efficiency photovoltaics. *Materials Chemistry Frontiers*, 1: 1520–1525.

[67] Gil-Escrig, L., Momblona, C., La-Placa, M. G., Boix, P. P., Sessolo, M., Bolink, H. J. (2018). Vacuum deposited triple-cation mixed-halide perovskite solar cells. *Advanced Energy Materials*, 8: 1703506.

[68] Roß, M., Severin, S., Stutz, M. B., Wagner, P., Köbler, H., Favin-Lévêque, M., Al-Ashouri, A., Korb, P., Tockhorn, P., Abate, A., et al. (2021). Co-evaporated formamidinium lead iodide based perovskites with 1000 h constant stability for fully textured monolithic perovskite/silicon tandem solar cells. *Advanced Energy Materials*, 11: 2101460.

[69] Lohmann, K. B., Motti, S. G., Oliver, R. D. J., Ramadan, A. J., Sansom, H. C., Yuan, Q., Elmestekawy, K. A., Patel, J. B., Ball, J. M., Herz, L. M., et al. (2022). Solvent-free method for defect reduction and improved performance of p-i-n vapor-deposited perovskite solar cells. *ACS Energy Letters*, 7: 1903–1911.

[70] Li, J., Dewi, H. A., Wang, H., Zhao, J., Tiwari, N., Yantara, N., Malinauskas, T., Getautis, V., Savenije, T. J., Mathews, N., et al. (2021). Co-evaporated $MAPbI_3$ with graded Fermi levels enables highly performing, scalable, and flexible p-i-n perovskite solar cells. *Advanced Functional Materials*, 31: 2103252.

[71] Roß, M., Gil-Escrig, L., Al-Ashouri, A., Tockhorn, P., Jošt, M., Rech, B., Albrecht, S. (2020). Co-evaporated p-i-n perovskite solar cells beyond 20% efficiency: Impact of substrate temperature and hole-transport layer. *ACS Applied Materials & Interfaces*, 12: 39261–39272.

[72] Feng, J., Jiao, Y., Wang, H., Zhu, X., Sun, Y., Du, M., Cao, Y., Yang, D., Liu, S. (2021). High-throughput large-area vacuum deposition for high-performance formamidine-based perovskite solar cells. *Energy & Environmental Science*, 14: 3035–3043.

[73] Chen, C. W., Kang, H. W., Hsiao, S. Y., Yang, P. F., Chiang, K. M., Lin, H. W. (2014). Efficient and uniform planar-type perovskite solar cells by simple sequential vacuum deposition. *Advanced Materials*, 26: 6647–6652.

[74] Hsiao, S. Y., Lin, H. L., Lee, W. H., Tsai, W. L., Chiang, K. M., Liao, W. Y., Ren-Wu, C. Z., Chen, C. Y., Lin, H. W. (2016). Efficient all-vacuum deposited perovskite solar cells by controlling reagent partial pressure in high vacuum. *Advanced Materials*, 28: 7013–7019.

[75] Tong, G., Li, H., Li, G., Zhang, T., Li, C., Yu, L., Xu, J., Jiang, Y., Shi, Y., Chen, K. (2018). Mixed cation perovskite solar cells by stack-sequence chemical vapor deposition with self-passivation and gradient absorption layer. *Nano Energy*, 48: 536–542.

[76] Luo, L., Zhang, Y., Chai, N., Deng, X., Zhong, J., Huang, F., Peng, Y., Ku, Z., Cheng, Y.B. (2018). Large-area perovskite solar cells with $Cs_xFA_{1-x}PbI_{3-y}Br_y$ thin films deposited by a vapor–solid reaction method. *Journal of Materials Chemistry A*, 6: 21143–21148.

[77] Luo, L., Ku, Z., Li, W., Zheng, X., Li, X., Huang, F., Peng, Y., Ding, L., Cheng, Y. B. (2021). 19.59% Efficiency from $Rb_{0.04}Cs_{0.14}FA_{0.86}Pb(Br_yI_{1-y})_3$ perovskite solar cells made by vapor-solid reaction technique. *Science Bulletin*, 66: 962–964.

[78] Zhang, G., Luo, W., Dai, H., Li, N., Li, Y., Peng, Y., Huang, F., Ku, Z., Cheng, Y.B. (2022). Ultrafast growth of high-quality $Cs_{0.14}FA_{0.86}Pb(Br_xI_{1-x})_3$ thin films achieved using super-close-space sublimation. *ACS Applied Energy Materials*, 5: 5797–5803.

[79] Leyden, M. R., Ono, L. K., Raga, S. R., Kato, Y., Wang, S., Qi, Y. (2014). High performance perovskite solar cells by hybrid chemical vapor deposition. *Journal of Materials Chemistry A*, 2: 18742–18745.

[80] Qiu, L., He, S., Jiang, Y., Son, D. Y., Ono, L. K., Liu, Z., Kim, T., Bouloumis, T., Kazaoui, S., Qi, Y. (2019). Hybrid chemical vapor deposition enables scalable and stable Cs-FA mixed cation perovskite solar modules with a designated area of 91.8 cm^2 approaching 10% efficiency. *Journal of Materials Chemistry A*, 7: 6920–6929.

[81] Fei, C., Guo, L., Li, B., Zhang, R., Fu, H., Tian, J., Cao, G. (2016). Controlled growth of textured perovskite films towards high performance solar cells. *Nano Energy*, 27: 17–26.

[82] Ma, Z., Liu, Z., Lu, S., Wang, L., Feng, X., Yang, D., Wang, K., Xiao, G., Zhang, L., Redfern, S. A. T., et al. (2018). Pressure-induced emission of cesium lead halide perovskite nanocrystals. *Nature Communications*, 9: 4506.

[83] Guo, F., Qiu, S., Hu, J., Wang, H., Cai, B., Li, J., Yuan, X., Liu, X., Forberich, K., Brabec, C. J., et al. (2019). A generalized crystallization protocol for scalable deposition of high-quality perovskite thin films for photovoltaic applications. *Advanced Science*, 6: 1901067.

[84] Stranks, S. D., Eperon, G. E., Grancini, G., Menelaou, C., Alcocer, M. J., Leijtens, T., Herz, L. M., Petrozza, A., Snaith, H. J. (2013). Electron-hole diffusion lengths exceeding 1 micrometer in an organometal trihalide perovskite absorber. *Science*, 342: 341–344.

[85] Lu, H., Krishna, A., Zakeeruddin, S. M., Grätzel, M., Hagfeldt, A. (2020). Compositional and interface engineering of organic-inorganic lead halide perovskite solar cells. *iScience*, 23: 101359.

[86] Lee, J. W., Kim, D. H., Kim, H. S., Seo, S. W., Cho, S. M., Park, N. G. (2015). Formamidinium and cesium hybridization for photo- and moisture-stable perovskite solar cell. *Advanced Energy Materials*, 5: 1501310.

[87] Eperon, G. E., Stranks, S. D., Menelaou, C., Johnston, M. B., Herz, L. M., Snaith, H. J. (2014). Formamidinium lead trihalide: A broadly tunable perovskite for efficient planar heterojunction solar cells. *Energy & Environmental Science*, 7: 982–988.

[88] Pang, S., Hu, H., Zhang, J., Lv, S., Yu, Y., Wei, F., Qin, T., Xu, H., Liu, Z., Cui, G. (2014). $NH_2CH{=}NH_2PbI_3$: An alternative organolead iodide perovskite sensitizer for mesoscopic solar cells. *Chemistry of Materials*, 26: 1485–1491.

[89] Yang, C., Wang, H., Miao, Y., Chen, C., Zhai, M., Bao, Q., Ding, X., Yang, X., Cheng, M. (2021). Interfacial molecular doping and energy level alignment regulation for perovskite solar cells with efficiency exceeding 23%. *ACS Energy Letters*, 6: 2690–2696.

[90] Luo, D., Yang, W., Wang, Z., Sadhanala, A., Hu, Q., Su, R., Shivanna, R., Trindade, G. F., Watts, J. F., Xu, Z., et al. (2018). Enhanced photovoltage for inverted planar heterojunction perovskite solar cells. *Science*, 360: 1442–1446.

[91] Min, H., Kim, M., Lee, S. U., Kim, H., Kim, G., Choi, K., Lee, J. H., Seok, S. I. (2019). Efficient, stable solar cells by using inherent bandgap of α-phase formamidinium lead iodide. *Science*, 366: 749–753.

[92] Kim, M., Kim, G. H., Lee, T. K., Choi, I. W., Choi, H. W., Jo, Y., Yoon, Y. J., Kim, J. W., Lee, J., Huh, D., et al. (2019). Methylammonium chloride induces intermediate phase stabilization for efficient perovskite solar cells. *Joule*, 3: 2179–2192.

[93] Lu, H., Liu, Y., Ahlawat, P., Mishra, A., Tress, W. R., Eickemeyer, F. T., Yang, Y., Fu, F., Wang, Z., Avalos, C. E., et al. (2020). Vapor-assisted deposition of highly efficient, stable black-phase $FAPbI_3$ perovskite solar cells. *Science*, 370: eabb8985.

[94] Ahmad, S., Fu, P., Yu, S., Yang, Q., Liu, X., Wang, X., Wang, X., Guo, X., Li, C. (2019). Dion-jacobson phase 2D layered perovskites for solar cells with ultrahigh stability. *Joule*, 3: 794–806.

[95] Chen, P., Bai, Y., Wang, S., Lyu, M., Yun, J. H., Wang, L. (2018). Perovskite solar cells: *in situ* growth of 2D perovskite capping layer for stable and efficient perovskite solar cells. *Advanced Functional Materials*, 28: 1706923.

[96] Chen, J., Seo, J. Y., Park, N. G. (2018). Simultaneous improvement of photovoltaic performance and stability by *in situ* formation of 2D perovskite at $(FAPbI_3)_{0.88}(CsPbBr_3)_{0.12}$/CuSCN interface. *Advanced Energy Materials*, 8: 1702714.

[97] Ma, C., Shen, D., Huang, B., Li, X., Chen, W. C., Lo, M. F., Wang, P., Lam, M. H. W., Lu, Y., Ma, B., et al. (2019). High performance low-dimensional perovskite solar cells based on a one dimensional lead iodide perovskite. *Journal of Materials Chemistry A*, 7: 8811–8817.

[98] Zhan, Y., Yang, F., Chen, W., Chen, H., Shen, Y., Li, Y., Li, Y. (2021). Elastic lattice and excess charge carrier manipulation in 1D-3D perovskite solar cells for exceptionally long-term operational stability. *Advanced Materials*, 33: e2105170.

[99] Wu, G., Liang, R., Ge, M., Sun, G., Zhang, Y., Xing, G. (2022). Surface passivation using 2D perovskites toward efficient and stable perovskite solar cells. *Advanced Materials*, 34: 2105635.

[100] Mahmud, M. A., Duong, T., Yin, Y., Pham, H. T., Walter, D., Peng, J., Wu, Y., Li, L., Shen, H., Wu, N., et al. (2020). Double-sided surface passivation of 3D perovskite film for high-efficiency mixed-dimensional perovskite solar cells. *Advanced Functional Materials*, 30: 1907962.

[101] Chen, S., Shen, N., Zhang, L., Zhang, L., Cheung, S. H., Chen, S., So, S. K., Xu, B. (2020). Understanding the interplay of binary organic spacer in ruddlesden–popper perovskites toward efficient and stable solar cells. *Advanced Functional Materials*, 30: 1907759.

[102] Azmi, R., Ugur, E., Seitkhan, A., Aljamaan, F., Subbiah, A. S., Liu, J., Harrison, G. T., Nugraha, M. I., Eswaran, M. K., Babics, M., et al. (2022). Damp heat-stable perovskite solar cells with tailored-dimensionality 2D/3D heterojunctions. *Science*, 376: 73–77.

[103] Wang, Z., Lin, Q., Chmiel, F. P., Sakai, N., Herz, L. M., Snaith, H. J. (2017). Efficient ambient-air-stable solar cells with 2D-3D heterostructured butylammonium-caesium-formamidinium lead halide perovskites. *Nature Energy*, 2: 17135.

[104] Yuan, S., Xian, Y., Long, Y., Cabot, A., Li, W., Fan, J. (2021). Chromium-based metal–organic framework as A-site cation in $CsPbI_2Br$ perovskite solar cells. *Advanced Functional Materials*, 31: 2106233.

[105] Mahmud, M. A., Duong, T., Peng, J., Wu, Y., Shen, H., Walter, D., Nguyen, H. T., Mozaffari, N., Tabi, G. D., Catchpole, K. R., et al. (2022). Origin of efficiency and stability enhancement in high-performing mixed dimensional 2D-3D perovskite solar cells: A review. *Advanced Functional Materials*, 32: 2009164.

[106] Jang, Y. W., Lee, S., Yeom, K. M., Jeong, K., Choi, K., Choi, M., Noh, J. H. (2021). Intact 2D/3D halide junction perovskite solar cells via solid-phase in-plane growth. *Nature Energy*, 6: 63–71.

[107] Fan, J., Ma, Y., Zhang, C., Liu, C., Li, W., Schropp, R. E. I., Mai, Y. (2018). Thermodynamically self-healing 1D–3D hybrid perovskite solar cells. *Advanced Energy Materials*, 8: 1703421.

[108] Liu, P., Xian, Y., Yuan, W., Long, Y., Liu, K., Rahman, N. U., Li, W., Fan, J. (2020). Lattice-matching structurally-stable 1D@3D perovskites toward highly efficient and stable solar cells. *Advanced Energy Materials*, 10: 1903654.

[109] Kong, T., Xie, H., Zhang, Y., Song, J., Li, Y., Lim, E. L., Hagfeldt, A., Bi, D. (2021). Perovskitoid-templated formation of a 1D@3D perovskite structure toward highly efficient and stable perovskite solar cells. *Advanced Energy Materials*, 11: 2101018.

[110] Long, Y., Xian, Y., Yuan, S., Liu, K., Sun, M., Guo, Y., Rahman, N. U., Fan, J., Li, W. (2021). π-π conjugate structure enabling the channel construction of carrier-facilitated transport in 1D-3D multi-dimensional $CsPbI_2Br$ solar cells with high stability. *Nano Energy*, 89: 106340.

[111] Liu, K., Yuan, S., Xian, Y., Long, Y., Yao, Q., Rahman, N. U., Guo, Y., Sun, M., Xue, Q., Yip, H. L., et al. (2021). Architecturing 1D-2D-3D multidimensional coupled $CsPbI_2$ Br perovskites toward highly effective and stable solar cells. *Small*, 17: e2100888.

[112] Yang, N., Zhu, C., Chen, Y., Zai, H., Wang, C., Wang, X., Wang, H., Ma, S., Gao, Z., Wang, X., et al. (2020). An *in situ* cross-linked 1D/3D perovskite heterostructure improves the stability of hybrid perovskite solar cells for over 3000 h operation. *Energy & Environmental Science*, 13: 4344–4352.

[113] Li, W., Zhang, C., Ma, Y., Liu, C., Fan, J., Mai, Y., Schropp, R. E. I. (2018). *In situ* induced core/shell stabilized hybrid perovskites *via* gallium(iii) acetylacetonate intermediate towards highly efficient and stable solar cells. *Energy & Environmental Science*, 11: 286–293.

[114] Bai, F., Zhang, J., Yuan, Y., Liu, H., Li, X., Chueh, C. C., Yan, H., Zhu, Z., Jen, A. K. (2019). A 0D/3D heterostructured all-inorganic halide perovskite solar cell with high performance and enhanced phase stability. *Advanced Materials*, 31: e1904735.

[115] Zhu, J., He, B., Yao, X., Chen, H., Duan, Y., Duan, J., Tang, Q. (2022). Phase control of Cs-Pb-Br derivatives to suppress 0D Cs_4PbBr_6 for high-efficiency and stable all-inorganic $CsPbBr_3$ perovskite solar cells. *Small*, 18: e2106323.

[116] Fan, Y., Wang, X., Miao, Y., Zhao, Y. (2021). The chemical design in high-performance lead halide perovskite: Additive vs dopant. *Journal of Physical Chemistry Letters*, 12: 11636–11644.

[117] Zhao, Y., Zhu, K. (2014). CH_3NH_3Cl-assisted one-step solution growth of $CH_3NH_3PbI_3$: Structure, charge-carrier dynamics, and photovoltaic properties of perovskite solar cells. *Journal of Physical Chemistry C*, 118: 9412–9418.

[118] Zhao, Y., Zhu, K. (2014). Efficient planar perovskite solar cells based on 1.8 eV band gap $CH_3NH_3PbI_2Br$ nanosheets via thermal decomposition. *Journal of the American Chemical Society*, 136: 12241–12244.

[119] Zuo, C., Tan, L., Dong, H., Chen, J., Hao, F., Yi, C., Ding, L. (2023). Natural drying yields efficient perovskite solar cells. *DeCarbon*, 2: 100020.

[120] Zuo, C., Ding, L. (2014). An 80.11% FF record achieved for perovskite solar cells by using the NH_4Cl additive. *Nanoscale*, 6: 9935–9938.

[121] Zhao, Y., Zhu, K. (2015). Three-step sequential solution deposition of PbI_2-free $CH_3NH_3PbI_3$ perovskite. *Journal of Materials Chemistry A*, 3: 9086–9091.

[122] Ke, W., Spanopoulos, I., Stoumpos, C. C., Kanatzidis, M. G. (2018). Myths and reality of $HPbI_3$ in halide perovskite solar cells. *Nature Communications*, 9: 4785.

[123] Wang, Y., Liu, X., Zhang, T., Wang, X., Kan, M., Shi, J., Zhao, Y. (2019). The role of dimethylammonium iodide in $CsPbI_3$ perovskite fabrication: Additive or dopant. *Angewandte Chemie International Edition*, 58: 16691–16696.

[124] Tan, S., Yu, B., Cui, Y., Meng, F., Huang, C., Li, Y., Chen, Z., Wu, H., Shi, J., Luo, Y., Li, D., et al. (2022). Temperature-reliable low-dimensional perovskites passivated black-phase $CsPbI_3$ toward stable and efficient photovoltaics. *Angewandte Chemie International Edition*, 61: e202201300.

[125] Kim, D. H., Muzzillo, C. P., Tong, J., Palmstrom, A. F., Larson, B. W., Choi, C., Harvey, S. P., Glynn, S., Whitaker, J. B., Zhang, F., et al. (2019). Bimolecular additives improve wide-band-gap perovskites for efficient tandem solar cells with CIGS. *Joule*, 3: 1734–1745.

[126] Abdi-Jalebi, M., Andaji-Garmaroudi, Z., Cacovich, S., Stavrakas, C., Philippe, B., Richter, J. M., Alsari, M., Booker, E. P., Hutter, E. M., Pearson, A. J., et al. (2018). Maximizing and stabilizing luminescence from halide perovskites with potassium passivation. *Nature*, 555: 497–501.

[127] Bai, S., Da, P., Li, C., Wang, Z., Yuan, Z., Fu, F., Kawecki, M., Liu, X., Sakai, N., Wang, J. T. W., et al. (2019). Planar perovskite solar cells with long-term stability using ionic liquid additives. *Nature*, 571: 245–250.

[128] Deng, Y., Zheng, X., Bai, Y., Wang, Q., Zhao, J., Huang, J. (2018). Surfactant-controlled ink drying enables high-speed deposition of perovskite films for efficient photovoltaic modules. *Nature Energy*, 3: 560–566.

[129] Chen, S., Dai, X., Xu, S., Jiao, H., Zhao, L., Huang, J. (2021). Stabilizing perovskite-substrate interfaces for high-performance perovskite modules. *Science*, 373: 902–907.

[130] Bi, D., Yi, C., Luo, J., Décoppet, J. D., Zhang, F., Zakeeruddin, S. M., Li, X., Hagfeldt, A., Grätzel, M. (2016). Polymer-templated nucleation and crystal growth of perovskite films for solar cells with efficiency greater than 21%. *Nature Energy*, 1: 16142.

[131] Peng, J., Kremer, F., Walter, D., Wu, Y., Ji, Y., Xiang, J., Liu, W., Duong, T., Shen, H., Lu, T., et al. (2022). Centimetre-scale perovskite solar cells with fill factors of more than 86 per cent. *Nature*, 601: 573–578.

[132] Kim, J. E., Kim, S. S., Zuo, C., Gao, M., Vak, D., Kim, D. Y. (2019). Humidity-tolerant roll-to-roll fabrication of perovskite solar cells via polymer-additive-assisted hot slot die deposition. *Advanced Functional Materials*, 29: 1809194.

[133] Zhao, Y., Zhu, K. (2014). Solution chemistry engineering toward high-efficiency perovskite solar cells. *Journal of Physical Chemistry Letters*, 5: 4175–4186.

[134] Chen, H., Wei, Z., He, H., Zheng, X., Wong, K. S., Yang, S. (2016). Solvent engineering boosts the efficiency of paintable carbon-based perovskite solar cells to beyond 14%. *Advanced Energy Materials*, 6: 1502087.

[135] Bai, Y., Xiao, S., Hu, C., Zhang, T., Meng, X., Li, Q., Yang, Y., Wong, K. S., Chen, H., Yang, S. (2017). A pure and stable intermediate phase is key to growing aligned and vertically monolithic perovskite crystals for efficient PIN planar perovskite solar cells with high processibility and stability. *Nano Energy*, 34: 58–68.

[136] Yan, K., Long, M., Zhang, T., Wei, Z., Chen, H., Yang, S., Xu, J. (2015). Hybrid halide perovskite solar cell precursors: Colloidal chemistry and coordination engineering behind device processing for high efficiency. *Journal of the American Chemical Society*, 137: 4460–4468.

[137] Zhang, K., Wang, Z., Wang, G., Wang, J., Li, Y., Qian, W., Zheng, S., Xiao, S., Yang, S. (2020). A prenucleation strategy for ambient fabrication of perovskite solar cells with high device performance uniformity. *Nature Communications*, 11: 1006.

[138] Yang, G., Zhang, H., Li, G., Fang, G. (2019). Stabilizer-assisted growth of formamdinium-based perovskites for highly efficient and stable planar solar cells with over 22% efficiency. *Nano Energy*, 63: 103835.

[139] Wu, C., Wang, D., Zhang, Y., Gu, F., Liu, G., Zhu, N., Luo, W., Han, D., Guo, X., Qu, B., et al. (2019). $FAPbI_3$ flexible solar cells with a record efficiency of 19.38% fabricated in air via ligand and additive synergetic process. *Advanced Functional Materials*, 29: 1902974.

[140] Tavakoli, M. M., Saliba, M., Yadav, P., Holzhey, P., Hagfeldt, A., Zakeeruddin, S. M., Grätzel, M. (2019). Synergistic crystal and interface engineering for efficient and stable perovskite photovoltaics. *Advanced Energy Materials*, 9: 1802646.

[141] Xie, F., Chen, C. C., Wu, Y., Li, X., Cai, M., Liu, X., Yang, X., Han, L. (2017). Vertical recrystallization for highly efficient and stable formamidinium-based inverted-structure perovskite solar cells. *Energy & Environmental Science*, 10: 1942–1949.

[142] Meng, X., Wang, Z., Qian, W., Zhu, Z., Zhang, T., Bai, Y., Hu, C., Xiao, S., Yang, Y., Yang, S. (2019). Excess cesium iodide induces spinodal decomposition of $CsPbI_2Br$ perovskite films. *Journal of Physical Chemistry Letters*, 10: 194–199.

[143] Meng, X., Li, Y., Qu, Y., Chen, H., Jiang, N., Li, M., Xue, D. J., Hu, J. S., Huang, H., Yang, S. (2021). Crystallization kinetics modulation of $FASnI_3$ films with pre-nucleation clusters for efficient lead-free perovskite solar cells. *Angewandte Chemie International Edition*, 60: 3693–3698.

[144] Bu, T., Ono, L. K., Li, J., Su, J., Tong, G., Zhang, W., Liu, Y., Zhang, J., Chang, J., Kazaoui, S., et al. (2022). Modulating crystal growth of formamidinium-caesium perovskites for over 200 Cm2 photovoltaic sub-modules. *Nature Energy*, 7: 528–536.

[145] Kim, Y. Y., Yang, T. Y., Suhonen, R., Kemppainen, A., Hwang, K., Jeon, N. J., Seo, J. (2020). Roll-to-roll gravure-printed flexible

perovskite solar cells using eco-friendly antisolvent bathing with wide processing window. *Nature Communications*, 11: 5146.
[146] Wang, Y., Wu, J., Zhang, P., Liu, D., Zhang, T., Ji, L., Gu, X., Chen, Z. D., Li, S. (2017). Stitching triple cation perovskite by a mixed anti-solvent process for high performance perovskite solar cells. *Nano Energy*, 39: 616–625.
[147] Gedamu, D., Asuo, I. M., Benetti, D., Basti, M., Ka, I., Cloutier, S. G., Rosei, F., Nechache, R. (2018). Solvent-antisolvent ambient processed large grain size perovskite thin films for high-performance solar cells. *Scientific Reports*, 8: 12885.
[148] Lou, L., Liu, T., Xiao, J., Xiao, S., Long, X., Zheng, S., Yang, S. (2020). Controlling apparent coordinated solvent number in the perovskite intermediate phase film for developing large-area perovskite solar modules. *Energy Technology*, 8: 1900972.
[149] Bai, Y., Xiao, S., Hu, C., Zhang, T., Meng, X., Lin, H., Yang, Y., Yang, S. (2017). Dimensional engineering of a graded 3D–2D halide perovskite interface enables ultrahigh V_{oc} enhanced stability in the p-i-n photovoltaics. *Advanced Energy Materials*, 7: 1701038.
[150] Liu, Q., Jiang, Y., Jin, K., Qin, J., Xu, J., Li, W., Xiong, J., Liu, J., Xiao, Z., Sun, K., et al. (2020). 18% Efficiency organic solar cells. *Science Bulletin*, 65: 272–275.
[151] Al-Dainy, G., Watanabe, F., Biris, A. S., Bourdo, S. E. (2021). Surface passivation of triple-cation perovskite via organic halide-saturated antisolvent for inverted planar solar cells. *ACS Applied Energy Materials*, 4: 3297–3309.
[152] Zhou, L., Chang, J., Liu, Z., Sun, X., Lin, Z., Chen, D., Zhang, C., Zhang, J., Hao, Y. (2018). Enhanced planar perovskite solar cell efficiency and stability using a perovskite/PCBM heterojunction formed in one step. *Nanoscale*, 10: 3053–3059.
[153] Zhang, F., Shi, W., Luo, J., Pellet, N., Yi, C., Li, X., Zhao, X., Dennis, T. J. S., Li, X., Wang, S., et al. (2017). Isomer-pure bis-PCBM-assisted crystal engineering of perovskite solar cells showing excellent efficiency and stability. *Advanced Materials*, 29: 1606806.
[154] Niu, T., Lu, J., Munir, R., Li, J., Barrit, D., Zhang, X., Hu, H., Yang, Z., Amassian, A., Zhao, K., et al. (2018). Stable high-performance perovskite solar cells via grain boundary passivation. *Advanced Materials*, 30: e1706576.
[155] Li, F., Yuan, J., Ling, X., Zhang, Y., Yang, Y., Cheung, S. H., Ho, C. H. Y., Gao, X., Ma, W. (2018). A universal strategy to utilize polymeric semiconductors for perovskite solar cells with enhanced efficiency and longevity. *Advanced Functional Materials*, 28: 1706377 [166] Li, F., Yuan, J., Ling, X., Zhang, Y., Yang, Y., Hang Cheung, S., Hoi Yi Ho, C., Gao, X., Ma, W. (2018). A universal strategy to utilize polymeric semiconductors for perovskite solar cells with enhanced effciency and longevity. *Advanced Functional Materials*, 28: 1706377.
[156] Leijtens, T., Eperon, G. E., Pathak, S., Abate, A., Lee, M. M., Snaith, H. J. (2013). Overcoming ultraviolet light instability of sensitized TiO_2 with meso-superstructured organometal tri-halide perovskite solar cells. *Nature Communications*, 4: 2885.
[157] Liu, D., Kelly, T. L. (2014). Perovskite solar cells with a planar heterojunction structure prepared using room-temperature solution processing techniques. *Nature Photonics*, 8: 133–138.
[158] Shin, S. S., Yeom, E. J., Yang, W. S., Hur, S., Kim, M. G., Im, J., Seo, J., Noh, J. H., Seok, S. I. (2017). Colloidally prepared La-doped $BaSnO_3$ electrodes for efficient, photostable perovskite solar cells. *Science*, 356: 167–171.
[159] Shin, S. S., Yang, W. S., Noh, J. H., Suk, J. H., Jeon, N. J., Park, J. H., Kim, J. S., Seong, W. M., Seok, S. I. (2015). High-performance flexible perovskite solar cells exploiting Zn_2SnO_4 prepared in solution below 100 ℃. *Nature Communications*, 6: 7410.
[160] Liu, J., Gao, C., Luo, L., Ye, Q., He, X., Ouyang, L., Guo, X., Zhuang, D., Liao, C., Mei, J., et al. (2015). Low-temperature, solution processed metal sulfide as an electron transport layer for efficient planar perovskite solar cells. *Journal of Materials Chemistry A*, 3: 11750–11755.
[161] Yoon, H., Kang, S. M., Lee, J. K., Choi, M. (2016). Hysteresis-free low-temperature-processed planar perovskite solar cells with 19.1% efficiency. *Energy & Environmental Science*, 9: 2262–2266.
[162] Wang, S., Huang, Z., Wang, X., Li, Y., Günther, M., Valenzuela, S., Parikh, P., Cabreros, A., Xiong, W., Meng, Y. S. (2018). Unveiling the role of tBP-LiTFSI complexes in perovskite solar cells. *Journal of the American Chemical Society*, 140: 16720–16730.
[163] Kong, J., Shin, Y., Röhr, J. A., Wang, H., Meng, J., Wu, Y., Katzenberg, A., Kim, G., Kim, D. Y., Li, T. D., et al. (2021). CO_2 doping of organic interlayers for perovskite solar cells. *Nature*, 594: 51–56.
[164] Jeong, M., Choi, I. W., Yim, K., Jeong, S., Kim, M., Choi, S. J., Cho, Y., An, J. H., Kim, H. B., Jo, Y., et al. (2022). Large-area perovskite solar cells employing spiro-Naph hole transport material. *Nature Photonics*, 16: 119–125.
[165] Jeong, M. J., Yeom, K. M., Kim, S. J., Jung, E. H., Noh, J. H. (2021). Spontaneous interface engineering for dopant-free poly(3-hexylthiophene) perovskite solar cells with efficiency over 24%. *Energy & Environmental Science*, 14: 2419–2428.
[166] Fu, Q., Xu, Z., Tang, X., Liu, T., Dong, X., Zhang, X., Zheng, N., Xie, Z., Liu, Y. (2021). Multifunctional two-dimensional conjugated materials for dopant-free perovskite solar cells with efficiency exceeding 22%. *ACS Energy Letters*, 6: 1521–1532.
[167] Fu, Q., Tang, X., Liu, H., Wang, R., Liu, T., Wu, Z., Woo, H. Y., Zhou, T., Wan, X., Chen, Y., et al. (2022). Ionic dopant-free polymer alloy hole transport materials for high-performance perovskite solar cells. *Journal of the American Chemical Society*, 144: 9500–9509.
[168] Arora, N., Dar, M. I., Hinderhofer, A., Pellet, N., Schreiber, F., Zakeeruddin, S. M., Grätzel, M. (2017). Perovskite solar cells with CuSCN hole extraction layers yield stabilized efficiencies greater than 20%. *Science*, 358: 768–771.
[169] Christians, J. A., Fung, R. C., Kamat, P. V. (2014). An inorganic hole conductor for organo-lead halide perovskite solar cells. Improved hole conductivity with copper iodide. *Journal of the American Chemical Society*, 136: 758–764.
[170] Hu, L., Li, M., Yang, K., Xiong, Z., Yang, B., Wang, M., Tang, X., Zang, Z., Liu, X., Li, B., et al. (2018). PEDOT: PSS monolayers to enhance the hole extraction and stability of perovskite solar cells. *Journal of Materials Chemistry A*, 6: 16583–16589.
[171] Hu, L., Fu, J., Yang, K., Xiong, Z., Wang, M., Yang, B., Wang, H., Tang, X., Zang, Z., Li, M., et al. (2019). Inhibition of In-plane charge transport in hole transfer layer to achieve high fill factor for inverted planar perovskite solar cells. *Solar RRL*, 3: 1900104.
[172] Li, Z., Li, B., Wu, X., Sheppard, S. A., Zhang, S., Gao, D., Long, N. J., Zhu, Z. (2022). Organometallic-functionalized interfaces for highly efficient inverted perovskite solar cells. *Science*, 376: 416–420.
[173] Zhu, Z., Bai, Y., Zhang, T., Liu, Z., Long, X., Wei, Z., Wang, Z., Zhang, L., Wang, J., Yan, F., et al. (2014). High-performance hole-extraction layer of sol-gel-processed NiO nanocrystals for inverted planar perovskite solar cells. *Angewandte Chemie International Edition*, 53: 12571–12575.
[174] Hou, F., Su, Z., Jin, F., Yan, X., Wang, L., Zhao, H., Zhu, J., Chu, B., Li, W. (2015). Efficient and stable planar heterojunction perovskite solar cells with an MoO_3/PEDOT: PSS hole transporting layer. *Nanoscale*, 7: 9427–9432.
[175] Cheng, M., Li, Y., Safdari, M., Chen, C., Liu, P., Kloo, L., Sun, L. (2017). Efficient perovskite solar cells based on a solution processable nickel(II) phthalocyanine and vanadium oxide integrated hole transport layer. *Advanced Energy Materials*, 7:
[176] Grimme, S., Antony, J., Ehrlich, S., Krieg, H. (2010). A consistent and accurate *ab initio* parametrization of density functional dispersion correction (DFT-D) for the 94 elements H-Pu. *The Journal of Chemical Physics*, 132: 154104.
[177] Yin, W.J., Shi, T., Yan, Y. (2014). Unusual defect physics in CH_3NH_3PbI3 perovskite solar cell absorber. *Applied Physics Letters*, 104: 063903.
[178] Bai, Y., Lin, Y., Ren, L., Shi, X., Strounina, E., Deng, Y., Wang, Q., Fang, Y., Zheng, X., Lin, Y., et al. (2019). Oligomeric silica-

wrapped perovskites enable synchronous defect passivation and grain stabilization for efficient and stable perovskite photovoltaics. *ACS Energy Letters*, 4: 1231–1240.

[179] Jung, M., Shin, T. J., Seo, J., Kim, G., Seok, S. I. (2018). Structural features and their functions in surfactant-armoured methylammonium lead iodide perovskites for highly efficient and stable solar cells. *Energy & Environmental Science*, 11: 2188–2197.

[180] Xiong, Z., Chen, S., Zhao, P., Cho, Y., Odunmbaku, G. O., Zheng, Y., Jones, D. J., Yang, C., Sun, K. (2021). Phase transition modulation and defect suppression in perovskite solar cells enabled by a self-sacrificed template. *Solar RRL*, 5: 2100448.

[181] Yu, B., Zhang, L., Wu, J., Liu, K., Wu, H., Shi, J., Luo, Y., Li, D., Bo, Z., Meng, Q. (2020). Application of a new π-conjugated ladder-like polymer in enhancing the stability and efficiency of perovskite solar cells. *Journal of Materials Chemistry A*, 8: 1417–1424.

[182] Li, M., Li, H., Zhuang, Q., He, D., Liu, B., Chen, C., Zhang, B., Pauporté, T., Zang, Z., Chen, J. (2022). Stabilizing perovskite precursor by synergy of functional groups for NiO_x-based inverted solar cells with 23.5 % efficiency. *Angewandte Chemie International Edition*, 61: e202206914.

[183] Li, X., Zhang, W., Guo, X., Lu, C., Wei, J., Fang, J. (2022). Constructing heterojunctions by surface sulfidation for efficient inverted perovskite solar cells. *Science*, 375: 434–437.

[184] Gu, L., Wang, S., Chen, Y., Xu, Y., Li, R., Liu, D., Fang, X., Jia, X., Yuan, N., Ding, J. (2021). Stable high-performance perovskite solar cells via passivation of the grain boundary and interface. *ACS Applied Energy Materials*, 4: 6883–6891.

[185] de Quilettes, D. W., Koch, S., Burke, S., Paranji, R. K., Shropshire, A. J., Ziffer, M. E., Ginger, D. S. (2016). Photoluminescence lifetimes exceeding 8 μs and quantum yields exceeding 30% in hybrid perovskite thin films by ligand passivation. *ACS Energy Letters*, 1: 438–444.

[186] Noel, N. K., Abate, A., Stranks, S. D., Parrott, E. S., Burlakov, V. M., Goriely, A., Snaith, H. J. (2014). Enhanced photoluminescence and solar cell performance via Lewis base passivation of organic-inorganic lead halide perovskites. *ACS Nano*, 8: 9815–9821.

[187] Zhang, Y., Fei, Z., Gao, P., Lee, Y., Tirani, F. F., Scopelliti, R., Feng, Y., Dyson, P. J., Nazeeruddin, M. K. (2017). A strategy to produce high efficiency, high stability perovskite solar cells using functionalized ionic liquid-dopants. *Advanced Materials*, 29: 1702157.

[188] Liu, B., Bi, H., He, D., Bai, L., Wang, W., Yuan, H., Song, Q., Su, P., Zang, Z., Zhou, T., et al. (2021). Interfacial defect passivation and stress release via multi-active-site ligand anchoring enables efficient and stable methylammonium-free perovskite solar cells. *ACS Energy Letters*, 6: 2526–2538.

[189] Zhu, L., Zhang, X., Li, M., Shang, X., Lei, K., Zhang, B., Chen, C., Zheng, S., Song, H., Chen, J. (2021). Trap state passivation by rational ligand molecule engineering toward efficient and stable perovskite solar cells exceeding 23% efficiency. *Advanced Energy Materials*, 11: 2100529.

[190] Xiong, Z., Lan, L., Wang, Y., Lu, C., Qin, S., Chen, S., Zhou, L., Zhu, C., Li, S., Meng, L., et al. (2021). Multifunctional polymer framework modified SnO_2 enabling a photostable α-$FAPbI_3$ perovskite solar cell with efficiency exceeding 23%. *ACS Energy Letters*, 6: 3824–3830.

[191] Cong, S., Liu, X., Jiang, Y., Zhang, W., Zhao, Z. (2020). Surface enhanced Raman scattering revealed by interfacial charge-transfer transitions. *The Innovation*, 1: 100051.

[192] Chen, J., Zhao, X., Kim, S. G., Park, N. G. (2019). Multifunctional chemical linker imidazoleacetic acid hydrochloride for 21% efficient and stable planar perovskite solar cells. *Advanced Materials*, 31: e1902902.

[193] Zhou, Q., He, D., Zhuang, Q., Liu, B., Li, R., Li, H., Zhang, Z., Yang, H., Zhao, P., He, Y., et al. (2022). Revealing steric-hindrance-dependent buried interface defect passivation mechanism in efficient and stable perovskite solar cells with mitigated tensile stress. *Advanced Functional Materials*, 32: 2205507.

[194] Xiong, Z., Chen, X., Zhang, B., Odunmbaku, G. O., Ou, Z., Guo, B., Yang, K., Kan, Z., Lu, S., Chen, S., et al. (2022). Simultaneous interfacial modification and crystallization control by biguanide hydrochloride for stable perovskite solar cells with PCE of 24.4. *Advanced Materials*, 34: e2106118.

[195] Kim, M., Jeong, J., Lu, H., Lee, T. K., Eickemeyer, F. T., Liu, Y., Choi, I. W., Choi, S. J., Jo, Y., Kim, H. B., et al. (2022). Conformal quantum dot-SnO_2 layers as electron transporters for efficient perovskite solar cells. *Science*, 375: 302–306.

[196] Chen, J., Kim, S. G., Park, N. G. (2018). $FA_{0.88}Cs_{0.12}PbI_{3-x}(PF_6)_x$ interlayer formed by ion exchange reaction between perovskite and hole transporting layer for improving photovoltaic performance and stability. *Advanced Materials*, 30: 1801948.

[197] Meng, L., Sun, C., Wang, R., Huang, W., Zhao, Z., Sun, P., Huang, T., Xue, J., Lee, J. W., Zhu, C., et al. (2018). Tailored phase conversion under conjugated polymer enables thermally stable perovskite solar cells with efficiency exceeding 21. *Journal of the American Chemical Society*, 140: 17255–17262.

[198] Fu, Q., Liu, H., Tang, X., Wang, R., Chen, M., Liu, Y. (2022). Multifunctional two-dimensional polymers for perovskite solar cells with efficiency exceeding 24%. *ACS Energy Letters*, 7: 1128–1136.

[199] Degani, M., An, Q., Albaladejo-Siguan, M., Hofstetter, Y. J., Cho, C., Paulus, F., Grancini, G., Vaynzof, Y. (2021). 23.7% Efficient inverted perovskite solar cells by dual interfacial modification. *Science Advances*, 7: eabj7930.

[200] Hu, L., Sun, K., Wang, M., Chen, W., Yang, B., Fu, J., Xiong, Z., Li, X., Tang, X., Zang, Z., et al. (2017). Inverted planar perovskite solar cells with a high fill factor and negligible hysteresis by the dual effect of NaCl-doped PEDOT: PSS. *ACS Applied Materials & Interfaces*, 9: 43902–43909.

[201] Liu, X., Li, B., Zhang, N., Yu, Z., Sun, K., Tang, B., Shi, D., Yao, H., Ouyang, J., Gong, H. (2018). Multifunctional RbCl dopants for efficient inverted planar perovskite solar cell with ultra-high fill factor, negligible hysteresis and improved stability. *Nano Energy*, 53: 567–578.

[202] Yablonovitch, E. (1982). Statistical ray optics. *Journal of the Optical Society of America*, 72: 899–907.

[203] Wang, Y., Wang, P., Zhou, X., Li, C., Li, H., Hu, X., Li, F., Liu, X., Li, M., Song, Y. (2018). Solar cells: Diffraction-grated perovskite induced highly efficient solar cells through nanophotonic light trapping. *Advanced Energy Materials*, 8: 1702960.

[204] Kang, S. M., Jang, S., Lee, J. K., Yoon, J., Yoo, D. E., Lee, J. W., Choi, M., Park, N. G. (2016). Moth-eye TiO_2 layer for improving light harvesting efficiency in perovskite solar cells. *Small*, 12: 2443–2449.

[205] Wang, Y., Li, M., Zhou, X., Li, P., Hu, X., Song, Y. (2018). High efficient perovskite whispering-gallery solar cells. *Nano Energy*, 51: 556–562.

[206] Hörantner, M. T., Zhang, W., Saliba, M., Wojciechowski, K., Snaith, H. J. (2015). Templated microstructural growth of perovskite thin films *via* colloidal monolayer lithography. *Energy & Environmental Science*, 8: 2041–2047.

[207] Wei, J., Xu, R.P., Li, Y.Q., Li, C., Chen, J.D., Zhao, X.D., Xie, Z.Z., Lee, C. S., Zhang, W.J., Tang, J.X. (2017). Perovskite solar cells: Enhanced light harvesting in perovskite solar cells by a bioinspired nanostructured back electrode. *Advanced Energy Materials*, 7: 1700492.

[208] Pascoe, A. R., Meyer, S., Huang, W., Li, W., Benesperi, I., Duffy, N. W., Spiccia, L., Bach, U., Cheng, Y.B. (2016). Enhancing the optoelectronic performance of perovskite solar cells via a textured $CH_3NH_3PbI_3$Morphology. *Advanced Functional Materials*, 26: 1278–1285.

[209] Guo, P., Zhu, H., Zhao, W., Liu, C., Zhu, L., Ye, Q., Jia, N., Wang, H., Zhang, X., Huang, W., et al. (2021). Interfacial embedding of laser-manufactured fluorinated gold clusters enabling stable perovskite solar cells with efficiency over 24. *Advanced Materials*, 33: e2101590.

[210] Schuster, C. S., Kowalczewski, P., Martins, E. R., Patrini, M., Scullion, M. G., Liscidini, M., Lewis, L., Reardon, C., Andreani, L. C., Krauss, T. F. (2013). Dual gratings for enhanced light trapping in thin-film solar cells by a layer-transfer technique. *Optics Express*, 21: A433–A439.

[211] Wang, K. X., Yu, Z., Liu, V., Cui, Y., Fan, S. (2012). Absorption enhancement in ultrathin crystalline silicon solar cells with antireflection and light-trapping nanocone gratings. *Nano Letters*, 12: 1616–1619.

[212] Wang, Y., Lan, Y., Song, Q., Vogelbacher, F., Xu, T., Zhan, Y., Li, M., Sha, W. E. I., Song, Y. (2021). Perovskite solar cells: Colorful efficient moiré-perovskite solar cells. *Advanced Materials*, 33: e2008091.

[213] Song, Q., Wang, Y., Vogelbacher, F., Zhan, Y., Zhu, D., Lan, Y., Fang, W., Zhang, Z., Jiang, L., Song, Y., et al. (2021). Moiré perovskite photodetector toward high-sensitive digital polarization imaging. *Advanced Energy Materials*, 11: 2100742.

[214] Shi, X.B., Liu, Y., Yuan, Z., Liu, X.K., Miao, Y., Wang, J., Lenk, S., Reineke, S., Gao, F. (2018). Optical energy losses in organic–inorganic hybrid perovskite light-emitting diodes. *Advanced Optical Materials*, 6: 1800667.

[215] Meng, S. S., Li, Y. Q., Tang, J. X. (2018). Theoretical perspective to light outcoupling and management in perovskite light-emitting diodes. *Organic Electronics*, 61: 351–358.

[216] Mao, J., Sha, W. E. I., Zhang, H., Ren, X., Zhuang, J., Roy, V. A. L., Wong, K. S., Choy, W. C. H. (2017). Novel direct nanopatterning approach to fabricate periodically nanostructured perovskite for optoelectronic applications. *Advanced Functional Materials*, 27: 1606525.

[217] Zhang, Q., Tavakoli, M. M., Gu, L., Zhang, D., Tang, L., Gao, Y., Guo, J., Lin, Y., Leung, S. F., Poddar, S., et al. (2019). Efficient metal halide perovskite light-emitting diodes with significantly improved light extraction on nanophotonic substrates. *Nature Communications*, 10: 727.

[218] Chen, Z., Li, Z., Chen, Z., Xia, R., Zou, G., Chu, L., Su, S. J., Peng, J., Yip, H. L., Cao, Y. (2021). Utilization of trapped optical modes for white perovskite light-emitting diodes with efficiency over 12%. *Joule*, 5: 456–466.

[219] Jeon, S., Zhao, L., Jung, Y. J., Kim, J. W., Kim, S. Y., Kang, H., Jeong, J. H., Rand, B. P., Lee, J. H. (2019). Perovskite light-emitting diodes with improved outcoupling using a high-index contrast nanoarray. *Small*, 15: e1900135.

[220] Shen, Y., Cheng, L. P., Li, Y. Q., Li, W., Chen, J. D., Lee, S. T., Tang, J. X. (2019). High-efficiency perovskite light-emitting diodes with synergetic outcoupling enhancement. *Advanced Materials*, 31: e1901517.

[221] Pitarke, J. M., Silkin, V. M., Chulkov, E. V., Echenique, P. M. (2007). Theory of surface plasmons and surface-plasmon polaritons. *Reports on Progress in Physics*, 70: 1–87.

[222] Li, Z., Moon, J., Gharajeh, A., Haroldson, R., Hawkins, R., Hu, W., Zakhidov, A., Gu, Q. (2018). Room-temperature continuous-wave operation of organometal halide perovskite lasers. *ACS Nano*, 12: 10968–10976.

[223] Saliba, M., Wood, S. M., Patel, J. B., Nayak, P. K., Huang, J., Alexander-Webber, J. A., Wenger, B., Stranks, S. D., et al. (2016). Structured organic-inorganic perovskite toward a distributed feedback laser. *Advanced Materials*, 28: 923–929.

[224] Shen, Y., Li, M. N., Li, Y., Xie, F. M., Wu, H. Y., Zhang, G. H., Chen, L., Lee, S. T., Tang, J. X. (2020). Rational interface engineering for efficient flexible perovskite light-emitting diodes. *ACS Nano*, 14: 6107–6116.

[225] Shi, Z., Li, Y., Li, S., Li, X., Wu, D., Xu, T., Tian, Y., Chen, Y., Zhang, Y., Zhang, B., et al. (2018). Luminescence: Localized surface plasmon enhanced all-inorganic perovskite quantum dot light-emitting diodes based onCoaxial core/shell heterojunction architecture. *Advanced Functional Materials*, 28: 1707031.

[226] Yu, Z., Leilaeioun, M., Holman, Z. (2016). Selecting tandem partners for silicon solar cells. *Nature Energy*, 1: 16137.

[227] Leijtens, T., Bush, K. A., Prasanna, R., McGehee, M. D. (2018). Opportunities and challenges for tandem solar cells using metal halide perovskite semiconductors. *Nature Energy*, 3: 828–838.

[228] Sahli, F., Werner, J., Kamino, B. A., Bräuninger, M., Monnard, R., Paviet-Salomon, B., Barraud, L., Ding, L., Diaz Leon, J. J., Sacchetto, D., et al. (2018). Fully textured monolithic perovskite/silicon tandem solar cells with 25.2% power conversion efficiency. *Nature Materials*, 17: 820–826.

[229] Hou, Y., Aydin, E., De Bastiani, M., Xiao, C., Isikgor, F. H., Xue, D. J., Chen, B., Chen, H., Bahrami, B., Chowdhury, A. H., et al. (2020). Efficient tandem solar cells with solution-processed perovskite on textured crystalline silicon. *Science*, 367: 1135–1140.

[230] Xu, J., Boyd, C. C., Yu, Z. J., Palmstrom, A. F., Witter, D. J., Larson, B. W., France, R. M., Werner, J., Harvey, S. P., Wolf, E. J., et al. (2020). Triple-halide wide-band gap perovskites with suppressed phase segregation for efficient tandems. *Science*, 367: 1097–1104.

[231] Al-Ashouri, A., Köhnen, E., Li, B., Magomedov, A., Hempel, H., Caprioglio, P., Márquez, J. A., Morales Vilches, A. B., Kasparavicius, E., Smith, J. A., et al. (2020). Monolithic perovskite/silicon tandem solar cell with >29% efficiency by enhanced hole extraction. *Science*, 370: 1300–1309.

[232] Eperon, G. E., Leijtens, T., Bush, K. A., Prasanna, R., Green, T., Wang, J. T., McMeekin, D. P., Volonakis, G., Milot, R. L., May, R., et al. (2016). Perovskite-perovskite tandem photovoltaics with optimized band gaps. *Science*, 354: 861–865.

[233] Rajagopal, A., Yang, Z., Jo, S. B., Braly, I. L., Liang, P.W., Hillhouse, H. W., Jen, A. K. Y. (2017). Highly efficient perovskite–perovskite tandem solar cells reaching 80% of the theoretical limit in photovoltage. *Advanced Materials*, 29: 1702140.

[234] Zhao, D., Chen, C., Wang, C., Junda, M. M., Song, Z., Grice, C. R., Yu, Y., Li, C., Subedi, B., Podraza, N. J., et al. (2018). Efficient two-terminal all-perovskite tandem solar cells enabled by high-quality low-bandgap absorber layers. *Nature Energy*, 3: 1093–1100.

[235] Tong, J., Song, Z., Kim, D. H., Chen, X., Chen, C., Palmstrom, A. F., Ndione, P. F., Reese, M. O., Dunfield, S. P., Reid, O. G., et al. (2019). Carrier lifetimes of >1 μs in Sn-Pb perovskites enable efficient all-perovskite tandem solar cells. *Science*, 364: 475–479.

[236] Xiao, K., Lin, R., Han, Q., Hou, Y., Qin, Z., Nguyen, H. T., Wen, J., Wei, M., Yeddu, V., Saidaminov, M. I., et al. (2020). All-perovskite tandem solar cells with 24.2% certified efficiency and area over 1 cm2 using surface-anchoring zwitterionic antioxidant. *Nature Energy*, 5: 870–880.

[237] Lin, R., Xiao, K., Qin, Z., Han, Q., Zhang, C., Wei, M., Saidaminov, M. I., Gao, Y., Xu, J., Xiao, M., et al. (2019). Monolithic all-perovskite tandem solar cells with 24.8% efficiency exploiting comproportionation to suppress Sn(ii) oxidation in precursor ink. *Nature Energy*, 4: 864–873.

[238] Li, L., Wang, Y., Wang, X., Lin, R., Luo, X., Liu, Z., Zhou, K., Xiong, S., Bao, Q., Chen, G., et al. (2022). Flexible all-perovskite tandem solar cells approaching 25% efficiency with molecule-bridged hole-selective contact. *Nature Energy*, 7: 708–717.

[239] Lin, R., Xu, J., Wei, M., Wang, Y., Qin, Z., Liu, Z., Wu, J., Xiao, K., Chen, B., Park, S. M., et al. (2022). All-perovskite tandem solar cells with improved grain surface passivation. *Nature*, 603: 73–78.

[240] Green, M. A., Dunlop, E. D., Hohl-Ebinger, J., Yoshita, M., Kopidakis, N., Bothe, K., Hinken, D., Rauer, M., Hao, X. (2022). Solar cell efficiency tables (Version 60). *Progress in Photovoltaics: Research and Applications*, 30: 687–701.

[241] Xiao, K., Lin, Y. H., Zhang, M., Oliver, R. D. J., Wang, X., Liu, Z., Luo, X., Li, J., Lai, D., Luo, H., et al. (2022). Scalable processing for realizing 21.7%-efficient all-perovskite tandem solar modules. *Science*, 376: 762–767.

[242] Palmstrom, A. F., Eperon, G. E., Leijtens, T., Prasanna, R., Habisreutinger, S. N., Nemeth, W., Gaulding, E. A., Dunfield, S. P., Reese, M., Nanayakkara, S., et al. (2019). Enabling flexible all-perovskite tandem solar cells. *Joule*, 3: 2193–2204.

[243] Zhang, Z., Li, Z., Meng, L., Lien, S.Y., Gao, P. (2020). Perovskite-

based tandem solar cells: Get the most out of the Sun. *Advanced Functional Materials*, 30: 2001904.

[244] Fang, Z., Zeng, Q., Zuo, C., Zhang, L., Xiao, H., Cheng, M., Hao, F., Bao, Q., Zhang, L., Yuan, Y., et al. (2021). Perovskite-based tandem solar cells. *Science Bulletin*, 66: 621–636.

[245] Jošt, M., Kegelmann, L., Korte, L., Albrecht, S. (2020). Monolithic perovskite tandem solar cells: A review of the present status and advanced characterization methods toward 30% efficiency. *Advanced Energy Materials*, 10: 1904102.

[246] Todorov, T., Gershon, T., Gunawan, O., Lee, Y. S., Sturdevant, C., Chang, L.Y., Guha, S. (2015). Monolithic perovskite-CIGS tandem solar cells via *in situ* band gap engineering. *Advanced Energy Materials*, 5: 1500799.

[247] Han, Q., Hsieh, Y. T., Meng, L., Wu, J. L., Sun, P., Yao, E. P., Chang, S. Y., Bae, S. H., Kato, T., Bermudez, V., et al. (2018). High-performance perovskite/Cu(In, Ga)Se_2 monolithic tandem solar cells. *Science*, 361: 904–908.

[248] Al-Ashouri, A., Magomedov, A., Roß, M., Jošt, M., Talaikis, M., Chistiakova, G., Bertram, T., Márquez, J. A., Köhnen, E., Kasparavi čius, E., et al. (2019). Conformal monolayer contacts with lossless interfaces for perovskite single junction and monolithic tandem solar cells. *Energy & Environmental Science*, 12: 3356–3369.

[249] Jošt, M., Köhnen, E., Al-Ashouri, A., Bertram, T., Tomšič, Š., Magomedov, A., Kasparavicius, E., Kodalle, T., Lipovšek, B., Getautis, V., et al. (2022). Perovskite/CIGS tandem solar cells: From certified 24.2% toward 30% and beyond. *ACS Energy Letters*, 7: 1298–1307.

[250] Yuan, J., Zhang, Y., Zhou, L., Zhang, G., Yip, H. L., Lau, T. K., Lu, X., Zhu, C., Peng, H., Johnson, P. A., et al. (2019). Single-junction organic solar cell with over 15% efficiency using fused-ring acceptor with electron-deficient core. *Joule*, 3: 1140–1151.

[251] Xiao, Z., Jia, X., Ding, L. (2017). Ternary organic solar cells offer 14% power conversion efficiency. *Science Bulletin*, 62: 1562–1564.

[252] Meng, L., Zhang, Y., Wan, X., Li, C., Zhang, X., Wang, Y., Ke, X., Xiao, Z., Ding, L., Xia, R., et al. (2018). Organic and solution-processed tandem solar cells with 17.3% efficiency. *Science*, 361: 1094–1098.

[253] Liu, L., Xiao, Z., Zuo, C., Ding, L. (2021). Inorganic perovskite/organic tandem solar cells with efficiency over 20%. *Journal of Semiconductors*, 42: 020501.

[254] Chen, C. C., Bae, S. H., Chang, W. H., Hong, Z., Li, G., Chen, Q., Zhou, H., Yang, Y. (2015). Perovskite/polymer monolithic hybrid tandem solar cells utilizing a low-temperature, full solution process. *Materials Horizons*, 2: 203–211.

[255] Liu, Y., Renna, L. A., Bag, M., Page, Z. A., Kim, P., Choi, J., Emrick, T., Venkataraman, D., Russell, T. P. (2016). High efficiency tandem thin-perovskite/polymer solar cells with a graded recombination layer. *ACS Applied Materials & Interfaces*, 8: 7070–7076.

[256] Chen, X., Jia, Z., Chen, Z., Jiang, T., Bai, L., Tao, F., Chen, J., Chen, X., Liu, T., Xu, X., et al. (2020). Efficient and reproducible monolithic perovskite/organic tandem solar cells with low-loss interconnecting layers. *Joule*, 4: 1594–1606.

[257] Zeng, Q., Liu, L., Xiao, Z., Liu, F., Hua, Y., Yuan, Y., Ding, L. (2019). A two-terminal all-inorganic perovskite/organic tandem solar cell. *Science Bulletin*, 64: 885–887.

[258] Wang, P., Li, W., Sandberg, O. J., Guo, C., Sun, R., Wang, H., Li, D., Zhang, H., Cheng, S., Liu, D., et al. (2021). Tuning of the interconnecting layer for monolithic perovskite/organic tandem solar cells with record efficiency exceeding 21. *Nano Letters*, 21: 7845–7854.

[259] Qin, S., Lu, C., Jia, Z., Wang, Y., Li, S., Lai, W., Shi, P., Wang, R., Zhu, C., Du, J., et al. (2022). Constructing monolithic perovskite/organic tandem solar cell with efficiency of 22.0% via reduced open-circuit voltage loss and broadened absorption spectra. *Advanced Materials*, 34: e2108829.

[260] Chen, W., Zhu, Y., Xiu, J., Chen, G., Liang, H., Liu, S., Xue, H., Birgersson, E., Ho, J. W., Qin, X., et al. (2022). Monolithic perovskite/organic tandem solar cells with 23.6% efficiency enabled by reduced voltage losses and optimized interconnecting layer. *Nature Energy*, 7: 229–237.

[261] Brinkmann, K. O., Becker, T., Zimmermann, F., Kreusel, C., Gahlmann, T., Theisen, M., Haeger, T., Olthof, S., et al. (2022). Perovskite-organic tandem solar cells with indium oxide interconnect. *Nature*, 604: 280–286.

[262] Aydin, E., Allen, T. G., De Bastiani, M., Xu, L., Ávila, J., Salvador, M., Van Kerschaver, E., De Wolf, S. (2020). Interplay between temperature and bandgap energies on the outdoor performance of perovskite/silicon tandem solar cells. *Nature Energy*, 5: 851–859.

[263] Liu, J., Aydin, E., Yin, J., De Bastiani, M., Isikgor, F. H., Rehman, A. U., Yengel, E., Ugur, E., Harrison, G. T., Wang, M., et al. (2021). 28.2%-efficient, outdoor-stable perovskite/silicon tandem solar cell. *Joule*, 5: 3169–3186.

[264] Wang, S., Wang, P., Chen, B., Li, R., Ren, N., Li, Y., Shi, B., Huang, Q., Zhao, Y., Grätzel, M., et al. (2022). Suppressed recombination for monolithic inorganic perovskite/silicon tandem solar cells with an approximate efficiency of 23%. *eScience*, 2: 339–346.

[265] Zheng, J., Mehrvarz, H., Liao, C., Bing, J., Cui, X., Li, Y., Gonçales, V. R., Lau, C. F. J., Lee, D. S., Li, Y., et al. (2019). Large-area 23%-efficient monolithic perovskite/homojunction-silicon tandem solar cell with enhanced UV stability using down-shifting material. *ACS Energy Letters*, 4: 2623–2631.

[266] Zheng, J., Mehrvarz, H., Ma, F.J., Lau, C. F. J., Green, M. A., Huang, S., Ho-Baillie, A. W. Y. (2018). 21.8% efficient monolithic perovskite/homo-junction-silicon tandem solar cell on 16 cm^2. *ACS Energy Letters*, 3: 2299–2300.

[267] Li, J., Xia, R., Qi, W., Zhou, X., Cheng, J., Chen, Y., Hou, G., Ding, Y., Li, Y., Zhao, Y., et al. (2021). Encapsulation of perovskite solar cells for enhanced stability: Structures, materials and characterization. *Journal of Power Sources*, 485: 229313.

[268] Li, Y., Wu, H., Qi, W., Zhou, X., Li, J., Cheng, J., Zhao, Y., Li, Y., Zhang, X. (2020). Passivation of defects in perovskite solar cell: From a chemistry point of view. *Nano Energy*, 77: 105237.

[269] Yang, W., Zhong, D., Shi, M., Qu, S., Chen, H. (2019). Toward highly thermal stable perovskite solar cells by rational design of interfacial layer. *iScience*, 22: 534–543.

[270] Belisle, R. A., Bush, K. A., Bertoluzzi, L., Gold-Parker, A., Toney, M. F., McGehee, M. D. (2018). Impact of surfaces on photoinduced halide segregation in mixed-halide perovskites. *ACS Energy Letters*, 3: 2694–2700.

[271] Bush, K. A., Palmstrom, A. F., Yu, Z. J., Boccard, M., Cheacharoen, R., Mailoa, J. P., McMeekin, D. P., Hoye, R. L. Z., Bailie, C. D., Leijtens, T., et al. (2017). 23.6%-efficient monolithic perovskite/silicon tandem solar cells with improved stability. *Nature Energy*, 2: 17009.

[272] Oxford pv sets world record for perovskite solar cell. 2018, 2023(7): https://www.oxfordpv.com/news/oxford-pv-sets-world-record-perovskite-solar-cell

[273] Oxford pv perovskite solar cell achieves 28% efficiency. 2018, 2023(7): https://www.oxfordpv.com/news/oxford-pv-perovskite-solar-cell-achieves-28-efficiency

[274] Helmholtz center achieves 29.80% efficiency for perovskite/silicon tandem solar cell. 2021, 2023(7):https://www.pv-magazine.com/2021/11/22/helmholtz-center-achieves-29-80-efficiency-for-perovskite-silicon-tandem-solar-cell/

[275] Sahli, F., Kamino, B. A., Werner, J., Bräuninger, M., Paviet-Salomon, B., Barraud, L., Monnard, R., Seif, J. P., Tomasi, A., Jeangros, Q., et al. (2018). Improved optics in monolithic perovskite/silicon tandem solar cells with a nanocrystalline silicon recombination junction. *Advanced Energy Materials*, 8: 1701609.

[276] Kamino, B. A., Paviet-Salomon, B., Moon, S. J., Badel, N., Levrat, J., Christmann, G., Walter, A., Faes, A., Ding, L., Diaz Leon, J. J., et al. (2019). Low-temperature screen-printed metallization for the scale-up of two-terminal perovskite–silicon tandems. *ACS Applied Energy Materials*, 2: 3815–3821.